CHEMICAL HEAT STORAGE FOR SAVING EXHAUST GAS ENERGY IN INTERNAL COMBUSTION ENGINES

By

Duc Luong Cao

A thesis in fulfilment of the requirement for the degree of

Doctor of Philosophy

Under the supervision of Associate Professor **Guang Hong**

University of Technology Sydney

Faculty of Engineering and Information Technology

August 2019

Certificate of Original Authorship

I, Duc Luong Cao declare that this thesis is submitted in fulfilment of the requirements for the award of Doctoral degree in the School of Mechanical and Mechatronic Engineering, Faculty of Engineering and Information Technology, at the University of Technology Sydney.

This thesis is wholly my own work unless otherwise reference or acknowledged. In addition, I certify that all information sources and literature used are indicated in the thesis.

This document has not been submitted for qualifications at any other academic institution.

This research is supported by the Australian Government Research Training Program

Signature:

Production Note:
Signature removed prior to publication.

Date: 23/08/2019

Acknowledgements

First of all, I owe my deepest gratitude to my principal supervisor, Associate Professor Guang Hong for her continuous supports, guidance, time, patience and inspiration. I have learnt a lot from her ideas, critical review of my study plans and papers, knowledge and motivation which encouraged me to overcome many difficulties in the research as well as other aspects of life to achieve this milestone. I also would like to thank my co-supervisory Professor Tuan Anh Le who supported my experiments at Hanoi University of Science and Technology.

I gratefully acknowledge the Vietnam International Education Development (VIED) under the Ministry of Education and Training, Vietnam (MOET) and University of Technology Sydney (UTS) for awarding me the UTS - VIED Scholarship.

I gratefully appreciate Yuhan Huang and Nizar Al-Muhsen for their time and assistance in the engine experiments at UTS. I would also like to thank Yuhan Huang for his valuable support in the CFD modelling.

I gratefully thank my close friends Van Truong Hoang, Yuhan Huang, Nizar Al-Muhsen, Peter Abdo, etc. for the wonderful time we spent together at UTS.

Finally, I am hugely indebted to my wife Thi Hong Tuyet Nguyen, my son Thanh Lam Cao and my family for their emotional supports, unconditional love and guidance.

List of Publications

Journal Articles

[1] **Duc Luong Cao**, Guang Hong, Jack Wang. Chemical heat storage for saving the exhaust gas energy in a spark ignition engine. *Journal of Clean Energy Technologies*, 2018; 6: 41-46.

Conference proceedings

[1] **Duc Luong Cao**, Guang Hong, Jack Wang. Preliminary investigation to the feasibility of chemical heat storage for saving the exhaust gas energy in a spark ignition engine. *The 20th Australasian Fluid Mechanics Conference*, Australasian Fluid Mechanics Society, Perth Australia 2016.

[2] **Duc Luong Cao**, Guang Hong, Tuan Anh Le. Preliminary comparison of chemical heat storage systems for saving exhaust gas energy in gasoline and diesel engines.*11th Asia-Pacific Conference on Combustion,* The combustion Institute, Sydney Australia 2017.

[3] **Duc Luong Cao**, Guang Hong, Tuan Anh Le. Investigation of chemical heat storage processes for recovering exhaust gas energy in internal combustion engines. T*he 21st Australasian Fluid Mechanics Conference*, Australasian Fluid Mechanics Society, Adelaide Australia 2018.

[4] **Duc Luong Cao**, Guang Hong, Tuan Anh Le. Numerical investigation of heat storage in a chemical heat storage system for saving exhaust gas energy in internal

combustion engines. *Internal conference on Sustainable Energy and Green Technology*. Bangkok, Thailand 2019

Content

Nomenclatures

Symbol	Description	Unit
A	Area	m^2
C_{ex}	Specific heat of the exhaust gas	kJ/kg.K
$C_{EM8block}$	Specific heat of EM8block	kJ/kg.K
C_r	Specific heat of the reactor	kJ/kg.K
$E_{captured}$	Captured energy of the reactor	kW
E_{com}	Energy of exhaust gas components	kW
E_{ex}	Energy of the exhaust gas	kW
$E_{EM8block}$	Energy for heating EM8block	kW
E_{other}	Other energy losses and storage	kW
E_r	Energy for heating the reactor	kW
E_{total}	Total energy of IC engine	kW
h	Heat transfer coefficient	$W/m^2.K$
h_{com}	Enthalpy of the exhaust gas component	kJ/kg
k_d	Dehydration rate of EM8block	s^{-1}
m_a	Intake air mass flow rate	kg/s
m_{air}	Air mass flow rate	kg/s
m_{com}	Exhaust gas component mass flow rate	kg/s
m_{ex}	Exhaust gas mass flow rate	kg/s
$m_{EM8block}$	Mass of reacted EM8block	kg

m_{fuel}	Fuel mass flow rate	kg/s
m_{H_2O}	Mass of water vapour generating in the dehydration reaction	kg
	Mass of condensed water in the water tank in the heat storage process	
$m_{Mg(OH)_2}$	Mass of $Mg(OH)_2$ in EM8block	kg
m_r	Mass of the reactor	kg
m_{total}	Total mass of EM8block	g
M_{H_2O}	Mole mass of the water	g/mol
$M_{Mg(OH)_2}$	Mole mass of $Mg(OH)_2$	g/mol
$q_{d,v}$	Volumetric storage capacity of the dehydration reaction	kJ/m^3
$q_{h,v}$	Volumetric storage capacity of the hydration reaction	kJ/m^3
$Q_{ex,in}$	Total energy of the exhaust gas at the reactor inlet	kJ
$Q_{ex,out}$	Total energy of the exhaust gas at the reactor outlet	kJ
Q_{HV}	Heating value of the fuel	kJ/kg
Q_{stored}	Stored energy inside the reactor in the heat storage process	kJ
$r_{captured}$	Percentage of the captured exhaust gas energy of the reactor	%
r_{com}	Mass percentage of the exhaust gas component	%
$r_{EM8block}$	Percentage of the reacted EM8block	%
r_{mix}	Mass mixing ration.	
r_{stored}	Percentage of stored exhaust gas energy	%
S	Heat source inside EM8block	kJ/m^3

t	Time	s
T_1	Exhaust gas temperature at the reactor inlet in the heat storage process	^{0}C
T_2	Exhaust gas temperature at the reactor outlet in the heat storage process	^{0}C
T_3	Temperature of EM8block in the heat storage process	^{0}C
T_4	Intake air temperature at the reactor inlet in the heat output process	^{0}C
T_5	Heated air temperature at the reactor outlet in the heat output process	^{0}C
T_6	Temperature of the reactor wall in the heat output process	^{0}C
T_a	Average temperature of the intake air in the reactor	^{0}C
T_w	Temperature of the reactor wall	^{0}C
T_{ex}	Temperature of the exhaust gas	^{0}C
x_d	Reacted fraction of the dehydration reaction	
x_d^0	Initial reacted fraction of the dehydration reaction	
$V_{Em8block}$	Volume of EM8block inside the reactor	m^3
Δx_d	Mole reacted fraction change of the dehydration reaction	
Δx_h	Mole reacted fraction change of the hydration process.	
$\Delta\tau$	Time step	s
ΔH_r^o	Reaction enthalpy of the dehydration reaction	kJ/mol
$\rho_{EM8block}$	Density of EM8block	kg/m^3
α_{ex}	Convection heat transfer coefficient of the exhaust gas	$W/m^2.K$

λ_{ex}	Thermal conductivity of the exhaust gas	W/m.K
λ_r	Effective thermal conductivity of the reactor wall	W/m.K
ϵ	Emission coefficient of the wall	
σ	Stefan - Boltzman constant	

Abbreviations

ASC	Ammonia Slip Catalyst
CFD	Computational fluid dynamics
CHS	Chemical heat storage
DHW	Domestic hot water
DNS	Direct Numerical Simulation
DOC	Diesel Oxidation Catalyst
DPF	Diesel Particulate Filter
EG	Expanded graphite
EGHR	Exhaust gas heat recovery
EM4	Compound of $Mg(OH)_2$ and EG in the mass mixing ratio of 4:1
EGR	Exhaust gas recirculation system
EM8	Compound of $Mg(OH)_2$ and EG in the mass mixing ratio of 8:1
EM16	Compound of $Mg(OH)_2$ and EG in the mass mixing ratio of 16:1
EM8block	Compound of $Mg(OH)_2$ and EG in the mass mixing ratio of 8:1 in block state
$EM8block_p$	Solid product of the dehydration reaction of EM8block
HVAC	Heating, ventilation and air conditioning
LES	Large Eddy Simulation
NEDC	New European Driving Cycle
PCM	Phase change material

RANS	Reynolds Averaged Navier-Stokes Simulation
SCR	Selective Catalytic Reduction
SST	Shear Stress Transport
TEG	Thermoelectric generation
TES	Thermal energy storage

List of Tables

List of Figures

Abstract

Utilizing the wasted energy is one of the important strategies for addressing the current issue of sustainability by increasing the energy system overall efficiency. Thermal energy storage (TES) systems have been in development to address the above strategy by storing the wasted energy and reusing it when needed. Chemical heat storage (CHS) system is one kind of TES systems, with its advantages of high energy density and long storage time and has been studied in recent years. CHS systems have been applied to storing the solar energy for domestic hot water, air-conditioning, etc. and heat energy required in the thermal power plants. However, research is needed to exploit more applications of CHS to store and utilize the wasted heat energy.

Internal combustion (IC) engines have been and are still the main power resource for vehicles and stationary electricity generation systems. However, the heat lost through the exhaust gases of an IC engine is significant and it is the major factor limiting the engine thermal efficiency. Technologies for instantaneously converting the heat energy of the engine exhaust gas to be other forms of energy have become mature, such as thermoelectric generation (TEG) and heat exchangers. Difference from them, CHS stores the wasted energy and reuses it when needed. However, applying CHS in the IC engine is still new. This study was aimed to develop a CHS system using magnesium hydroxide ($Mg(OH)_2$) and its dehydration and hydration reactions to store the engine exhaust gas energy rather than instantaneous energy conversion until the stored energy was need.

To experimentally investigate the performance of the CHS system, a CHS system was developed and tested on a Diesel engine (D1146TI). In the heat storage process, the experiments were conducted at 60%, 70% and 80% engine load conditions. Experimental

results showed that at 80% engine load, 61.4% of chemical material reacted and 5.05 % heat energy of exhaust gas was stored in an hour. The percentage of the stored exhaust gas energy reduced with the decrease of engine load due to the decrease of the exhaust gas energy. In the heat output process, as one of the proposed applications, the engine intake air was heated with the stored energy by hydrating MgO at the ambient temperature. The experimental results showed that the intake air could be heated to the temperature 5.7^0C - 17.3^0C higher than the ambient temperature of 23^0C.

To further investigate the CHS system in engine conditions more than that in experiments, a CFD model of the CHS system was developed using the commercial code of ANSYS FLUENT as a platform. The model was verified by comparing the simulation and experimental results. In the heat storage process and 60 minutes mode, the maximum stored energy in the CHS system was 21.9 MJ which was equivalent to 4.78% of exhaust gas energy with 72.54% of the EM8block reacted at the full engine load. The stored energy and the percentage of reacted EM8block decreased with the decrease of the engine load. In the full charge mode, the simulation results showed that the time on fully charge of the CHS reduced with the increase of the engine load and that the shortest time was 67.1 minutes at full engine load. This time on full charging increased to 110.3 minutes at 50% engine load. The simulation results also showed that the maximum percentage of the exhaust gas energy stored in the CHS system was 7.14% at 70% engine load. In the heat output process, the CFD model was used to test the CHS system at different ambient temperature values. Simulation results showed that the temperature of the engine intake air heated by the CHS could be increased from the ambient temperature of -10^0C to 12.15^0C.

Numerical simulation was also performed to investigate the CHS system modified with two wings added to the exterior wall of the tube of the reactor, aiming to enhance the heat transfer between the exhaust gas and the reactant. In the heat storage process in 60 minutes mode, both the percentage of the stored exhaust gas energy and reacted EM8block increased. Compared with the original CHS system, the percentage of reacted EM8block increased from 72.54% to 81.6% and the percentage of stored exhaust gas energy increased from 4.78% to 5.47% at the full engine load. The effect of the modified CHS system became stronger with the increase of the engine load. In the full charge mode, using the modified CHS system, the full charge time reduced 3.1 minutes at the full engine load and 8.2 minutes at 50% engine load compared with the original CHS system. Furthermore, the maximum percentage of stored exhaust gas energy increased from 7.14 % to 7.58% at 70% engine load. In the heat output process, the effect of the modified CHS system was stronger at the lower ambient temperature and higher reactor wall temperature. In the same condition at the ambient temperature of -10^0C and the reactor wall of 85^0C, the heated air temperature in the modified CHS system was 1.2^0C higher than that in the original one.

Chapter One

1 Introduction

1.1 Research background and motivation

The problems of fossil resources and greenhouse gas emissions have become more and more severe. Research on thermal energy storage (TES) is required to minimize energy consumption by storing the wasted thermal energy and reusing it when needed. Chemical heat storage (CHS) is considered as one of the promising methods for storing and releasing heat energy through the reversible reaction of chemical material. With CHS, heat energy is stored in chemical material with the high energy density, long storing time and small heat loss as the products of chemical reaction are stored separately in the ambient temperature. At present, CHS systems have been applied to store the solar energy for domestic hot water, air-conditioning, etc. and heat energy in the industrial processes and the thermal power plant. However, applying CHS to store heat energy in other areas has not been fully exploit.

Internal combustion (IC) engines have been widely used in many fields. However, a significant amount of fuel energy has to be lost as wasted heat through exhaust gas. The energy loss is 71% of the total energy in an IC engine including 22% through the exhaust gases [1]. Therefore, if the waste heat of exhaust gas could be reused, the overall efficiency of the IC engine will increase and the fuel and the pollutant emissions will reduce.

Some techniques have been developed to recover the heat energy of exhaust gas of IC engines including thermoelectric generation (TEG), and heat exchangers. However, they convert and use the heat energy of exhaust gas to be another form of energy instantaneously. On the other hand, they are not effective in the cold-start process when the temperature of the exhaust gas is low. Different from the existing techniques, CHS can store the heat energy to be used in the cold-start process. Although the application potential of CHS in IC engines is significant, the research in this area cannot fully exploit.

1.2 Research methodology and objectives

Based on experimental and simulation works, the current research focuses on applying CHS to recovering exhaust gas energy of IC engines by using the stored energy for heating purposes of the vehicle. In the current study, the prototype of the CHS reactor using $Mg(OH)_2$ was designed and built. Experiments were conducted on a Diesel engine (D1146TI) equipped with the CHS to investigate the performance of this CHS system and its application to heating the engine intake air. The high-temperature intake air could be used to heat the engine, catalyst, lubricant in IC engine vehicles or the batteries and the cabin in hybrid vehicles or defrosting system in the ice-areas.

Although, experiments had been conducted to demonstrate the advantages of the CHS system in recovering thermal energy of exhaust gas of IC engine, the multidimensional computational fluid dynamic (CFD) model had been built to reduce both times and cost in design, production and experiment. The CFD code ANSYS FLUENT had been used to investigate the CHS system in conditions more than that in experiments. Detailed aims of the project are described as follows:

- To develop a CHS system which can be used for experimental investigation.
- To investigate the performance of CHS system in the heat storage and heat output processes.
- To investigate the performance of the modified CHS system when two wings added to the exterior wall of the tube of the reactor.
- To identify possible applications of CHS system in IC engine and hybrid vehicles.

1.3 Thesis outline

This thesis consists of eight chapters with the following structure.

Chapter One: Introduction. This chapter presents the research background, together with the methodology and the objectives of the research. Chapter 1 finishes with the layout of the thesis.

Chapter Two: Literature review. This chapter presents the fundamental knowledge about thermal energy storage, including CHS and current applications of the CHS system. The chapter also reviews the background information of IC engine and solutions to recover exhaust gas heat energy. Besides, the main parameters of the chemical material using in the research (EM8block) is presented in this chapter. The chapter finishes with the reviews about the CFD modellings.

Chapter Three: CHS system. The chapter presents the principle of the CHS system using EM8block to recover exhaust gas energy of IC engine. The chapter also presents the main parameter of the tested engine. The chapter finishes with the design of the main device of CHS, the reactor.

Chapter Four: Experimental and Numerical methods. This chapter shows the processes to make EM8block and the experimental apparatus of the heat storage and heat output processes in the engine test bed. This chapter also presents the CFD model using ANSYS FLUENT verifying against the experimental results.

Chapter Five: CHS in heat storage processes. This chapter presents the criteria for evaluating the performance of CHS in the heat storage process. This chapter also presents the experimental and simulation results in the heat storage process of the CHS system in the 60 minutes and full charge modes.

Chapter Six: CHS in heat output processes. This chapter presents the experimental and simulation results of the heat output process. The results are compared with other thermal energy storage systems using to recover exhaust gas energy of IC engine to evaluate the operation of the CHS system.

Chapter Seven: Numerical investigation to improve the CHS system. This chapter presented the modified CHS system when two wings added in the exterior wall of the tube of the reactor. The performance of the modified CHS system in the heat storage and heat output processes are investigated using the verified CFD model and compared with the original one.

Chapter Eight: Conclusions and Future work. The chapter summaries the major finding and the contribution of the research. The proposed application of the CHS system in IC engine and hybrid vehicles, the suggestions for future work are also presented in this chapter.

Chapter Two

2 Literature Review

2.1 Chemical heat storage (CHS)

2.1.1 Thermal energy storage systems

TES systems have been applied to storing energy wasted in power systems and using the stored energy when it is needed. TES technology involves three main steps: heat charging, storage and heat recharging. Sensible, latent and chemical heat storages (CHS) are classified as TES systems.

Sensible heat storage technology results in the change of dry-bulb temperature of material which stores the heat energy [2, 3]. In the heat charging process, the material receives heat energy, thus, increasing its temperature and energy capacity.

In the discharging process, the temperature of the material decreases while the stored heat is released. The rate of storage sensible heat storage system, Q, can be calculated with Eq. (2.1).

$$Q = m\Delta h \quad (2.1)$$

Where m is the mass flow rate of the material (kg) and Δh is the enthalpy change of the material.

Water is the most well-known sensible heat storage material [4, 5]. The hot water storage system is applying to store the thermal energy of solar thermal collectors or co-generation

energy supply system for district heating. In Ulm, Germany, a pressurized hot water storage with the storage capacity 140 MWh was connected with two biomass co-generation plants to store the wasted heat energy and use for the city's district heating system [6]. Similarly, in the co-generation plants in Munich, Germany, an underground seasonal hot water storage was adopted in the solar district heating "Am Ackermann-Bogen" to supply space heating and domestic hot water for 320 apartments with 30.400 m^2 of living area[7]. A back-up system using a big hot water storage with the storage capacity 1200 MWh was adopted in the co-generation plant in Potsdam, Germany [8]. The stored energy of the co-generation plant could be used as a back-up system or help to enable to shut down of the co-generation during weak load periods.

Thermal oils [9], molten salts [10, 11], liquid metal [12], concrete blocks, rock [13, 14] are other main materials using in the sensible heat storage systems. They are applied to store solar energy [15] or wasted energy of industrial processes for space heating [16, 17] or domestic hot water.

In the latent heat storage systems, the thermal energy is stored in the phase change material (PCM) [18]. In the charging step, PCM absorbs heat energy and changes to a new phase. When this energy is released in the discharging process, PCM releases heat and changes back to the initial phase. The rate of stored latent heat storage, Q, can be express as follows:

$$Q = m\Delta H \quad (2.2)$$

Where m is the mass flow rate of PCM (kg) and ΔH is the change in latent heat of PCM (kJ/kg).

Depending on PCM, the latent heat storage system should be used for both cold and hot storages. Ice is presented as the main PCM for cold storage. In French, ice storage is using for the cold network to increase the cooling capacity and better reliability of cold supply at the business district of Paris La Defense [8]. Besides, seasonal snow storage is adopted to reduce the need for cooling machine in the hospital in Sundsvall, Sweden [19]. In Hokkaido, Japan, snow, and ice cryogenic energies are currently applied in agricultural facilities, housing complexes and welfare facilities [20]. Snow and ices are stored in the winter and used as cold sources in the summer to reduce the use of energy for the HVAC system. For cool storage, salt hydrate is another potential PCM. A latent heat storage using commercial salt hydrate was suggested by Pepe at Chalmers University of Technology, Sweden [21]. The heat storage system is charged by the campus cooling system during the night and supplies the additional cold energy during daytime. It helps to reduce the use of energy in the on-peak time, therefore, reducing the energy cost.

For hot storage, latent heat storage systems have been applied to stored wasted heat energy from the building, solar collectors, industrial processes or thermal power plants. There are two main types of PCM using for hot storage systems, organic and inorganic materials. Paraffin [22, 23], fatty acids [24], esters [24], alcohols [25], glycols [2] are classified as organic PCMs. The organic PCMs are usually adopted in the medium temperature TES systems. The main inorganic PCMs include salts, salt hydrates [26, 27], metals and alloys [28-30]. Inorganic PCMs are usually applied in high-temperature TES systems.

Both organic and inorganic PCMs are used [31] for heating and cooling purposes in active and passive storage systems in the building [32]. PCMs can be incorporated in construction materials to store heat energy on the sun day and use for cooling, heating

systems [33]. The use of latent heat storage in the building provides thermal comfort with minimal use of HVAC energy. Besides, PCM could be applied to store solar energy from the solar collector system. Palomba in [34] suggested using PlusICE A82, a commercial paraffinic material, as PCM with the melting temperature of 82^0C to support hot water for the building. The latent heat storage system using PlusICE A82 supported hot water at 65^0C, and the storage efficiency is 30%. In the industry, a latent heat storage using sodium nitrate as PCM was adopted in a co-generation plant in Saarland, Germany [35]. In the plant, one of the customers requires a constant high- quality steam. To ensure the delivery, a backup boiler is kept at the minimal load. With the latent TES system, the stored energy will supply the necessary steam and the backup boiler can be reduced to a warm load. It will reduce the use of fossil fuel of the plant.

It can be seen that, sensible and latent heat storage systems are based on physical processes. Different from them, chemical heat storage systems uses chemical materials as heat storage materials [2] and it is based on the reversible reaction of the chemical materials as described in Eq. (2.3).

$$A + \text{heat} \leftrightarrow B + C \quad (2.3)$$

Where A is the initial chemical material, B and C are products from the endothermic reaction.

In the charging process, the thermochemical material A absorbs heat energy to become two components B and C in the endothermic reaction (B and C are stored separately). During the discharging process, the reverse reaction occurs when two products B and C react together to become the initial form A and heat energy is released in the exothermic reaction. The stored energy of this technology could be estimated using Eq. (2.4).

$$Q = n_A H_r \quad (2.4)$$

Where n_A is the mole number of the reactant A and H_r is the reaction enthalpy (kJ/mol).

Compared with sensible and latent TES systems, two main advantages of the CHS can be summarized as follows [36-38]:

- CHS has higher thermal capacity compared with sensible and latent heat storage.
- CHS has longer storing time and with small heat loss. Products, B and C, are stored separately, and in the ambient temperature, so the heat lost to the environment is minimal.

However, CHS system is more complex than sensible and latent TES systems [37]. Thus, the cost of complete system for this technology will be higher.

2.1.2 Classification of CHS systems

Depending on the material and the chemical reaction, CHS can be classified into three main groups: gas-gas reaction, liquid-gas reaction and solid-gas reaction CHS systems [39].

2.1.2.1 Gas-gas reaction CHS

In the gas-gas reaction CHS, both initial material A and products B and C are gases. The gas-gas reaction CHS bases on the following form.

$$gas\ (1) + Heat \leftrightarrow gas(2) + gas\ (3) \quad (2.5)$$

The gas-gas reaction CHS usually has high reaction enthalpy but it has the following disadvantages [40].

- It has poor heat transfer characteristic and needs more space to store materials (the density of gases are small).
- Products are in the state of gas so it is difficult to separate them.
- Gas products usually need pressure vessels to store so it makes the investment cost increase.

Some main chemical materials using for gas-gas reaction CHS systems are shown in Table 2.1.

Table 2.1 *Chemical materials for gas-gas reaction CHS*

Chemical material	**Chemical reaction**	**Reaction Enthalpy (kJ/mol)**	**Working temperature (K)**	**Reference**
Ammonia (NH_3)	$2NH_3(g) \leftrightarrow N_2(g) + 3H_2(g)$	66.8	Below 673	[41][42]
Sulphur trioxide (SO_3)	$2SO_3(g) \leftrightarrow 2SO_2(g) + O_2(g)$	98.94	1073-1273	[43]
Methanol (CH_3OH)	$CH_3OH(g) \leftrightarrow 2H_2(g) + CO(g)$	95.04	373 – 473	[43]
Cyclohexane ($C_6H_{12}OH$)	$C_6H_{12}(g) \leftrightarrow C_6H_6(g) + 3H_2(g)$		478 – 589	[40]
Methane (CH_4)	$CH_4(g) + H_2O \leftrightarrow 3H_2(g) + CO(g)$ $CH_4(g) + CO_2 \leftrightarrow 2H_2(g) + 2CO(g)$	206.2 247.4	973 – 1133 973 – 1133	[40][44]

2.1.2.2 Liquid-gas reaction CHS

Different from the gas-gas CHS systems, in the liquid-gas reaction CHS systems, the initial material A is liquid and reaction products B and C are gases. Equation 2.6 shows the reversible reaction of a liquid-gas reaction CHS system.

$$liquid(1) + heat \leftrightarrow gas(2) + gas(3) \quad (2.6)$$

Compared with sensible, latent TES or gas-gas CHS systems, the liquid-gas CHS has higher reaction enthalpy but it has the following disadvantages.

- It is difficult to separate reaction products when all of them are in the gas state.
- Pressure vessels can be used to store products in the gas state, so it makes the investment cost increased.

Some candidates for the liquid-gas reaction CHS system are shown in Table 2.2.

Table 2.2 *Chemical materials for liquid-gas reaction CHS*

Chemical material	**Chemical reaction**	**Reaction Enthalpy (kJ/mol)**	**Working temperature (K)**	**Reference**
Isopropanol $(CH_3)_2CHOH$	$(CH_3)_2CHOH(l) \leftrightarrow (CH_3)_3CO(g) + H_2(g)$	Endothermic reaction: 100.4 Exothermic reaction: 55	353 – 483	[45] [46]
Ammonium hydrogen sulfate NH_4HSO_4	$NH_4HSO_4(l) \leftrightarrow NH_3(g) + H_2O(g) + SO_3(g)$	336.5	436 – 1173	[47] [48]

2.1.2.3 Solid-gas reaction CHS

In the solid-gas reaction CHS system, the initial material A and product B are solids and product C is in the gas state. This CHS system bases on the following form.

$$solid(1) + Heat \leftrightarrow solid(2) + gas(3) \quad (2.7)$$

Compared with gas-gas and liquid-gas reactions CHS systems, solid-gas CHS system has some advantages as follows:

- The reactions are very attractive with high reaction enthalpy.
- Products are in the difference states (solid and gas) so it is easy to separate and store them.
- The density of solid is much higher than gas and liquid so solid-gas reaction. CHS system will be more compact than gas-gas or liquid-gas reaction CHS systems.

Besides advantages, the major problem of the solid –gas reaction CHS system is the thermal conductivity of solid materials is small and it affects the efficiency of the whole system. There are three main solid-gas reaction CHS systems based on the chemical material including metal oxides, carbonate and hydroxide CHS systems.

Metal oxides CHS

Metal oxides CHS system is based on the thermal dissociation reaction of metal oxides, MO_{2x+1} as follows:

$$MO_{2x+1}(s) + Heat \leftrightarrow MO(s) + xO_2(g) \quad (2.8)$$

The working temperature and reaction enthalpy of metal oxides CHS systems depends on the material are shown in Table 2.3.

Table 2.3 *Metal oxide materials for solid-gas reaction CHS*

Chemical material	**Chemical reaction**	**Reaction Enthalpy (kJ/mol)**	**Working temperature (K)**	**Reference**
BaO_2	$BaO_2(s) \leftrightarrow BaO + 1/2\,O_2$	80.9	1011	[49]
PbO_2	$PbO_2(s) \leftrightarrow PbO + 1/2O_2$	55.1	565	[48]
CuO	$CuO(s) \leftrightarrow Cu_2O + 1/2O_2$	143.1	1298	[50]
MnO_2	$MnO_2(s) \leftrightarrow MnO + 1/2O_2$	133.9	1226	
Li_2O_2	$Li_2O_2(s) \leftrightarrow Li_2O + 1/2O_2$	38.4	460	[51]
Na_2O_2	$Na_2O_2(s) \leftrightarrow Na_2O + 1/2O_2$	99.6	1200	
SrO_2	$SrO_2(s) \leftrightarrow SrO + 1/2O_2$	48.1	416	
MgO	$MgO(s) \leftrightarrow Mg + 1/2O_2$	752	3360	
CaO	$CaO(s) \leftrightarrow Ca + 1/2O_2$	828	3800	
SrO	$SrO(s) \leftrightarrow Sr + 1/2O_2$	755	3550	
BaO	$BaO(s) \leftrightarrow Ba + 1/2O_2$	729	3600	
Li_2O	$Li_2O(s) \leftrightarrow 2Li + 1/2O_2$	906	2650	
Na_2O	$Na_2O(s) \leftrightarrow 2Na + 1/2O_2$	634	1880	
K_2O	$K_2O(s) \leftrightarrow 2K + 1/2O_2$	544	1652	
Rb_2O	$Rb_2O(s) \leftrightarrow 2Rb + 1/2O_2$	502	1494	
Cs_2O	$Cs_2O(s) \leftrightarrow 2Cs + 1/2O_2$	481	1432	

Carbonate CHS

Carbonate CHS system is based on the decarbonation reaction of carbonate. $CaCO_3$,$PbCO_3$, $MgCO_3$, $ZnCO_3$, $SrCO_3$ can be selected as candidates for a carbonate CHS. All of them are usually used in high temperature CHS systems. Equation 2.9 shows the decarbonation reaction of carbonate in a carbonate CHS system.

$$MCO_3(s) + Heat \leftrightarrow MO(s) + CO_2(g) \quad (2.9)$$

The working temperature and reaction enthalpy of candidates depend on the material as shown in Table 2.4.

Table 2.4 *Carbonate materials for solid-gas reaction CHS*

Chemical material	**Chemical reaction**	**Reaction Enthalpy (kJ/mol)**	**Working temperature (K)**	**Reference**
$CaCO_3$	$CaCO_3(s) \leftrightarrow CaO(s) + CO_2(g)$	178	Heat charge: 1133 K Heat release: 1153 K	[37] [52]
$PbCO_3$	$PbCO_3(s) \leftrightarrow PbO(s) + CO_2(g)$	88	Heat charge: 723 K Heat release: 573 K	[37]
$MgCO_3$	$MgCO_3(s) \leftrightarrow MgO(s) + CO_2(g)$	125	670	[53]
$ZnCO_3$	$ZnCO_3(s) \leftrightarrow ZnO(s) + CO_2(g)$	67	406	[53]
$SrCO_3$	$SrCO_3(s) \leftrightarrow SrO(s) + CO_2(g)$	234	1281	[53]

The challenge of the carbonate CHS system is that the CO_2 is rather difficult to liquefy [48]. To store the product, CO_2 is cooled down from the reaction temperature to 373K and is compressed and stored at 1100 kPa [53]. This system is called as CO_2 compressed system. CO_2 is stored in high-pressure vessel so it makes the cost for a carbonate CHS system increases.

Hydroxide CHS

The hydroxide CHS system is based on the dehydration and hydration reaction of hydroxides. $Ca(OH)_2$ and $Mg(OH)_2$ are two main materials in the system. The main properties of $Ca(OH)_2$ and $Mg(OH)_2$are shown in Table 2.5. Hydroxide CHS system using hydroxide, $M(OH)_2$,is based on the reversible reaction as follows:

$$M(OH)_2(s) + heat \leftrightarrow MO(s) + H_2O(g) \quad (2.10)$$

Table 2.5 *Hydroxide materials for solid-gas reaction CHS*

Chemical material	**Chemical reaction**	**Reaction Enthalpy (kJ/mol)**	**Working temperature (K)**	**Reference**
$Ca(OH)_2$	$Ca(OH)_2(s) + heat \leftrightarrow CaO(s) + H_2O(g)$	148.6	780	[54][55]
$Mg(OH)_2$	$Mg(OH)_2(s) \leftrightarrow MgO(s) + H_2O(g)$	81	540	[56]

In the charging process, $M(OH)_2$ absorbs heat energy from a heat source to become MO and H_2O in the dehydration reaction. Products, MO and H_2O, are stored separately at the ambient temperature. In the discharging process, two products react to become the initial material $M(OH)_2$ and heat energy is released.

2.1.3 Current application of CHS systems

CHS systems have been applied to store the wasted heat energy in domestic heating, industrial processes and power plants in order to bring a wide range of advantages.

For domestic heating, in the Netherland, to harvest the solar energy in the summer and support the hot water demand in the winter, an active solar heating and domestic hot water (DHW) system using $MgCl_2.6H_2O$ is being researched [57]. In the summer, the chemical material, $MgCl_2.6H_2O$, can be dehydrated by the solar energy through solar thermal evacuated tube collectors. In the winter, it will be hydrated by moist air from the ambient and heat energy will be released and used for DHW.

For industrial processes, in Italy, a CHS was developed for low-temperature storage. It absorbs the wasted heat energy from industrial processes at the low temperature ($T<100^0C$) and uses for equipment and space cooling. The principle of the CHS system is shown in Figure 2.1 [8].

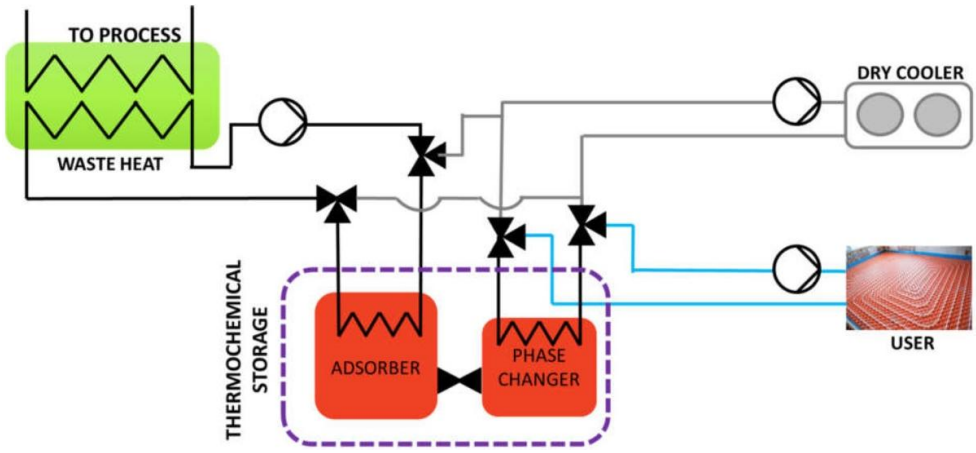

Figure 2.1 *Process diagram of CHS system for industrial processes*

As shown in Figure 2.1, a CHS system consists of two chambers, for the absorber (the dimensions of 250 x 353 x 774) and the phase change (the dimension of 240 x 543 x 769) [58]. The experimental results show that the CHS was able to store from 620 Wh at the charging temperature 75^0C up to 1100 Wh at 91^0C. The cooling temperature of the system was from 5 to 10^0C when the efficiency was between 30 and 42%.

Besides domestic and industrial areas, CHS systems have been applied to store heat energy in the thermal power plants including solar, fossil fuel or nuclear power plants. Pardoe [59] and Sylvie [60] suggested using $Ca(OH)_2/CaO$ in a fluidized bed reaction to store heat energy of a concentrated solar power plant during the day. The principal of the $Ca(OH)_2/CaO$ CHS system using in the solar power plant is shown in Figure 2.2.

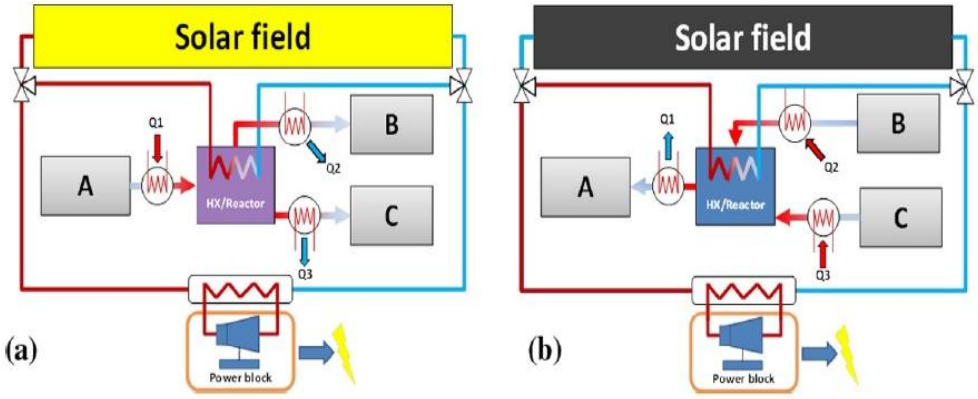

Figure 2.2 *Concentrated solar power plant using CHS: (a) heat storage process during the day, (b) heat output process during the night*

A is the initial chemical material ($Ca(OH)_2$) and B, C are products (CaO and H_2O). During the day, a part of solar energy from the solar field is stored in the reactor of the CHS system. The stored energy after that is used through the heat output process during the

night. It can be seen that using the CHS, the solar power plant can produce electricity during the night without the sun.

Zamengo [36] suggested using $Mg(OH)_2/MgO$ in a CHS system to store heat energy in the off-peak hours and release in the on-peak electricity times of a nuclear power plant. Therefore, it would make easier to manage the load variations of the power plant and contribution to the operation of a smart grid.

It can be seen that, CHS systems have been researched and applied in many fields to recover wasted heat energy. However, they still have a lot of potentials to be applied to other areas such as internal combustion (IC) engines.

2.2 Heat storage technology applied to internal combustion engines

2.2.1 Exhaust gas energy in internal combustion engines

In today's modern life, IC engines are still widely used in many fields, such as transportation, construction or agricultural sectors. However, a significant amount of fuel energy is lost as wasted heat through exhaust gas and cooling systems in IC engines.

As shown in Figure 2.3 [1], the total energy losses in a vehicle is 71% and 22% of total energy is lost in the exhaust gas of IC engines [1]. Therefore, if the heat loss in the exhaust gas can be stored and used, the efficiency of the IC engines will be increased. When a certain amount of exhaust gas heat could be recovered, the equivalent amount of primary fuel can be saved and the environment pollution could be reduced [61].

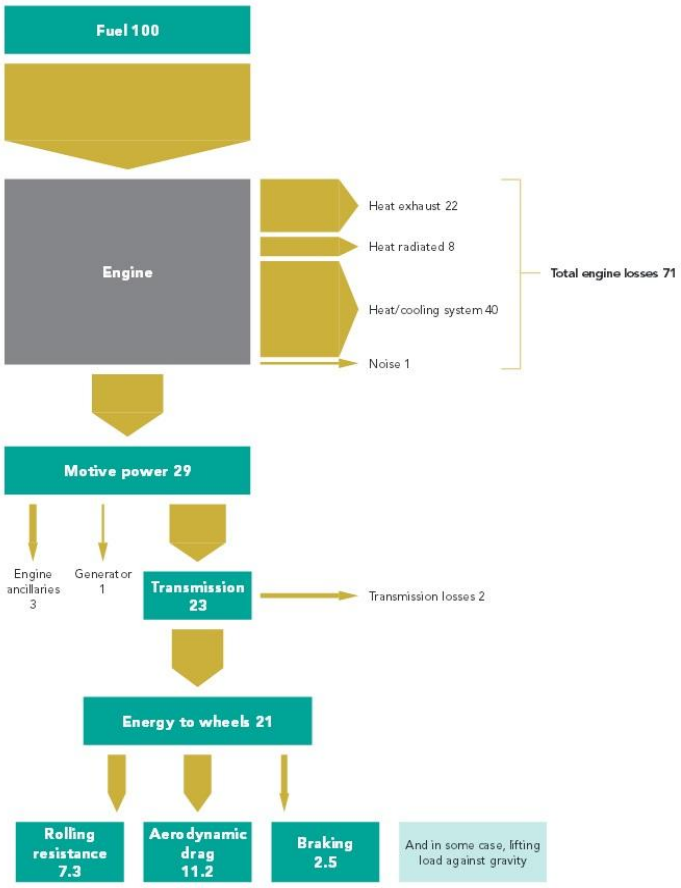

Figure 2.3 *Example map of energy flows in a vehicle*

2.2.2 Methods to recover engine exhaust gas energy

Thermoelectric generation (TEG), heat exchangers in direct and indirect heating methods and TES systems have been developed for recovering the heat energy in gasses exhausted from the combustion of IC engines.

2.2.2.1 Thermoelectric generation

Thermoelectric generation is used to convert the heat energy into electricity at the junction of difference materials [62]. When two dissimilar metal wires are formed into a closed

loop and its two junctions are held at different temperatures, it has the ability to deflect a galvanometer needle or having electrical current through the wires.

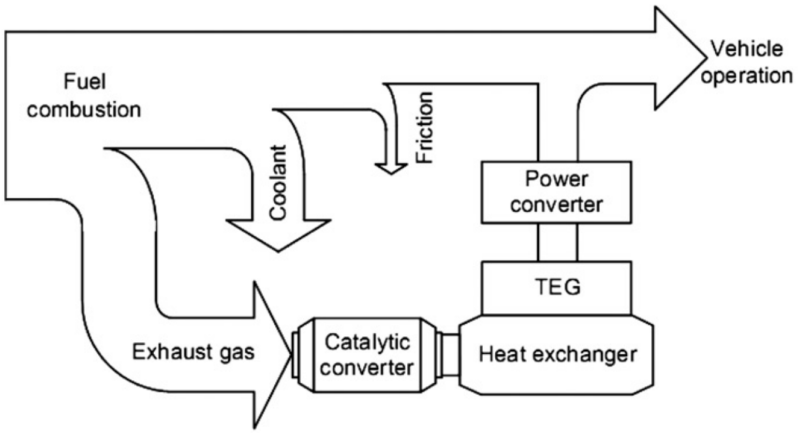

Figure 2.4 *Thermoelectric recovery for IC engines*

In IC engines, TEG can be used to convert heat energy from exhaust gas into electricity. A model of TEG applying for IC engines is shown in Figure 2.4 [63]. In the normal operation condition of IC engines, heat energy from the exhaust gas of IC engines is captured by a heat exchanger that is connected with the catalytic converter of the vehicle. Electricity generated from the TEG system is transmitted to a power converter and used for other vehicle needs.

TEG is a technology for directly converting thermal energy into electrical energy. It has no moving and complex mechanical parts so it is compact, silent operation, high reliability and environmentally friendly. However, there are some challengers of TEG as follows:

- Low efficiency: The efficiency of TEG depends on thermoelectric materials and the temperature of the hot side (the exhaust gas temperature). However, the

current efficiency of thermoelectric materials still low. To recover the exhaust gags energy of IC engines, the maximum efficiency of 8 TEGs using heat pipe of 62mm by 62 mm in size is 2.46% was reported by Bradley [64].

- A bigger size of the exhaust manifold: The voltage drop in a thermocouple is small so to have higher voltage, a lot of thermocouples is combined together. By this reason, using TEG needs a bigger size of the radiator and extended piping to the exhaust manifold [65]. It can increase the size of engines and vehicle.
- High initial cost: As recorded in [66], the investment cost for 1kW TEG system is 4773.77$ and for 5 kW TEG system is 19273.13$ (experiments and calculations were done on Cummins ISX 6 Cylinder diesel engine).

2.2.2.2 Heat exchangers

The main purpose of the lube oil in IC engine is to reduce friction losses. The performance of engine components lubricating by the lube oil depends on its viscosity that depends on its temperature. The viscosity of the lube oil is designed to get the highest efficiency at a warm-up temperature. The low temperature of the lube oil in the cold start process and in the cold weather makes the viscosity of the lube oil increases as shown in Figure 2.5 [67].

As shown in Figure 2.5, at the low temperature, the viscosity of the lubricant increases sharply. The high viscosity of the lube oil leads to the high friction losses of the engine and it affects to the engine efficiency. Therefore, heating the lube oil in the cold start process and the cold weather is necessary. As reported in [68], When the temperature of the lube oil increase 10^0C from 25^0C to 35^0C, the viscosity is reduced by 46%. Due to the reduction of the viscosity of the lube oil, it would be expected that the same reduction in

engine consumption. Therefore, a quite small increase in the temperature of the lube oil in the cold start process brings a significant diminution in fuel consumption.

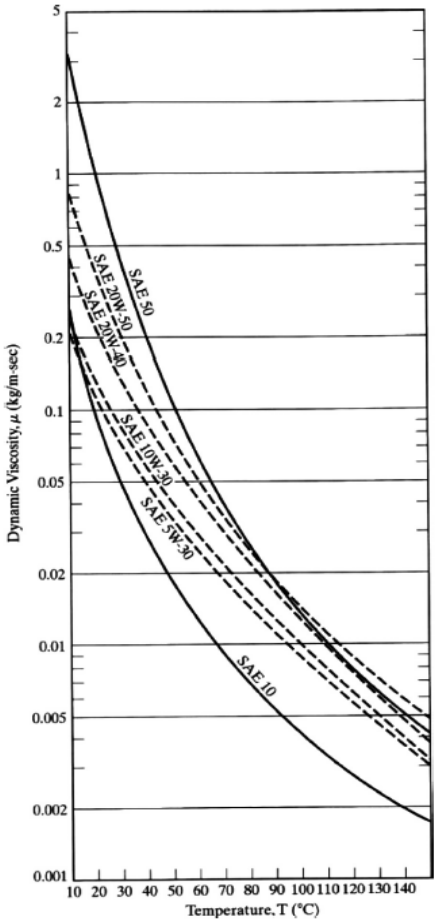

Figure 2.5 *Change in dynamic viscosity of the lube oil with temperature.*

To warm-up the lube oil, a heat exchanger system was installed in the lubrication system instead of the coolant system using the direct heating method in [69]. The main equipment of the system are shown in Figure 2.6. Exhaust gas from the catalyst flows to the heat exchanger to warm up directly the lube oil from the oil filter. The system was tested in a vehicle over the NEDC test cycle with the exhaust gas heat exchanger and without it. Over the test, the fuel economy of the engine was improved by 7%. Moreover, the carbon

dioxide (CO_2) emission reduced 21g/km, the carbon monoxide (CO) emission reduced 27% and NO_x was 19%.

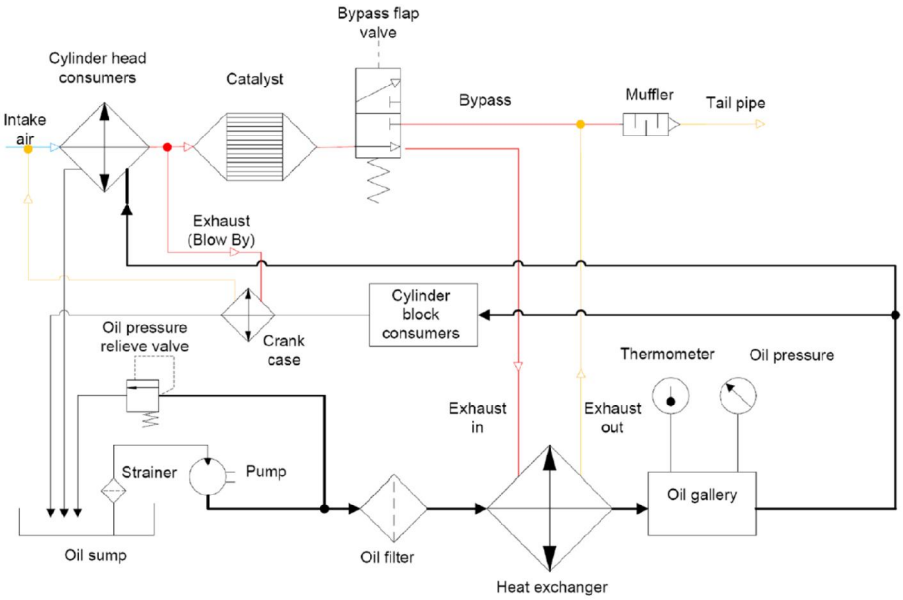

Figure 2.6 *Oil/exhaust gas heat exchanger system.*

In the indirect heating method, as reported in [68], water was used as an intermediate heat carrier to heat up the lube oil. The main principle of the exhaust gas heat exchanger using in the indirect method is shown in Figure 2.7 [68].

In this method, the exhaust gas heat exchanger was placed between the exhaust ports and the manifold inlet. In the heat exchanger, the water was heated from the ambient temperature (20^0C) to 35^0C by the exhaust gas. Water after that was used to heat the engine oil through an oil heater located between the oil filter and the sump. It can be seen that, because of the temperature of the water after going through the heat exchanger, the maximum temperature of the engine oil after going through the heating system was smaller than the temperature of the water after going through the heat exchanger.

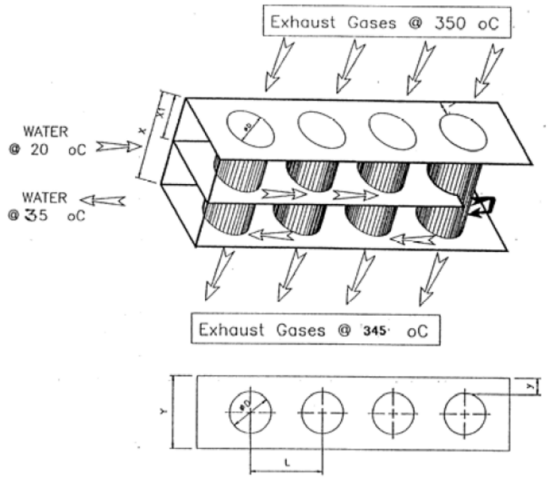

Figure 2.7 *Exhaust gas heat exchanger*

Using heat exchanger to recover the heat energy of the exhaust gas both in direct and indirect heating methods, the efficiency of the system highly depends on the efficiency of the heat exchanger.

2.2.2.3 Thermal energy storages

The solutions, as mentioned above, recover and use the heat energy of exhaust gas instantaneously and they are not effective in the cold-start process when the temperature of the exhaust gas is low. Different from the instantaneous energy conversion system, TES systems can store the heat energy of the exhaust gas until it is used including in the cold-start process.

V.Pandiyarajan [23] conducted the experiments using a TES tank and a shell and tube heat exchanger to recover heat energy from the exhaust gas of a diesel engine. The TES system in the research was the combination of sensible and latent heat storage systems. The experimental diagram is shown in Figure 2.8 [23].

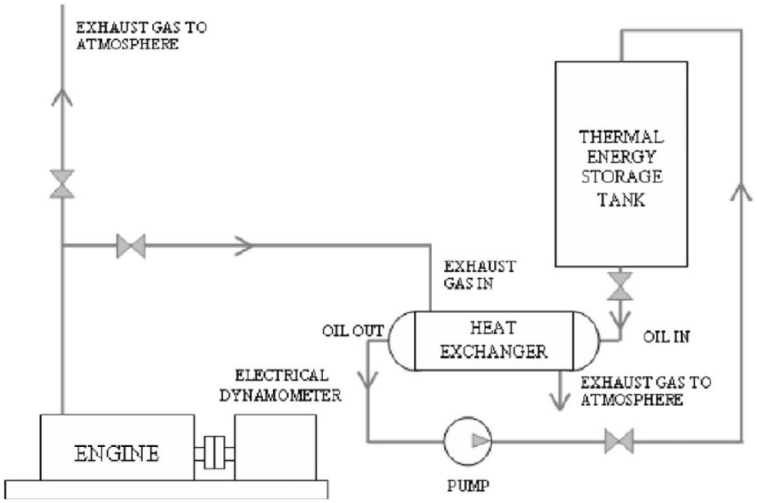

Figure 2.8 *Thermal energy storage for warming-up the lube oil*

With a heat exchanger (the diameter is 323 mm and length of shell is 500 mm), a 450 x 720 mm thermal energy storage tank and PCM was paraffin, the system as reported in [23] could store 10 – 15% of exhaust gas energy after 245 minutes, 180 minutes, 150 minutes and 85 minutes, respectively for 25%, 50% , 75% and full engine load. The maximum temperature of the storage material was 120^0C for all conditions.

However, after the heat storage process, in the storing time, the temperature of the TES tank (the temperature of PCM) was higher than the ambient temperature, so overtime the stored energy was lost to the ambient. The temperature of PCM decreases in the storing time as shown in Figure 2.9 [23]. It can be seen that, at ambient temperature 30^0C, the tank temperature decreased overtime and almost stored energy is gone after 5500 minutes of the storing time.

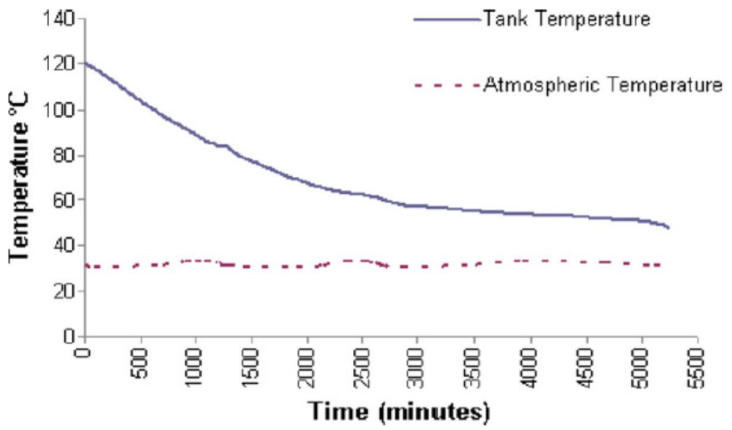

Figure 2.9 *Temperature of PCM in the storing period at the ambient temperature of* 30^0C

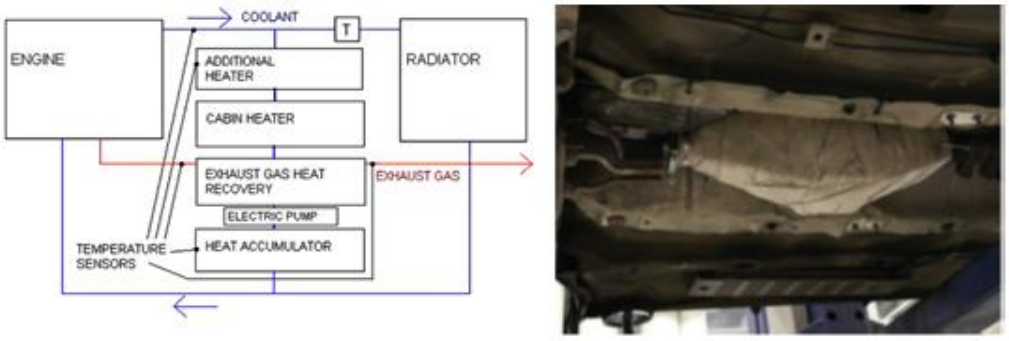

Figure 2.10 *Combination of the exhaust gas heat recovery system (EGHR) with a latent heat storage accumulator to reheating a diesel engine*

In the cold weather, it is difficult for the fuel in atomization, evaporation and the mixture with the air to create the correct air/fuel ratio for complete combustion. The incomplete combustion leads to the increase in the fuel consumption and pollutant emissions in the cold start process. Therefore, heating the engine in the cold weather is necessary to reduce the fuel consumption of the engine. In [70],the combination of the exhaust gas heat recovery system (EGHR) with a latent heat storage accumulator was used for preheating of the engine in the cold-start process and additional heating of the engine if the coolants

temperature drops below a thermostat set point during the drive cycle. The principle of this method is shown in Figure 2.10 [70].

In the system, EGHR and the heat storage accumulator were connected to the interior heat loop of the vehicle. An electric pump was added between EGHR and the heat accumulator to assist the engine water pump. In charging process, the hot coolant from EGHR would be used for charging the heat accumulator. The stored energy then was used to heat the coolant in the engine start-up. The experimental results showed that using the suggested system, during the engine start-up, it took 15 minutes for the coolant to reach 70^0C when the ambient temperature varied between -6 to -10^0C.

M.Gumus in[71] presented a latent heat storage system using $Na_2SO_4.10H_2O$ connection to the cooling system of the engine to preheating the engine in the cold start process. In the study, TES system was connected to the engine water jacket to store heat energy releasing from the engine in the charging process. In the discharging process, the stored energy was used to preheat the engine. The principle of this system is shown in Figure 2.11 [71].

The results showed that when the ambient temperature was 2^0C, using $Na_2SO_4.10H_2O$ CHS system, the temperature of the engine block cover can be increased to 17.4^0C after 500s. Furthermore, CO and HC emission decreased by approximately 64% and 15% respectively.

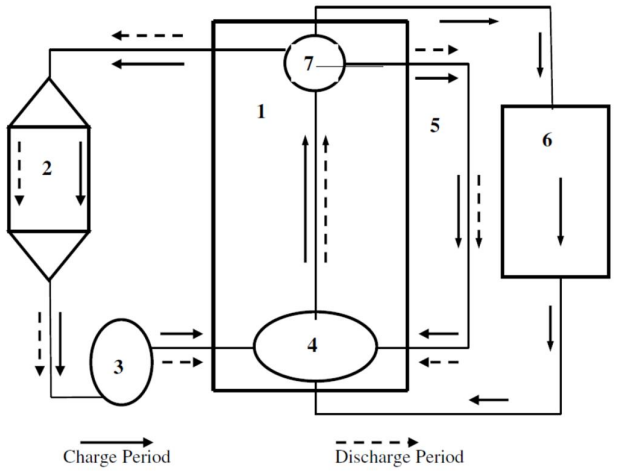

1. *Water jacket of engine*
2. *Heat storage*
3. *Pump working at discharge*
4. *Water pump of the engine*
5. *Line used for heater*
6. *Radiator*
7. *Thermostats*

Figure 2.11 *TES system for pre-heating the engine.*

Tessa thermal storage system is designed to stored exhaust gas energy of the IC engine and the stored energy can be used for pre-heating the engine, heating the cabin [72] or using as hot water and space heating in the building as shown in Figure 2.12 [73].

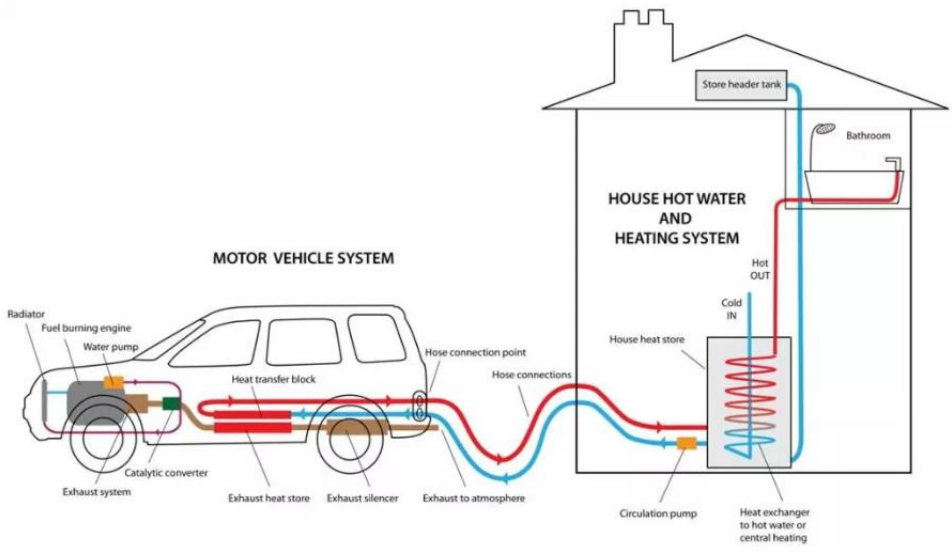

Figure 2.12 *Tessa-Thermal energy storage system for house hot water and heating system*

This system is in the final development stage with the energy unit cost is 160 £/kWh. The

weight of PCM is 36kg and the total weight of the CHS system is 60 kg. With the dimensions 610Width x710 Depth x230 Height, the system can stored 8.15 kWh at the temperature of 230^0C.

Besides sensible and latent heat storage, CHS with higher thermal capacity is also being researched to recover exhaust gas energy of IC engines. A CHS system using the stored energy of exhaust gas to heat the catalyst when starting the engine in [74].The updated versions of this research were published in 2016 and 2017 [75-77]. The main function of the catalytic converter in IC engine vehicle is purifying environment harmful elements such as CO_2, CO, NO_x, HC in the exhaust gas. The lowest limit for optimal temperature (for purification performance) of a catalyst is 150^0C. However, the temperature of exhaust gas immediately after starting the engines is around 100^0C lower than the requirement temperature of the catalyst. In the research presenting in [74-77] CHS system was used to warm up the catalyst to the active temperature in a shortest time. The exhaust gas purification system includes a CHS system is showed in Figure 2.13 [77].

When starting the engine, the temperature of exhaust gas is lower than the active temperature of the catalyst, the open-close valve is opened. When valve opens, ammonia from the absorber flows to the reactor through a connection tube. Heat creating from the chemical reaction between ammonia and reaction material inside the reactor is transferred to exhaust piper, whereby the temperature of DOC is increased to its active temperature.

When the temperature of the exhaust gas is higher than the active temperature of the catalysts, the dehydration reaction is taken place in the reactor by absorbing the exhaust gas heat energy, thereby generating ammonia. Through the connection valve, ammonia flows from the reactor to the absorber and it is absorbed by an absorbent.

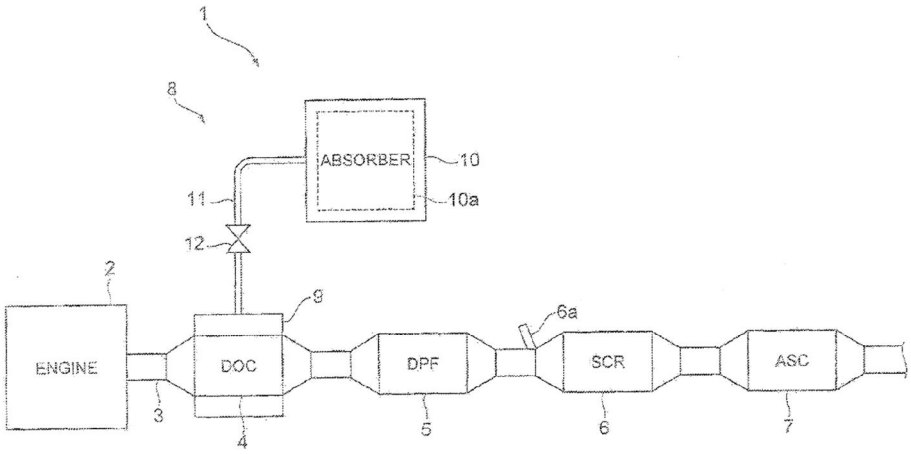

1: Exhaust gas purification system

2: Engine

3: Exhaust pipe

4: Diesel Oxidation Catalyst (DOC)

5: Diesel Particulate Filter (DPF)

6: Selective Catalytic Reduction (SCR)

7: Ammonia Slip Catalyst (ASC)

8: Chemical heat storage device

9: Reactor

10: Absorber

11: Connection tube

12: Open-close valve

***Figure 2.13** Exhaust purification system.*

In the present study, a new CHS system consisting of a reactor with $Mg(OH)_2$ as the initial chemical material has been developed and investigated to recover the exhaust gas energy of a diesel engine. The experiments were conducted to estimate the performance of the CHS system in the heat storage process at various engine operating conditions. In the heat output process, the stored energy was used to heat the engine intake air, aiming to extend this application to other heating required in IC engine and hybrid vehicles.

2.3 Chemical processes

The chemical material adopted in this research is Magnesium hydroxide ($Mg(OH)_2$). Compare with other candidate materials of CHS systems, $Mg(OH)_2$ has some advantages

as follows:

- It is an environmentally friendly material contained in the sea water.
- It is one candidate material of solid-gas reaction CHS system, so it has all advantages of this system such as high reaction enthalpy compared, higher density and easy to separate and store reaction products compared with gas-gas and liquid-gas reaction CHS systems.
- The working temperature of $Mg(OH)_2$ is suitable for the temperature of the exhaust gas of IC engines.

The CHS system using magnesium hydroxide is based on its reversible reaction as follows:

$$Mg(OH)_2(s) + heat \leftrightarrow MgO(s) + H_2O(g) \quad (2.11)$$

It was proposed that the wasted heat of exhaust gas of IC engines will be stored in the dehydration of $Mg(OH)_2$ to become MgO and H_2O, and releases the stored energy in the hydration of MgO. The storage density of this material is 81 kJ/mol and the reaction temperature of $Mg(OH)_2$ is around 540 K [78].

A drawback of the CHS system using pure $Mg(OH)_2$ is the thermal conductivity of the packed bed of $Mg(OH)_2$ pellets is too low (within 0.15 – 0.16 W/m.K) [78]. The low thermal conductivity of the pure $Mg(OH)_2$ pellets reduces the heat absorption capacity of chemical material and thereby decreases the efficiency of the system. To increase the heat transfer efficiency of $Mg(OH)_2$, a new compound was suggested by Massimiliano. It was the combination of $Mg(OH)_2$ and expanded graphite (EG) with the mass mixing ratio 8:1 and in the block state (EM8block). The EG, a nonhazardous material, with the high

thermal conductivity will help to enhance the heat transfer coefficient inside EM8block [36].

Table 2.6 *Main properties of pure $Mg(OH)_2$ pellets and EM8block*

Parameter	**Unit**	**$Mg(OH)_2$ pellets**	**EM8block**
Density of bed	g/cm^3	0.966	1.002
Working temperature	K	523-553	523-553
Reaction enthalpy	kJ/mol	81	81
Thermal conductivity	W/m.K	0.15 – 0.16	1.5 – 1.7

As reported in [78], the advantages of EM8block compared with pure $Mg(OH)_2$ include.

- Higher thermal conductivity: As shown in Table 2.6, the thermal conductivity of EM8block is ten times higher than that of the pure $Mg(OH)_2$ pellets.
- Higher density: Compare with the density of the bed with pure $Mg(OH)_2$ pellets were randomly arranged in the reactor, the density of EM8block is higher than that of $Mg(OH)_2$ pellets. The higher density means the size of the system will be more compact.
- Reduced void fraction of the bed: EM8block in the block state will enhance the contact between the packed material and the inner surface and consequently improve the thermal conductivity of the reactor.

EM8block, with its advantages as discussed above, was adopted in the present study. The exhaust gas energy will be stored in the dehydration process and the stored energy will be released in the hydration process of EM8block.

2.3.1 Dehydration reaction

In dehydration process, the volumetric heat storage capacity of EM8block can be estimated using Eq. (2.12) [36, 79].

$$q_{d,v} = \frac{-\Delta H_r^0}{M_{Mg(OH)_2}} \Delta x_d r_{mix} \rho_{EM8block} \quad (2.12)$$

Where $q_{d,v}$ is the volumetric heat storage capacity of the dehydration reaction of $Mg(OH)_2$ (kJ/m^3), ΔH_r^o is the reaction enthalpy of the dehydration reaction (kJ/mol), $M_{Mg(OH)_2}$ is mole mass of $Mg(OH)_2$ (g/mol), $\rho_{EM8block}$ is the density of EM8block (kg/m^3) and Δx_d is the mole reacted fraction change of the dehydration reaction.

The mass mixing ratio is expressed as follows:

$$r_{mix} = \frac{m_{Mg(OH)_2}}{m_{EM8block}} \quad (2.13)$$

Where $m_{Mg(OH)_2}$ is the mass of $Mg(OH)_2$ in EM8block (kg) and $m_{EM8block}$ is the mass of EM8block (kg) (r_{mix} = 8/9).

The mole reacted fraction change is showed in Eq. (2.14).

$$\Delta x_d = x_d - x_d^0 \quad (2.14)$$

Where x_d is the reacted fraction and x_d^0 is the initial reacted fraction of the dehydration reaction. The reacted fraction is defined as follows:

$$x_d = 1 + \frac{m_{H_2O}/M_{H_2O}}{m_{Mg(OH)_2}/M_{Mg(OH)_2}} \quad (2.15)$$

Where m_{H_2O} is the mass of water vapour generating from the dehydration reaction (kg), M_{H_2O} is the molemass of the water (g/mol). The reaction fraction of the dehydration reaction,x_d, depends on dehydration rate k_d (s^{-1}) and time t_d as follows:

$$lnx_d = -k_d.t_d + lnx_d^0 \quad (2.16)$$

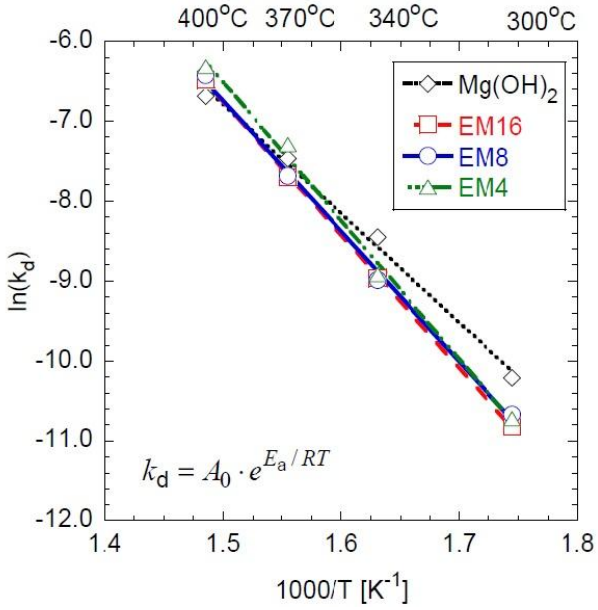

Figure 2.14 *Reaction rate for other materials*

The reaction fraction of pure $Mg(OH)_2$ and other compound of $Mg(OH)_2$ including EM4 (the compound of $Mg(OH)_2$ and EG in the mass mixing ratio is 4:1), EM8 (the compound of $Mg(OH)_2$ and EG in the mass mixing ratio is 8:1) and EM16 (the compound of $Mg(OH)_2$ and EG in the mass mixing ratio is 16:1) are shown in Figure 2.14 [36]. It can be seen that the reaction rate does not depend on the percentage of EG on the materials, it only depends on the temperature of the material. Moreover, the mole fraction of the materials highly depends on the temperature.

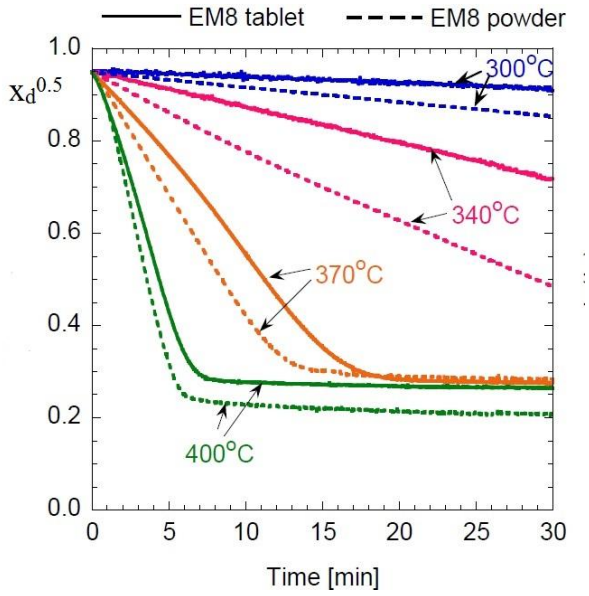

Figure 2.15 *Reacted fraction at 300, 340, 370 and 400^{0}C*

Figure 2.15 shows that the reaction rate at the high temperature is much higher than at low temperature. At 400^{0}C, after 7 minutes, more than 70% of the chemical material is decomposed. However, at 300^{0}C the reaction rate decreases very sharply.

As reported by Massimiliano in [36, 79], the volumetric heat storage of EM8block and other compounds are showed in Figure 2.16. As shown in Figure 2.16, the heat storage capacity of EM8block is 1.4 times higher than pure $Mg(OH)_2$ and EM8-b (the compound of $Mg(OH)_2$ and EG in the mass mixing ratio is 8:1 and in the state of pellets) in one hour working time.

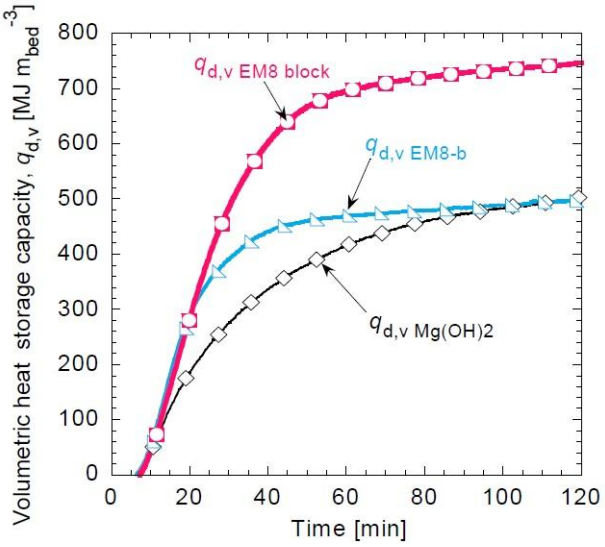

Figure 2.16 *Volumetric heat storage capacity of pure $Mg(OH)_2$, EM8 in the pellets state and EM8block*

In summary, compared with the pure $Mg(OH)_2$ and other compounds of $Mg(OH)_2$ and EG, EM8block has higher density and heat storage capacity. Therefore, CHS using EM8block will be more compact than other CHS systems using $Mg(OH)_2$ as the energy stored material. However, the reaction fraction of EM8block reduced sharply at the low temperature so CHS using EM8block is only suitable when the temperature of the heat source is higher than 300^0C. With IC engines, in almost operation condition, the temperature of the exhaust gas is higher than 300^0C so applying EM8block CHS in IC engines is feasible.

2.3.2 Hydration reaction

In the hydration process, the stored energy will be released. The volumetric heat storage capacity of EM8block in the hydration process can be estimated using Eq. (2.17) [36, 79].

$$q_{h,v} = \frac{-\Delta H_r^0}{M_{Mg(OH)_2}} \Delta x_h r_{mix} \rho_{Em8block} \quad (2.17)$$

Where $q_{h,v}$ is the volumetric heat output capacity of the hydration reaction of EM8block (kJ/m^3) and Δx_h is the mole reacted fraction change of the hydration process.

After the dehydration process, the solid product and water are stored separately and in the ambient condition. In the hydration process, the water vapour reacts with the solid products of the dehydration process to become the initial chemical material, EM8block. In the hydration process, the hydration pressure (water vapour pressure), P_h, affects directly to the temperature, the volumetric heat output of EM8block and the mole reacted fraction change of the hydration process Δx_h [80]. The properties of EM8block in the hydration process at the hydration pressure of 47 kPa, 101 kPa and 361 kPa [36], [81]are shown in Table 2.7.

Table 2.7 *EM8block properties in the hydration process at the water vapour pressure of 47 kPa, 101 kPa and 361 kPa*

Properties	**Unit**	**47 kPa**	**101 kPa**	**361 kPa**
Vapour temperature	^{0}C	79.69	100	139.95
EM8block temperature in the hydration reaction	^{0}C	130 – 140	150 – 175	220 – 230
Volumetric gross heat output after 60 min	MJ/m^3	347	588	911
Volumetric heat output rate after 30 min and 60 min	kW/m^3	118 (30’) 87 (60’)	300 (30’) -	400 (30’) 253 (60’)

As shown in Table 2.7, the higher pressure leads to the higher temperature and heat output of EM8block. However, with the higher temperature, the energy input (the required energy for evaporating the water) is higher. Moreover, at the high pressure, the pressure vessel makes the investment cost of the CHS system increases.

2.4 CFD modelling

An advantage of CFD model is reducing both times and cost in design, production and experiment. It makes possibility to analysis the geometrics, the operation condition changes. The commercial code of ANSYS FLUENT provides a system level modelling, meshing and complex flow simulations. CHS modelling using ANSYS FLUENT includes the modelling of the turbulence fields, the heat transfer, and the chemical reaction inside the CHS system.

2.4.1 Turbulence modelling

There are different approaches to calculate the turbulence flow, including Direct Numerical Simulation (DNS), Large Eddy Simulation (LES) and Reynolds Averaged Navier-Stokes Simulation (RANS). DNS offers the ability to provide 3D and time-dependent solutions of the Navier-Stokes equations. However, because of the inherent complexity of the transport equations, simulating the complex flow is impossible [82]. LES is a simulation method in CFD solves the spatially averaged Navier-Stokes equations. In this method, the large eddies are resolved directly but the eddies smaller than the mesh are modeled. Compared with DNS, LES is less expensive but the computational resources and efforts are still too large for practical applications [83]. RANS is the most widely used method. It solves time-average Navier-Stokes equations and is suitable with all turbulent length scales. As reported in [84], the computation cost of LES on the coarse grid is 80-100 times and on the basic grid is 160-400 times than steady RANS simulation on the basic grid. Moreover, LES is often referred to the turbulence model only. If applying LES in other model such as heat transfer and chemical reaction models, they should be modified to adapt with LES [85].

There are various RANS sub-models in ANSYS including one-equation model, two equation models (k-ε, k-ω models), three equation model (transition k-kl-ω model), four equation model (transition SST model) and seven equation model (Reynolds stress model) [86]. The computational cost per iteration increases with the increase of the number of equations in the model. The two equation models have advantages at computing efficiency [87].In these two equation models, the turbulent viscosity is based on the solutions of the equations for turbulent kinetic energy (k) and specific dissipation rate (ω) or turbulent dissipation rate (ε).

The k-ε model, a two equation model, is the most widely-used turbulence model. The k-ε model contains many sub-models for compressibility, combustion, buoyancy, etc. It is robust and accurate for a wide range of application. However, it is inaccurate for flows with a larger pressure gradient, strong separation and large streamline curvature. Compared with the k-ε model, the k-ω model has much better performance for boundary layer flows. With pressure gradient, k-ω accurate and robust for a wide range of boundary layer flows. However, the k-ω needs a higher computational cost than k- Ɛ model. To combine the merits of both the k-ε and the k-ω model, the Shear Stress Transport (SST) model, a sub-model of the k-ω model, is suggested in ANSYS. In the SST model, the k-ω model is applied for area closing to the wall and the k-ε model is used for the freestream.

To investigate the turbulence flow in the narrow area using CFD model, Hu in [88] compared the experimental results with the simulation results of four RANS turbulence models (standard k-ε, RNG k-ε, standard k-ω and SST k-ω models). He concluded that the best agreement between the experimental and numerical data with respect to the mean velocity vector fields and turbulent kinetic energy contours was obtained using the SST k-ω model [88].

2.4.2 Heat transfer modelling

Convection, radiation and conduction are three dominating mechanism of the heat transfer. In the cylindrical coordinates, the heat conduction inside a solid cylinder could be expressed as follows [89]:

$$\frac{\partial^2 T}{\partial r^2} + \frac{1}{r}\frac{\partial T}{\partial r} + \frac{1}{r^2}\frac{\partial^2 T}{\partial \emptyset^2} + \frac{\partial^2 T}{\partial z^2} + \frac{q^{\cdot}}{k} = \frac{1}{\alpha}\frac{\partial T}{\partial \tau} \quad (2.18)$$

Where T is the temperature (K), r is the radical distance (m), k is the thermal conductivity (W/m.K). $q^{\cdot}$ is the heat generated per unit volume (W/m^3), α is the thermal diffusivity of the material (m^2/s). The thermal diffusivity could be found from Eq. (2.19).

$$\alpha = \frac{k}{\rho c} \quad (2.19)$$

Where ρ is the density (kg/m^3) and c is the specific heat (kJ/kg) of the material.

At the high temperature of the fluid, the heat transfer between the fluid and the wall was presented as the combination of the heat convection and radiation. In this case, the heat transfer between the fluid and the reactor wall, $Q_{f,i,j}$ (W) could be presented by Eq. (2.20) [90, 91]

$$Q_{f,i,j} = \alpha_{i,j}\left(T_{f,i,j} - T_{w,i,j}\right)A_{i,j} + \epsilon\sigma\left(T_{f,i,j}^4 - T_{w,i,j}^4\right)A_{i,j} \quad (2.20)$$

Where $T_{w,i,j}$ is the temperature of the wall at the node i, j (K), $T_{f,i,j}$is the log mean temperature of the fluid (K),$\alpha_{i,j}$the heat convection coefficient of the fluid (W/m^2.K), ϵ is the emission coefficient of the wall, σ is the Stefan-Boltzmann constant and A is the surface area of the wall. The log mean temperature of the exhaust gas can be determined as follows [89]:

$$T_{f,i,j} = \frac{(T_{f\,in,i,j} - T_{w,i,j}) - (T_{f\,out,i,j} - T_{w,i,j})}{ln\frac{T_{f\,in\,i,j} - T_{w\,i,j}}{T_{f\,out\,i,j} - T_{w\ i,j}}} \quad (2.21)$$

Where $T_{f,i\,n,i,j}$, $T_{f,out,i,j}$ are the temperatures of the fluid at the inlet and outlet of the node i,j (K). When ignoring all heat loss from the system to the ambient, the heat transfer from the fluid to the wall $Q_{f,i,j}$is the energy change of the fluid in the node i, j presenting by Eq. (2.22).

$$Q_{f,i,j} = m_{f,i,j} C_{f,i,j} (T_{f\ i\ n,i,j} - T_{f\ out,i,j}) \quad (2.22)$$

Where $C_{f,i,j}$ is the specific heat of the fluid at the node i, j (kJ/kg.K), and $m_{f,i,j}$ is the mass flow rate of the fluid at the node i,j (kg/s).

2.4.3 Chemical reaction modelling

In the chemical reaction modelling, a typical chemical reaction is expressed as follows:

$$\sum_{n=1}^{N} \gamma'_{i,r} M_i \xleftrightarrow[k_{b,r}/k_{f,r}]{} \sum_{i=1}^{N} \gamma''_{i,r} M_i \quad (2.23)$$

where N is the number of chemicals,$\gamma'_{i,r}$ is the stoichiometric coefficient of reactant i in reaction r,$\gamma''_{i,r}$ is the stoichiometric coefficient of product i in reaction r,$k_{b,r}$ and $k_{f,r}$ are the reaction rate constant in reverse and forward reactions, respectively.

According to the Arrhenius law, the forward reaction rate is presented as follows [86]:

$$k_{f,r} = A_r T^{\beta_r} e^{-E_r/RT} \quad (2.24)$$

Where A_r is the pre-exponential factor, β_r is the temperature exponent, E_r is the activation energy and R is gas constant.

The reverse reaction rate is computed as follows [86]:

$$k_{b,r} = A_{b,r} T^{\beta_{b,r}} e^{-E_{b,r}/RT} \quad (2.25)$$

Where $A_{b,r}$ is the backward reaction pre-exponential factor, $\beta_{b,r}$ is the backward reaction temperature exponent, $E_{b,r}$ is the backward reaction activation energy.

After the reaction, the mass change of the solid material in the CFD model was developed based on the pyrolysis model. There are many pyrolysis models including single-step global mechanisms and semi-global multi-step mechanisms [92]. In the simplified models, the single or two-step Arrhenius reaction schemes were used to define devolatization rates [93]. The single-step model could be expressed as follows:

$$-\frac{dm_s}{dt} = k[m_s - (1 - f_v)m_{s,0}] \quad (2.26)$$

Where m_s is mass of the solid material, f_v is the mass fraction of volatiles initially, $m_{s,0}$ is the initial mass of the solid material, k is the reaction kinetic rate and it could be found from the single –step Arrhenius fashion as follow:

$$k = A_r \exp(\frac{-E}{RT}) \quad (2.27)$$

In the mathematical model of the chemical reaction proposed by Massimiliano in [36] the reaction rate of the reaction fraction at the node i, j at time $\tau + \Delta\tau$ of the solid material could be expressed as follows:

$$x'_{i,j} = x_{i,j}.\, e^{k_{i,j}.\Delta\tau} \quad (2.28)$$

Where $k_{i,j}$ is the reaction rate that is considered as constant between time τ and $\tau + \Delta\tau$, $x_{i,j}$ is the reaction fraction at time τ.

In the heat storage process, the exhaust gas energy will be stored in the dehydration process. Based on the amount of the reacted chemical material between time τ and $\tau + \Delta\tau$, the stored energy per time step $\Delta\tau$ is given by Eq. (2.29).

$$Q_{d,i,i} = \frac{-\Delta H}{\Delta\tau}\rho_{i,j}\Delta x_{d,i,j}V_{i,j} \quad (2.29)$$

Where $Q_{d,i,j}$ is the stored energy in the node i, j, ΔH is the reaction enthalpy of the chemical material, $\rho_{i,j}$ is the density and $V_{i,j}$ is the volume of node i, j. $\Delta x_{d,i,j}$ is the reaction fraction change of the node i, j in the heat storage process between time τ and $\tau + \Delta\tau$.

In the heat output process, the stored energy will be released in the hydration process. Based on the amount of the reacted chemical material in the heat output process between time τ and $\tau + \Delta\tau$, the stored energy per time step $\Delta\tau$ is given by Eq. (2.30).

$$Q_{h,i,i} = \frac{\Delta H}{\Delta\tau}\rho_{i,j}\Delta x_{h,i,j}V_{i,j} \quad (2.30)$$

Where $Q_{h,i,j}$ is the released energy in the node i, j and $\Delta x_{h,i,j}$ is the reaction fraction change of the node i, j in the heat output process between time τ and $\tau + \Delta\tau$.

Chapter Three

3 CHS system

3.1 Principle of CHS system using $Mg(OH)_2$

To store the waste heat of the exhaust gas, it was proposed that two main devices would be installed in the exhaust gas pathway of an IC engine, a reactor and a water tank. EM8block is stored inside the reactor. The water tank is for condensing the water vapour in the heat storage process and evaporating the water liquid in the heat output process. The reactor is located between the engine exhaust port and the catalytic converter. The principle of the heat storage process is shown in Figure 3.1.

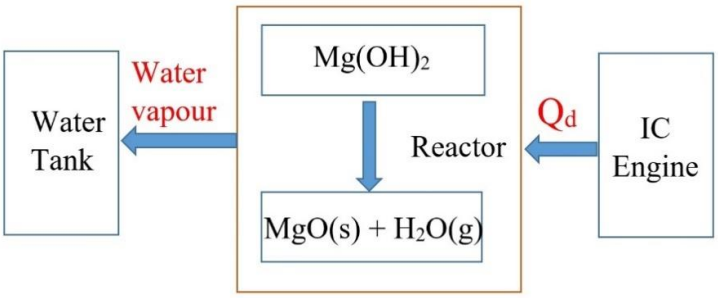

Figure 3.1 *Heat storage process*

As shown in Figure 3.1, in the heat storage process, heat energy, Q_d, is transferred from the exhaust gas to Magnesium hydroxide ($Mg(OH)_2$) and converts to magnesium oxide (MgO) and water vapour (H_2O) in the dehydration reaction in the reactor. The equilibriums are expressed as follows [94]:

$$Mg(OH)_2\ (s) + Q_d \rightarrow MgO(s) + H_2O(g) \qquad (3.1)$$

$$H_2O(g) \rightarrow H_2O(l) + \Delta H_1 \quad (3.2)$$

During this process, MgO is retained inside the reactor, the water vapour moves into the water tank and condenses into the liquid state. As the reaction products, MgO and water vapour are stored separately in the reactor and water tank.

In the heat output process, the stored heat is used to heat the intake air. The principle is shown in Figure 3.2.

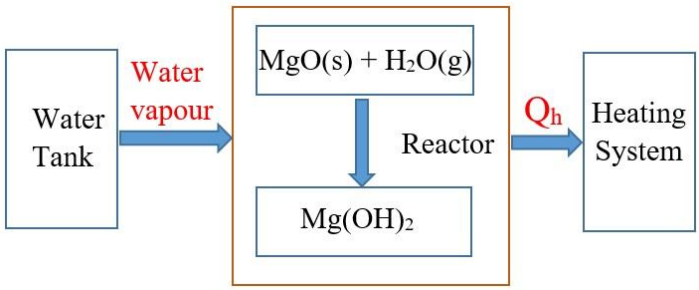

Figure 3.2 *Heat output process*

As shown in Figure 3.2, the water liquid in the water tank is heated by a small electrical resistor and evaporates. The water vapour flows from the water tank into the reactor and reacts with the solid retaining in the reactor after the heat storage process (MgO). Heat energy, Q_h, is released from the hydration reaction of MgO and water vapour as follows:

$$H_2O(l) + \Delta H_2 \rightarrow H_2O(g) \quad (3.3)$$

$$MgO(s) + H_2O(g) \rightarrow Mg(OH)_2(s) + Q_h \quad (3.4)$$

Heat energy releasing from the hydration reaction in the reactor, after that, is transferred to the object to be heated, here is the engine intake air.

3.2 Tested engine

Experiments were conducted on a Diesel engine, D1146TI, at the Engine Laboratory at the Hanoi University of Science & Technology in Vietnam. D1146T1 is a 4-stroke 6-cylinder Diesel engine for buses in Vietnam. The major specifications of the tested engine are shown in Table 3.1

Table 3.1 *Major specifications of the Diesel engine*

Parameters	**Unit**	**Value**
Number of cylinders		6
Number of strokes		4
Bore	mm	111
Stroke	mm	139
Displacement volume	cc	8071
Compression ration		16.7:1
Maximum power	kW	151@2200rpm
Maximum Torque	N.m	735@1400rpm

The total energy of the IC engine, E_{total}, is the amount of fuel chemical energy releasing in the combustion process. It can be written function of the fuel consumption of the engine and the heating value of the fuel as follows:

$$E_{total} = m_{fuel} Q_{HV} \quad (3.5)$$

Where Q_{HV} is the heating value of the fuel (kJ/kg) and m_{fuel} is the fuel mass flow rate (kg/s).

In IC engine, besides the useful work defining as the engine power, a part of the total energy is lost in the exhaust gas. The energy of the exhaust gas is determined by the sum of the energy of exhaust gas components (H_2O, CO_2, CO, O_2, NO_x, HC, etc.) at the exhaust gas temperature as follows:

$$E_{ex} = E_{H_2O} + E_{CO_2} + E_{CO} + E_{O_2} + E_{NO_x} + E_{HC} \quad (3.6)$$

Where E_{ex} is the energy of the exhaust gas (kW) and E_{H_2O}, E_{CO_2}, E_{CO}, E_{O_2}, E_{NO_x}, E_{HC} are the energy of the exhaust gas components (H_2O, CO_2, CO, O_2, NO_x, HC) (kW).

The energy of an exhaust gas component can be written function of the mass flow rate and the enthalpy of the exhaust gas component as follows:

$$E_{com} = m_{com} h_{com} \quad (3.7)$$

Where E_{com} is the energy of the exhaust gas component (H_2O, CO_2, CO, O_2, NO_x, HC) (kW), h_{com} is the enthalpy of the exhaust gas component (kJ/kg) and m_{com} is the mass flow rate of the exhaust gas component (kg/s). The mass flow rate of a component can be calculated with Eq. (3.8).

$$m_{com} = r_{com} . m_{ex} \quad (3.8)$$

Where r_{com} is the mass percentage of the component in the exhaust gas (%) and m_{ex} is the mass flow rate of the exhaust gas (kg/s). The mass flow rate of the exhaust gas is

defined as the sum of the mass flow rate of the fuel, m_{fuel} (kg/s), and the air, m_{air}(kg/s), at the inlet of IC engine as follows:

$$m_{ex} = m_{fuel} + m_{air} \quad (3.9)$$

Besides the engine power and the energy lost in the exhaust gas, the other energy losses of IC engine, E_{other} (kW), including energy losses in the combustion, transmission, noise, cooling systems, etc. is determined as follows:

$$E_{other} = E_{total} - P - E_{ex} \quad (3.10)$$

Where P is the engine power (kW).

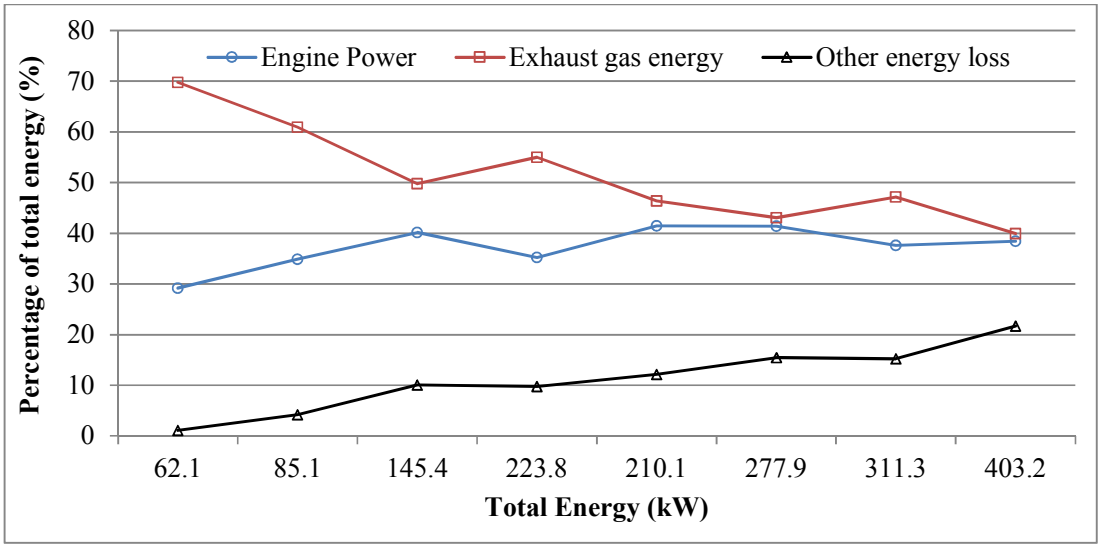

Figure 3.3 *Energy distribution varied with of the engine load*

Based on the experimental data and Equations 3.5, 3.6, 3.10, the energy distribution varied with the engine load of the diesel engine is calculated and shown in Figure 3.3 [95]. As shown in Figure 3.3, in the D1146TI diesel engine, the heat energy lost by the exhaust gas was higher than 40% of total energy, especially in some operation conditions,

this energy lost could be up to 70%. The aim of this research is to store and reuse as much as possible the wasted exhaust gas energy for heating purposes of the vehicle.

3.3 Reactor design

As mentioned in 3.1, to store the wasted heat energy of the exhaust gas, a reactor containing EM8block is connected with the exhaust gas manifold of the D1146TI diesel engine. The main requirements of the CHS using EM8block were defined as follows:

- It was small enough to be located in the vehicle.
- It could store enough EM8block for one hour at the full engine load.
- The maximum service temperature of the material chosen to fabricate the reactor must be greater than the temperature of exhaust gas of the engine.

The maximum exhaust gas temperature of the diesel engine in the current study was 850 K. Based on the maximum temperature of the exhaust gas of the diesel engine, the material chosen to fabric the reactor was the steel grade 153MA^{TM}with the maximum service temperature of 1273 K. It can be seen that the maximum service temperature of the steel is not only higher than the temperature of the exhaust gas of the diesel engine but also that of gasoline engines. The maximum temperature of the exhaust gas of the Toyota Aurion gasoline engine at UTS laboratory was 1078 K and 1113 K for the gasoline engine in Tianyou experiments [96]. Therefore, the CHS system in the current study could be extended to apply in gasoline engines in the future. The main properties of steel grade 153MA^{TM} [97]are shown in Table 3.2.

Table 3.2 *153MA^{TM} steel properties*

Properties	**Unit**	**Value**
Maximum service temperature	K	1273
Mass density	g/cm^3	7.8
Thermal conductivity	W/m.K	25.5
Heat capacity	J/kg.K	500

To design the reactor of CHS system, some assumptions were raised as follows:

- Ignore the heat loss in the connection piper between the exhaust manifold of the IC engine and the reactor: the properties of the exhaust gas at the reactor inlet are the properties of the exhaust gas at the exhaust manifold of the IC engine.
- Ignore the heat loss from the reactor to ambient: it means the energy change of the exhaust gas in the reactor is the absorbed energy of the reactor.
- Ignore the gap contact between the inside wall of the reactor and EM8block. EM8block was made in a mold before putting in the reactor, so in fact, there is some small gap contact between the reactor and EM8block. This gap was filled by the EM8 powder in the experiment.

Based on the requirements of the reactor and the volume of EM8block, the reactor was designed as a shell and tube heat exchanger using the reactor design process as shown in Figure 3.4. Based on the temperature of exhaust gas at the reactor inlet (T_1) and the hypothetical temperature at the reactor outlet (T_2), the heat energy of the exhaust gas at the inlet and outlet of the reactor could be defined by Equation 3.6. By ignoring the heat loss from the reactor to the ambient, the captured energy of the reactor ($Q_{captured}$, kJ) is

the energy change of the exhaust gas between outlet and inlet of the reactor.

$$Q_{captured} = (E_{ex,in} - E_{ex,out}).t \quad (3.11)$$

Where $E_{\mathrm{ex,in}}$ and $E_{\mathrm{ex,out}}$ are the energy of exhaust gas at the inlet and outlet of the reactor presenting by Equation 3.6 (kW) and t is the time (s).

The captured energy of the reactor will be used to increased the temperature of the reactor (Q_{r}), EM8block (Q_{Em8block}), from the ambient temperature to the reaction temperature of the reactant and stored in the dehydration reaction of EM8block (Q_{absorbed}). The energy for heating the reactor can be calculated using the Eq. (3.12).

$$Q_r = m_r C_r (T_r - T_{amb}) \quad (3.12)$$

The energy for heating EM8block can be estimated as follow.

$$Q_{EM8block} = m_{EM8block} C_{EM8block} (T_r - T_{amb}) \quad (3.13)$$

Where m_{r}, m_{EM8block} are the mass of the reactor and EM8block (kg); C_{r}, C_{Em8block} are the specific heat of the reactor and EM8block (kJ/kg.K); T_{r}, T_{amb} are the reaction temperature of EM8block and the ambient temperature.

The stored energy in the CHS system could be estimated using Eq. (3.14).

$$Q_{absorbed} = 81 \frac{r_{mix} m_{EM8block}}{M_{Mg(OH)_2}} 1000 \quad (3.14)$$

Where 81 kJ/mol is the reaction enthalpy of $Mg(OH)_2$, r_{mix} is the mass mixing ratio of EM8block (8/9).

The mass of EM8block stored inside the reactor could be found from Equations 3.11,

3.12, 3.13 and 3.14. The volume of EM8block inside the reactor can be written function of the mass,$m_{EM8block}$, and the density,$\rho_{EM8block}$, of EM8block as follows:

$$V_{Em8block} = \frac{m_{Em8block}}{\rho_{EM8block}} \quad (3.15)$$

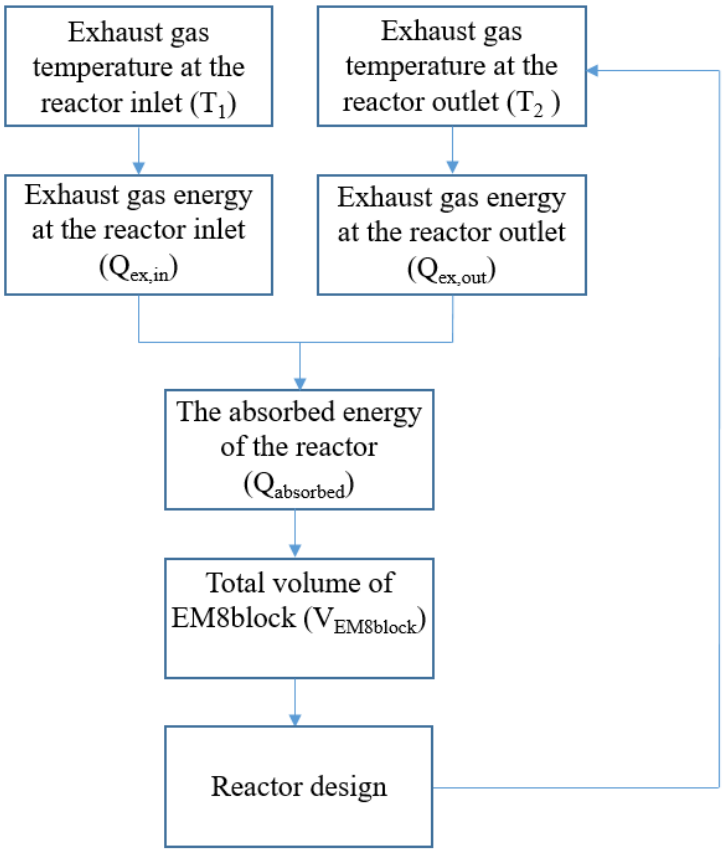

Figure 3.4 *Reactor design process*

From the volume of EM8block inside the reactor, the design of the reactor based on the shell and tube heat exchanger was proposed. After that, the temperature of the exhaust gas at the reactor outlet (T_2) was checked and adjusted based on the reactor design and used as the input temperature of the next loop as shown in Figure 3.4. The design process ended when the temperature difference of exhaust gas at the outlet of the reactor at the

input and output of the loop was smaller than 5%. The structure of the reactor is shown in Figure 3.5 and the parameters of the reactor of the CHS system are shown in Table 3.3.

As shown in Figure 3.5, the reactor consists of one shell and one tube. EM8block is stored inside the tube, and the exhaust gas flows in the space between the shell and the tube. EM8block was filled up to a height of 460 mm when the total mass of the material is 24.46 kg with the volume 0.0244 m^3.

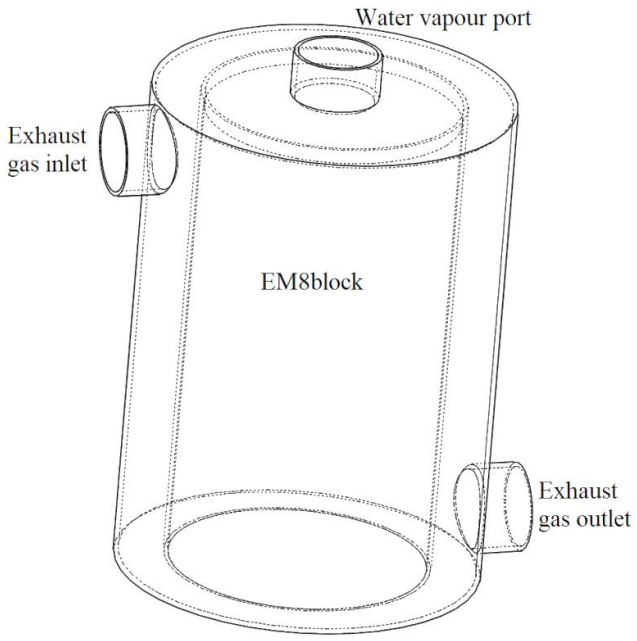

Figure 3.5 *Reactor design*

In the heat storage process, the exhaust gas flows into the reactor at the exhaust gas inlet and out at the exhaust gas outlet port, while heat energy is transferred from the exhaust gas to EM8block through the reactor wall. The dehydration reaction occurs inside the tube of the reactor when the temperature of EM8block reaches the reaction temperature of 280^0C. Water vapour from the dehydration reaction of $Mg(OH)_2$ flows from the reactor to the water tank at the water vapour port on the top of the reactor. After the heat storage

process, the solid product is stored inside the tube and the water vapour is condensed and retained inside the water tank.

Table 3.3 *Reactor parameters*

Parameter	**Internal diameter (mm)**	**Thickness (mm)**	**Length (mm)**
Tube	260	6.5	500
Shell	360	6.5	500
Exhaust gas inlet	88.9	3.05	
Exhaust gas outlet	88.9	3.05	
Vapour port	88.9	3.05	

In the heat output process, the water liquid in the water tank is heated by an electrical resistor and evaporates. The water vapour, after that, flows from the water tank to the tube of the reactor through the water vapour port and reacts with the solid product in the reactor. The hydration reaction between the solid product and water vapour occurs inside the tube and heat energy is released. The heat energy releasing from the hydration reaction in the reactor is then transferred to the engine intake air.

Chapter Four

4 Experimental and Numerical Methods

4.1 Experimental methods

4.1.1 Preparation of EM8block

As discussed in section 2, EM8block is the compound of $Mg(OH)_2$ and EG in the mass mixing ratio of 8:1 and in the block state. The EG was made by graphite flakes before mixing with $Mg(OH)_2$ at School of Chemical Engineering (SCE), Hanoi University of Science and Technology, Vietnam as follows:

- Pure $Mg(OH)_2$ was crushed to the average particle size smaller than 150 μm.
- $Mg(OH)_2$ was mixed with EG in the mass mixing ratio 8:1 and purified water was added. A spatula was used to mix the compound gently.
- The compound was placed in the furnace for 15 minutes at 120^0C.
- The compound was remixed before replacing in the drier for 15 minutes. This step was repeated to ensure that $Mg(OH)_2$ was mixed with EG perfectly.
- The compound was placed in the furnace until it was dry completely.
- The compound was removed from the furnace and crushed to the average particle size smaller than 150 μm.
- The compound was compressed in the mold to get the required parameters of EM8block.

(a) Expanded graphite *(b) Dried compound* *(c) EM8block in the reactor*

***Figure 4.1** Preparation of EM8block*

EM8block, after that, was removed from the mold and stored inside the reactor as shown in Figure 4.1.c. There was a small gap between EM8block and the reactor wall due to EM8block and reactor manufacturing processes. The gap was then filled by the compound powder.

The experiments were conducted in the heat storage and heat output processes. In the heat storage process, exhaust gas energy was stored in EM8block. In the heat output process, the stored energy was used to heat the engine intake air.

4.1.2 Heat storage process

In the heat storage process, the experiment apparatus was set up in the AVL engine test-bed as shown in Figure 4.2. Figure 4.3 shows its schematic diagram. The experiment devices and instruments include a dynamometer, a D1146TI Diesel engine, a fuel balance, a reactor, a water tank, a scale and other instruments used to analyze the exhaust gas and measure temperatures, the pressure difference between the inlet and outlet of the reactor. The reactor was manufactured based on the design in section 3.3. EM8block was made based on the process, as shown in section 4.1.

Figure 4.2 *Experimental apparatus of the heat storage process*

In the heat storage process, as shown in Figure 4.3, the reactor was located after the engine exhaust gas port and connected with the engine by a spring metal pipe. A thermostat was used to measure the exhaust gas temperatures at the inlet of the reactor (T_1). The exhaust gas after going through the reactor was collected by the exhaust gas system of the laboratory. At the outlet of the reactor, another thermostat was used to determine the temperature of the exhaust gas at this point (T_2). When the exhaust gas moved into the reactor, EM8block next to the reactor inlet was the hottest area. A thermostat was installed to measure the temperature of this area of EM8block (T_3). T_3 was used to recognize the

processes of the heat storage process inside the reactor. The pressure difference of the exhaust gas between the inlet and outlet of the reactor was recorded by a manometer. The water vapour from the dehydration reaction of EM8block inside the tube of the reactor flowed out at the water vapour port of the reactor and condensed in the water tank. It made the weight of water in the water tank changed. The weight of water in the water tank was measured by an electrical balance. All experimental data, including T_1, T_2, T_3, pressure difference, the weight of water in the water tank and operation data of the engine were recorded by the data acquisition system.

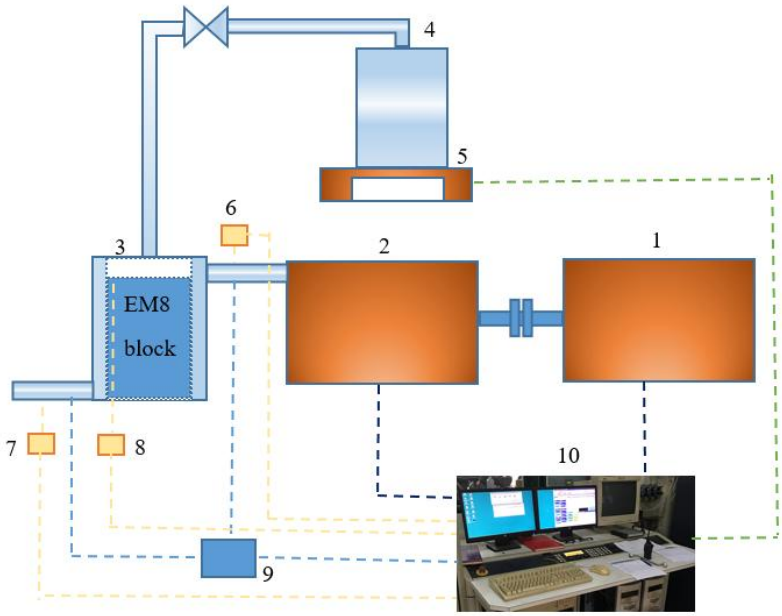

1. Dynamometer 2. Engine 3. Reactor 4. Water tank 5. Electrical balance 6, 7, 8 thermostats using to measure T_1, T_2, T_3 9. Manometer 10. Data acquisition

Figure 4.3 *Schematic diagram of the experimental apparatus of the heat storage process*

In the heat storage process, the experiments were conducted at 60%, 70%, and 80%

engine loads. At an engine load, the experiments took place in around 60 minutes, and the data was recorded every 2 minutes. Because of the moisture content of EM8block (from uncompleted drying process on EM8block built process and the environment), each experiment was performed in four stages as follows:

- Stage 1: The reactor received heat energy from the exhaust gas to increase the temperatures of the reactor and EM8block. The temperature of EM8block (T_3) increased from the ambient temperature to around 80^0C-90^0C. In this stage, the heat energy of the exhaust gas was used for heating the reactor and EM8block.
- Stage 2: The temperature inside EM8block was not uniform due to the heat transfer inside the reactor. The highest temperature of EM8block was at the outer layers and next to the reactor inlet. At other areas of EM8block, the temperature was smaller. At T_3 was 80-90^0C, the temperature of some hottest areas of EM8block reached to the saturation temperature of the water, 100^0C, and the moisture containing insideEM8block evaporated. This stage finished when the temperature ofEM8block, T_3, was around 110-120^0C. At this temperature, the temperature of all area inside EM8block was higher than the saturation temperature of the water and all moisture containing inside EM8block evaporated. The water vapour releasing from EM8block flowed to the water tank, and it made the weight of the water in the tank increased. In this stage, the heat energy of the exhaust gas was used not only for heating the EM8block and the reactor but also for evaporating the moisture inside EM8block.
- Stage 3: After all moisture evaporated and condensed in the water tank, the weight of the water in the water tank was constant. In this stage, when the exhaust gas continuously flowed in the reactor, the heat energy of exhaust gas was used for

heating the reactor and EM8block. This stage finished when T_3 reached around 250-280^{0}C (the reaction temperature of $Mg(OH)_2$).

- Stage 4: When the temperature, T_3, was in the range of 250^{0}C to 280^{0}C, the temperature of the hottest areas inside EM8block reached to the reaction temperature of $Mg(OH)_2$. At this temperature, the dehydration reaction of $Mg(OH)_2$ began inside EM8block. In this stage, the gas product of the dehydration reaction of $Mg(OH)_2$, the water vapour, moved out of the reactor and condensed in the water tank. The weight of the water in the water tank increased quickly. The heat energy of the exhaust gas in this stage was used for both heating EM8block, the reactor and storing in the dehydration reaction of $Mg(OH)_2$.

After the heat storage process, two products of the dehydration reaction were stored separately. The solid product ($EM8block_p$) was stored in the reactor and the gas product (water vapour) was condensed, and stored in the water tank.

4.1.3 Heat output process

In the heat output process, the stored energy was used to heat the engine intake air. The schematic diagram of the experimental apparatus of the heat output process is shown in Figure 4.4.

As shown in Figure 4.4, the reactor was connected with the water tank in the heat output process to heat the intake air supported by a small fan at the reactor inlet. After the heat storage process, the water was condensed and stored inside the water tank. In the heat output process, the water liquid in the water tank was heated by an electrical resistor to evaporate and flow into the reactor. The electrical energy was supported to keep the temperature of the water inside the water tank was 100^{0}C, and the evaporation occurred

continuously. Because of the evaporating of water in the water tank, the weight of the water tank decreased and it was measured by the electrical balance.

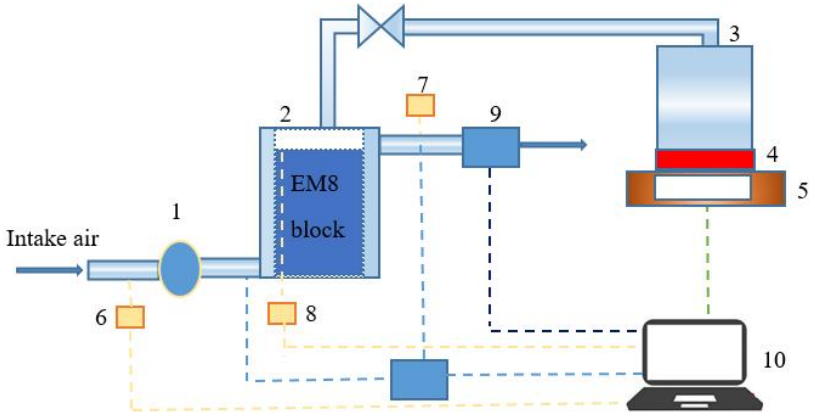

1. Fan 2. Reactor 3. Water tank 4. Electrical resister 5. Electrical balance 6, 7, 8. thermostats using to measure T_4, T_5, T_6 9.Velocity meter 10. Computer

Figure 4.4 *Schematic diagram of the experimental apparatus of the heat output process*

The solid product of the dehydration reaction ($EM8block_p$) storing inside the reactor reacted with the water vapour from the water tank in the hydration reaction to become the initial form, EM8block, and heat energy was released as shown in Equation 3.4. The releasing heat energy from the hydration reaction inside the reactor was used to heatEM8block and the reactor wall. Inside the reactor, the intake air absorbed heat energy from the reactor wall through heat convection process and flowed out at the reactor outlet. The engine intake air temperatures at the reactor inlet and outlet (T_4, T_5) and the wall temperature of the tube of the reactor (T_6) were recorded by three thermostats. The thermostat for measuring the temperature T_6 was located in the middle of the tube of the reactor. At the reactor outlet, a velocity meter was located to determine the velocity of

the heated air. The pressure difference of the engine intake air at the inlet and outlet of the reactor was recorded by a manometer.

In the air heating process, the heat energy from the hydration reaction of MgO and water vapour was used to heat EM8block and the reactor wall. It made the temperature of the reactor wall (T_6) increased over time. Each experiment in the air heating process was performed in two stages.

- Stage 1: The water vapour evaporating from the water tank flowed into and reacted with EM8block$_p$inside the reactor. The heat energy of the hydration reaction in this stage was used for heatingEM8block and the reactor wall and it made their temperatures increased.
- Stage 2: The hydration occurred inside the reactor continuously. In this process, the engine intake air supported by a fan flowed in the reactor at the reactor inlet. The intake air, after that, absorbed heat energy from the reactor wall, and its temperature increased. The heat energy of the hydration reaction in this stage was used not only for heating EM8block and the reactor but also for heating the engine intake air.

4.2 Numerical methods

To investigate the CHS system in engine conditions more than that in experiments, a CFD model of the CHS system was developed using the commercial code of ANSYS FLUENT as a platform. The model was verified by comparing the simulation results with the experimental ones. The verified model was then used to test the CHS system, which was further improved from the one used in the experiments.

4.2.1 Computational mesh

Based on the assumption of the symmetry of the CHS system, half of the reactor was simulated to minimize the simulation time. Figure 4.5 shows the computational mesh generated on the half of the reactor that includes the chemical material, EM8block, storing inside the tube of the reactor.

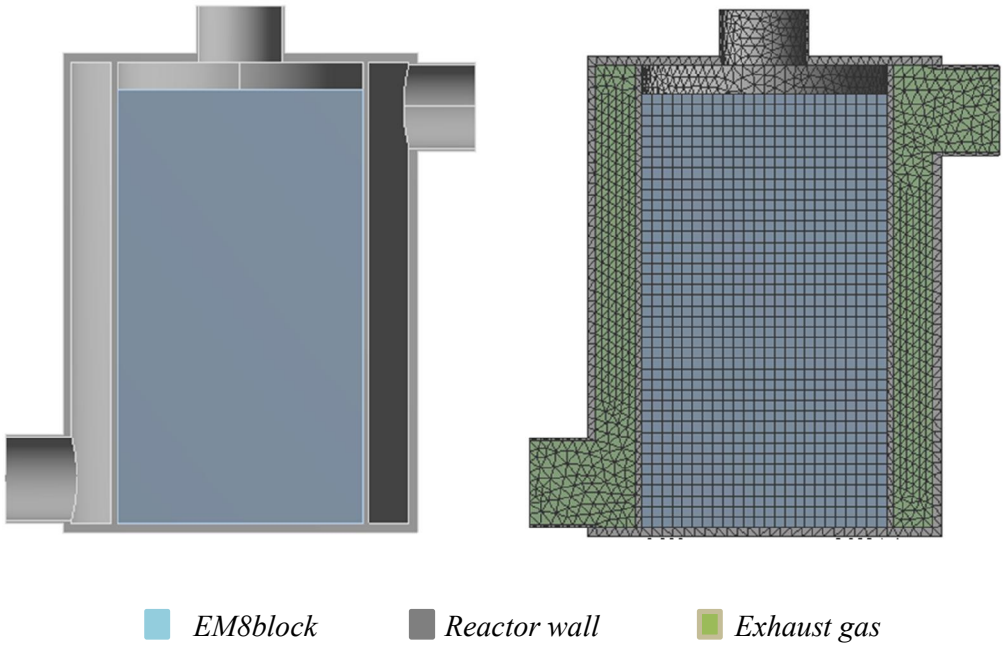

Figure 4.5 *Geometry and mesh structures of the reactor, EM8block and the exhaust gas*

The mesh of the reactor mainly consists of the tetrahedral grid. The computational mesh includes the reactor, EM8block, and the fluid body of the exhaust gas are shown in Figure 4.5.

The normal angle is the maximum allowable angle that one element edge is allowed to span. To make sure that the size of one element will not violate the size or the normal angle, the curvature size function was chosen to control the size computation. In the

computational mesh, the relevance center was fine, and the curvature size function on all edge and face zones was 18. The mesh with 101130 nodes was created with skewness was 0.2386, and the orthogonal quality was 0.77.

4.2.2 Heat transfer model

The inlet data of the heat storage model was the exhaust gas parameters. In the experiment, the exhaust gas velocity at the reactor inlet at all engine load was higher than 30 m/s, and the Reynolds number (Re) was higher than critical Reynolds number of the flow in a circular pipe (2000 → 3000), so the flow was turbulent in the reactor.

Standard two-equation turbulence models are often fail to predict the onset and the amount of flow separation under adverse pressure gradient conditions. To avoid this problem, the k-ω SST Model was used for the simulation. The SST model, as mentioned in section 2.4, is a hybrid two-equation model that combines the advantages of both k-ε and k-ω models. The k- ω model performs much better than k-ε models for boundary layer flows. In the SST model, the k- ω is applied for the area close to the wall and the k-ε model for the area in the freestream. It can give highly accurate predictions of the onset and the amount of flow separation under adverse pressure gradients by the inclusion of transport effects into the formulation of the eddy-viscosity.

In the heat storage model, the heat transfer process inside the reactor includes the heat transfer by convection and radiation from the exhaust gas to the reactor wall, conduction through the reactor wall and conduction in EM8block. The heat transfer by heat radiation and convection, $Q_{ex,i,j}$ (kW), between the exhaust gas and the reactor wall is mathematical described by Eq. (4.1).

$$Q_{ex,i,j} = \alpha_{ex,i,j}\left(T_{ex,i,j} - T_{w,i,j}\right)A_{i,j} + \epsilon\,\sigma\left(T_{ex,i,j}^4 - T_{w,i,j}^4\right)A_{i,j} \quad (4.1)$$

Where $A_{i,j}$is the contact area between the node i,j and the exhaust gas (m^2), $T_{w,i,j}$is the temperature of the reactor wall at the node i, j(K), $T_{ex,i,j}$ is the log mean temperature of the exhaust gas next to the node i,j (K) and $\alpha_{ex,i,j}$ is the convection heat transfer coefficient of the exhaust gas at the node i, j ($W/m^2.K$).The convection heat transfer coefficient of the exhaust gas could be found from the Nusselt number as follows:

$$\alpha_{ex,i,j} = \frac{\lambda_{ex}.\mathrm{Nu}}{\mathrm{l}} \quad (4.2)$$

Where λ_{ex} is the thermal conductivity of the exhaust gas (W/m.K), Nu is the Nusselt number and l is the characteristic dimension of the node (m). The Nusselt number of the turbulence heat transfer of exhaust gas could be estimated using Eq. (4.3).

$$Nu = 0.018\,Re^{0.8}Pr^{0.2} \quad (4.3)$$

Where Re, Pr are the Reynolds and Prandtl numbers.

To investigate the heat conduction process between the solid material inside a reactor, a 3D model was suggested by Zamengo in [36] as shown in Figure 4.6.

The reactor wall and EM8block are solid materials, so the heat transfer process are assumed as the heat conduction. Based on the model in [36],the heat conduction inside the reactor wall and EM8block in stages 1, 2 and 3 before the chemical reaction is shown by Eq. (4.4).

$$\frac{\lambda_{r\,i,j}A_{r\,out\,i,j}}{\Delta r}\left(T_{i,j+1}-T_{i,j}\right)+\frac{\lambda_{r\,i,j}A_{r\,in\,i,j}}{\Delta r}\left(T_{i,j-1}-T_{i,j}\right)+\frac{\lambda_{r\,i,j}A_{r\,top\,i,j}}{\Delta z}\left(T_{i-1,j}-T_{i,j}\right)+$$

$$\frac{\lambda_{r\,i,j}A_{r\,bottom\,i,j}}{\Delta z}\left(T_{i+1,j}-T_{i,j}\right)=\frac{\rho_{r\,i,j}\cdot c_{r\,i,j}}{\Delta\tau}V_{r\,i,j}\left(T_{r\,i,j\,\tau+\Delta\tau}-T_{r\,i,j\,\tau}\right) \quad (4.4)$$

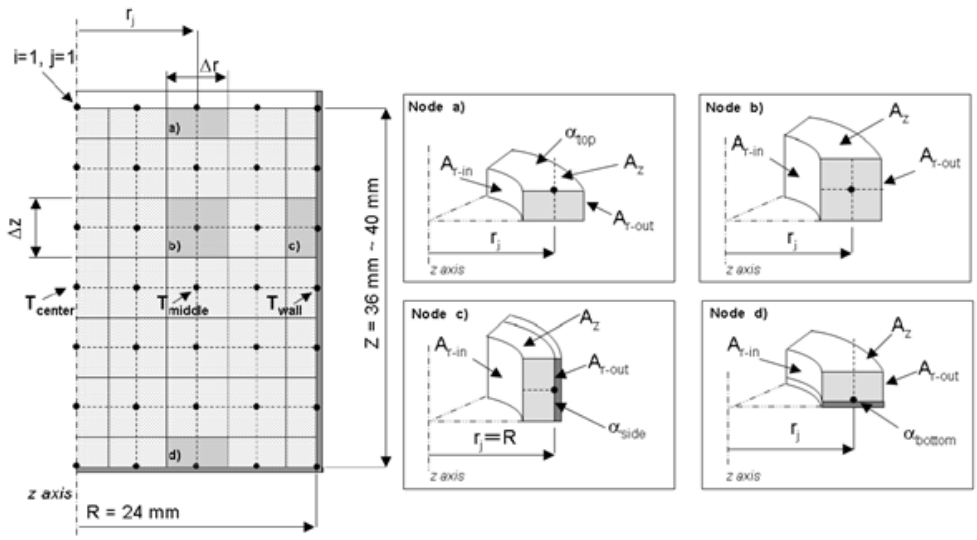

Figure 4.6 *Model of packed bed reactor: (a) the nodes on the top, (b) the nodes inside, (c) the nodes next to the side walls and (d) the nodes next to the bottom of the reactor*

When the temperature of a node is higher than the reaction temperature, the dehydration reaction occurred at the node. At this step, the node is assumed as a heat source, and it will absorb heat energy $Q_{a,i,j}$ (kJ) as follows:

$$\frac{\lambda_{r\,i,j}A_{r\,out\,i,j}}{\Delta r}\left(T_{i,j+1}-T_{i,j}\right)+\frac{\lambda_{r\,i,j}A_{r\,in\,i,j}}{\Delta r}\left(T_{i,j-1}-T_{i,j}\right)+\frac{\lambda_{r\,i,j}A_{r\,top\,i,j}}{\Delta z}\left(T_{i-1,j}-T_{i,j}\right)+$$

$$\frac{\lambda_{r\,i,j}A_{r\,bottom\,i,j}}{\Delta z}\left(T_{i+1,j}-T_{i,j}\right)=\frac{\rho_{r\,i,j}\cdot c_{r\,i,j}}{\Delta\tau}V_{r\,i,j}\left(T_{r\,i,j\,\tau+\Delta\tau}-T_{r\,i,j\,\tau}\right)+Q_{d,i,j} \quad (4.5)$$

Where λ_r is the thermal conductivity (W/m.K), A_r is the contact area (m^2), ρ_r is the density, V_r is the volume, c_r is the specific heat of the reactor wall or EM8block at the node i, j. $T_{i,j}$, $T_{i,j+1}$, $T_{i,j-1}$, $T_{i-1,j}$, $T_{i+1,j}$ are the temperature of the node i, j and next

nodes. $T_{r\,i,j\,\tau}$ and $T_{r\,i,j\,\tau+\Delta\tau}$ are the temperature of the node i, j at time τ and $\tau+\Delta\tau$. $Q_{d,i,j}$ is the dehydration reaction energy in the node i, j when the reaction occurs.

The dehydration reaction energy is described by the function of the mass of the node, $m_{i,j}$, and the enthalpy of the dehydration reaction (81 kJ/mol) as follows:

$$\mathrm{Q_{d,i,j}} = 81 r_{mi}\, x \frac{\mathrm{m_{i,j}}}{\mathrm{M_{Mg(OH)_2}}} 1000 \qquad (4.6)$$

The amount of the reacted EM8block after the heat storage in the simulation model is determined by the amount of EM8block with the temperature is higher than the reaction temperature of $Mg(OH)_2$. Therefore, the percentage of the reacted EM8block in the simulation could be found from the history of the temperature of EM8block.

In the heat output process, the stored energy was used to heat the intake air. The heat energy of the hydration reaction was used as a heat source for heating EM8block, the reactor, and the intake air. The heat source releasing from the hydration reaction, Q_h, is the enthalpy of the reaction, 81 kJ/mol. From the experiments, the heat transfer coefficient of the whole system, k (W/m.K), was found from the absorbed heat energy of the intake air, the average temperature of the intake air in the reactor and temperature of the reactor wall, T_6, as follows:

$$k = \frac{Q_a}{A(T_6 - T_a)} \qquad (4.7)$$

Where A is the outside area of the tube (m^2), Q_a (kW) is the absorbed energy of the intake air after going through the reactor, and T_a is the average temperature of the intake air in the reactor. The outside area, A, could be found from Eq. (4.8) as follows:

$$A = \pi d_t l \quad (4.8)$$

Where d_t is the outside diameter of the tube (m), l is the length of the reactor (m). The absorbed energy, Q_a, could be determined from Eq. (4.9).

$$Q_a = m_a . C_a . (T_5 - T_4) \quad (4.9)$$

Where m_a is the mass flow rate of the intake air (kg/s) and C_a is the specific heat of the air (kJ/kg.K). The average temperature of the intake air, T_a, could be found from T_4 and T_5 as follows:

$$T_a = \frac{T_4 + T_5}{2} \quad (4.10)$$

The heat transfer coefficient finding from the experiments was used in the CFD model to investigate the operation of the CHS system in the engine intake air heating process at other ambient temperatures.

4.2.3 Chemical reaction model

As discussed above, EM8block is the compound of $Mg(OH)_2$, and EG in the mass mixing ratio is 8:1. The operation of the CHS system in the current study is based on the reversible reaction of $Mg(OH)_2$. In the CFD model, the initial reaction is EM8block, and the solid product after the dehydration reaction is denoted as $EM8block_p$. The chemical reaction in the CFD model is presented by Eq. (4.11).

$$EM8block + heat \leftrightarrow EM8block_p + water\ vapour \quad (4.11)$$

To simulate the chemical reaction inside the reactor, the species transport and the reactions model were chosen in ANSYS FLUENT. The chemical reaction model chosen

is the particle model, and the turbulence-chemistry interaction was adopted as a finite-rate model. In the reaction model, the constituent species include EM8block, EM8block$_p$, and water vapour. EM8block and EM8block$_p$ were set as the solid material. Water vapour was in the gas state.

In the heat storage process, the chemical reaction occurs when the temperature of the node inside EM8block reaches the reaction temperature of $Mg(OH)_2$. After the dehydration reaction inside the reactor, EM8block$_p$ is retained in the reactor and water vapour flows out at the vapour port of the reactor.

In the heat output process, as presented in 2.3.2, the hydration reaction of EM8block$_p$ depends on the water vapour pressure. In the simulation, the water vapour pressure chosen is the ambient pressure. The water vapour was set from the database with the temperature at the water vapour port was the saturation temperature of water at the ambient pressure (100^0C). The mass flow rate of the water vapour in the heat output process was that in the experiments. The main parameters of EM8block and EM8block$_p$, were shown in Table 4.1.

Table 4.1 *Main properties of EM8block and EM8block$_p$*

Parameters	**Unit**	**EM8block**	**EM8block$_p$**
Initial density of bed	kg/m^3	1002	1001.446
Activation Energy	kJ/mol	81	81
Thermal conductivity	W/m.K	1.6	1.6
Reaction temperature	K	540	435

In the heat storage process, the reaction temperature of EM8block was set as the reaction temperature of the dehydration reaction, 540K. The reaction took place when the temperature of a node reaches the reaction temperature. At this temperature, EM8block absorbed activation energy to become $EM8block_p$ and water vapour.

In the heat output process, $EM8block_p$ reacted with water vapour to become the initial chemical material, EM8block. The reaction temperature in this process was it of $EM8block_p$, 435 K (162^0C). The mass diffusivity and thermal diffusion coefficient of the reaction were set following kinetic-theory in ANSYS FLUENT [86]. The hydration reaction took place when the water vapour contacted with $EM8block_p$. After the hydration reaction, the activation energy released from the reaction, and the temperature at the node increased to the reaction temperature of 435 K.

4.2.4 Boundary condition

In the heat storage process, the fluid material in the CFD model was set as the exhaust gas. In the CFD model, the heat lost from the exhaust gas manifold of the engine to the reactor was ignored. Therefore, the parameters of the exhaust gas at the reactor inlet was its parameters at the exhaust gas manifold of the engine in the experiment. At an engine load, the parameters of the exhaust gas were variable in 60 minutes of the experiment. The data was recorded every two minutes. In the simulation, the parameters of the exhaust gas were assumed as constant in a time step (two minutes), and they were the average parameters in a time step of the experimental data.

In the experiment, the reactor was well insulated. The heat lost from the reactor to the ambient was small. In the simulation, this heat loss was ignored, and the outside of the reactor was set as the free zone.

As discussed above, in the CFD model, only half of the reactor was simulated to reduce the time and computational cost. Therefore, the symmetry boundary was set for the contact area of the CFD model and the rest of the reactor.

4.2.5 Model verification

To verify the CFD model, the simulation results were compared with the experimental ones in both heat storage and heat output processes.

4.2.5.1 Heat storage process

In the heat storage process, the CFD model was run at 60%, 70% and 80% engine loads. The parameters of the exhaust gas at the reactor inlet was the parameters from the experiment as shown in Table 4.2.

Table 4.2 *Main parameters of the exhaust gas at the reactor inlet at 60%, 70% and 80% engine loads*

Parameter	**Unit**	**60%**	**70%**	**80%**
Fuel flow rate	Kg/h	14.34	17.53	18.66
Air flow rate	Kg/h	424.39	453.49	463.93
Exhaust gas temperature	K	656	720	761
Exhaust gas mass flow rate	Kg/s	0.122	0.131	0.134
Exhaust gas volume flow rate	m^3/s	0.319	0.367	0.391
Inlet area of the reactor	m^2	0.0065	0.0065	0.0065
Exhaust gas velocity	m/s	48.7	55.95	59.59
Reynolds number		21178.4	21759.9	21711.8

It can be seen that the Reynolds number in three engine loads were higher than the critical Reynolds number of the flow in the circular pipe, so the exhaust gas flow was turbulence as predicted.

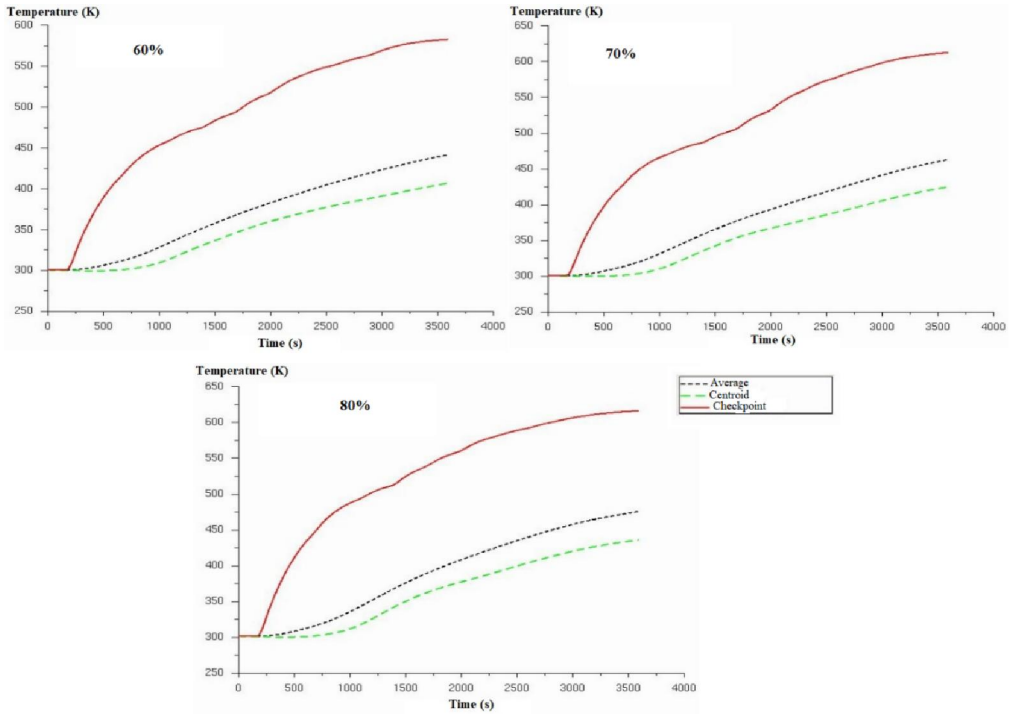

Figure 4.7 *Temperature at the centroid, checkpoint and average temperature of EM8block at 60%, 70% and 80% engine loads*

In the experiment, the temperature of EM8block, T_3, was recorded by a thermostat, and it was used to recognize stages in the heat storage process, as shown in section 4.2. Similar to that, in the CFD simulation, the temperature at the same point (checkpoint) was collected and compare with the experimental temperature. In the CFD simulation, besides the checkpoint temperature, the temperature at the centroid and the average temperature of EM8block were recorded. The CFD model was run in 60 minutes and three temperatures as mentioned above (the checkpoint, the centroid and the average

temperatures of EM8block) at three engine loads are shown in Figure 4.7. It can be seen that the temperature of the checkpoint was highest because it was located in the hottest area of EM8block. At the centroid of the reactor, the temperature was the smallest. At the engine started, the temperature at the centroid did not change. It need time for transferring the heat energy from the outer layers to the centroid of EM8block. After 60 minutes, the temperature profile of the outside surface of EM8bock at other engine loads are shown in Figure 4.8.

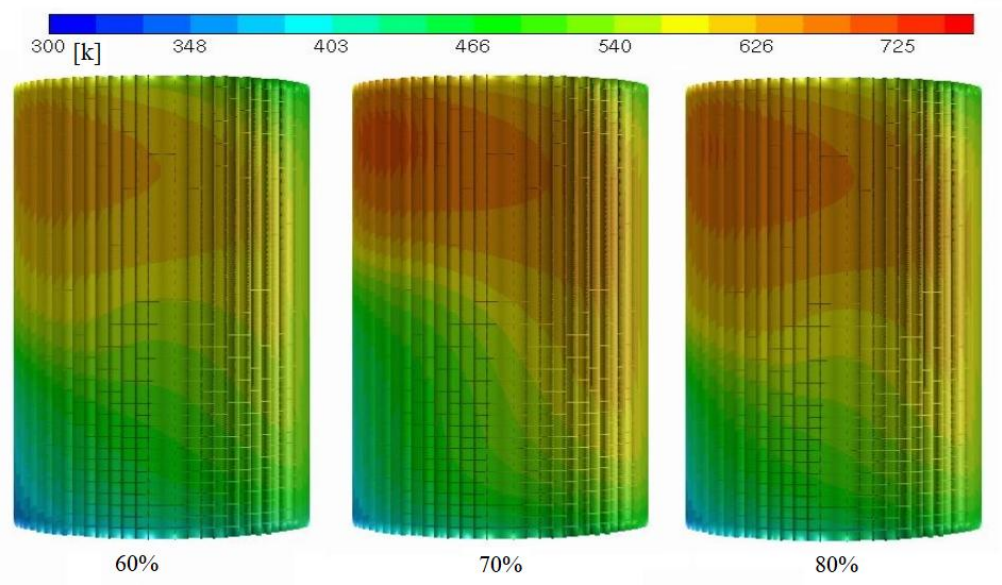

Figure 4.8 *Temperature distribution at the outside surface of EM8block 60 minutes after the engine starts at 60%, 70%, 80% engine loads*

As shown in Figure 4.8, the temperature of EM8block at the bottom and opposite to the reactor outlet is the smallest. The reason is that when the exhaust gas moved from the inlet to the outlet of the reactor, the area at the bottom and below the reactor inlet received the least heat energy from the exhaust gas.

To verify the CFD model, the temperature at the same point of EM8block in the experiment (T_3), and in the simulation (the checkpoint) were compared and the results at three engine loads (60%, 70%, 80%) are shown in Figure 4.9.

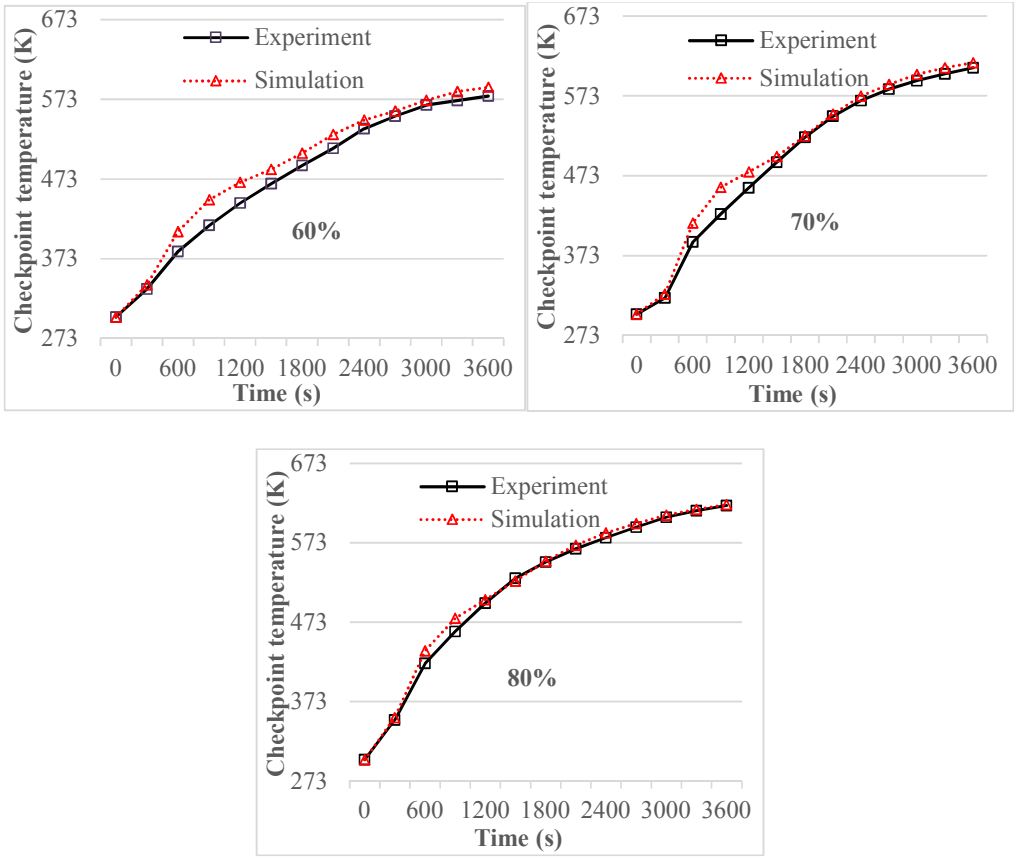

Figure 4.9 *Comparison of experimental and simulation results of the checkpoint temperature at 60%, 70%, 80% engine loads*

As shown in Figure 4.9, the difference between the experimental and simulation results at three engine loads were insignificant. The biggest average difference between simulation and experimental results is 3.34% at 70% engine load. At 80% and 60% engine loads, the difference reduced to 3.1% and 2.78%, respectively. In the experiment, the operation parameters of the engine changed overtime, especially in the engine start up. In

the simulation, based on the experimental data recording every two minutes, the parameters of the exhaust gas were set constant in 2 minutes. It led to the difference between the simulation and experimental results. Furthermore, in the experiment, the CHS system was well insulated, but the heat loss from the CHS system to the environment was inevitable. In the simulation, ignoring the heat loss from the CHS system to the environment led to the temperature of the checkpoint was slightly higher than it in the experiment. Another reason leading to the difference between the experimental and simulation results was the chemical material, EM8block. In the experiment, because EM8block was compressed in the mold before storing inside the reactor, there was a small gap between EM8block and the inside In the CFD model, the gap between EM8block and the inside surface of the tube of the reactor was ignored. The difference in the gap contact between the experiments and simulation could lead to the difference in the temperature of the checkpoint.

The temperature of a node inside EM8block depended on the operation condition of the engine and its position inside EM8block. As discussed in section 2, in the heat storage process, the dehydration reaction occurred when the temperature of a node was higher than the reaction temperature of $Mg(OH)_2$. The percentage of the reacted EM8block was determined by the weight of the reacted EM8block per the initial weight of EM8block. In the experiment, the weight of the reacted EM8lock was determined by the weight of the water condensing in the water tank and based on Equation 3.1. In the simulation model, the percentage of the reacted EM8block was determined by the percentage of EM8block with the temperature higher than the reaction temperature of $Mg(OH)_2$. This percentage at three engine loads could be found from the temperature profile of EM8block 60 minutes after the engine starts, as shown in Figure 4.10.

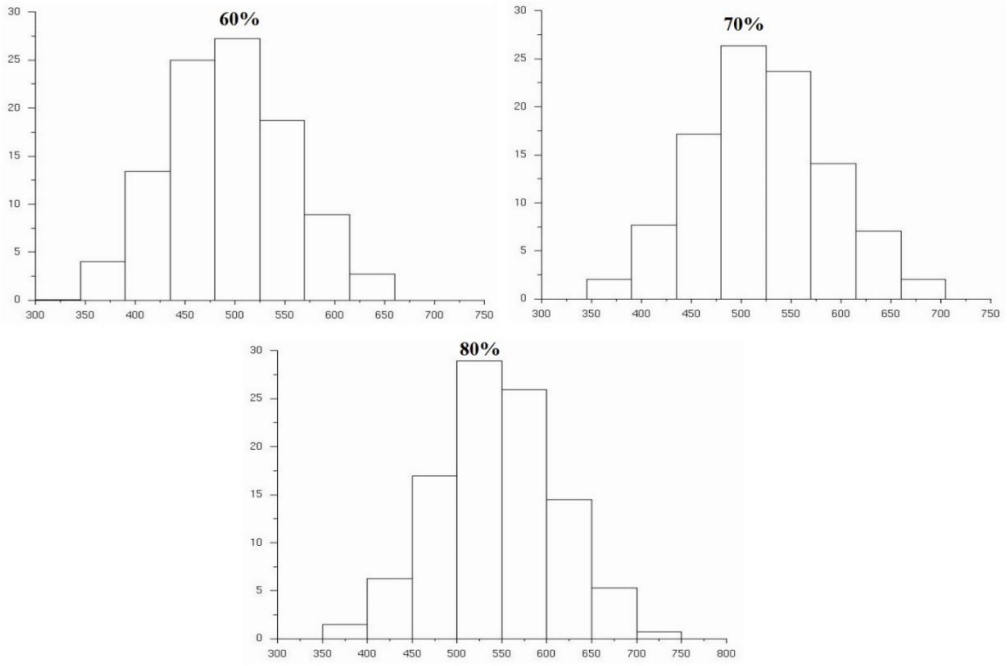

Figure 4.10 *Temperature history of EM8block at 60%, 70% and 80% engine loads*

It can be seen in Figure 4.10, the percentage of EM8block node having the temperature higher than the reaction temperature of $Mg(OH)_2$ at the high engine load (80%) was much higher than at the low load (60%). The reason was the higher exhaust gas temperature at the higher engine load. The difference in the percentage of the reacted EM8block between the experimental and simulation results at three engine loads are shown in Figure 4.11.

It can be seen that the percentage of reacted EM8block in the simulation is higher than in the experiment, however, the difference between experimental and simulation results is insignificant (smaller than 3%). Similar to the temperature of the checkpoint, the difference in the percentage of the reacted EM8block between the experimental and simulation results could be come from the difference in the operation condition, the heat loss from the CHS system to the ambient and the difference in the gap contact between EM8block and the reactor wall. However, as shown in Figure 4.9 and 4.11, the differences

between the simulation and experimental results are insignificant, so the accuracy of the simulation is considered in the heat storage process.

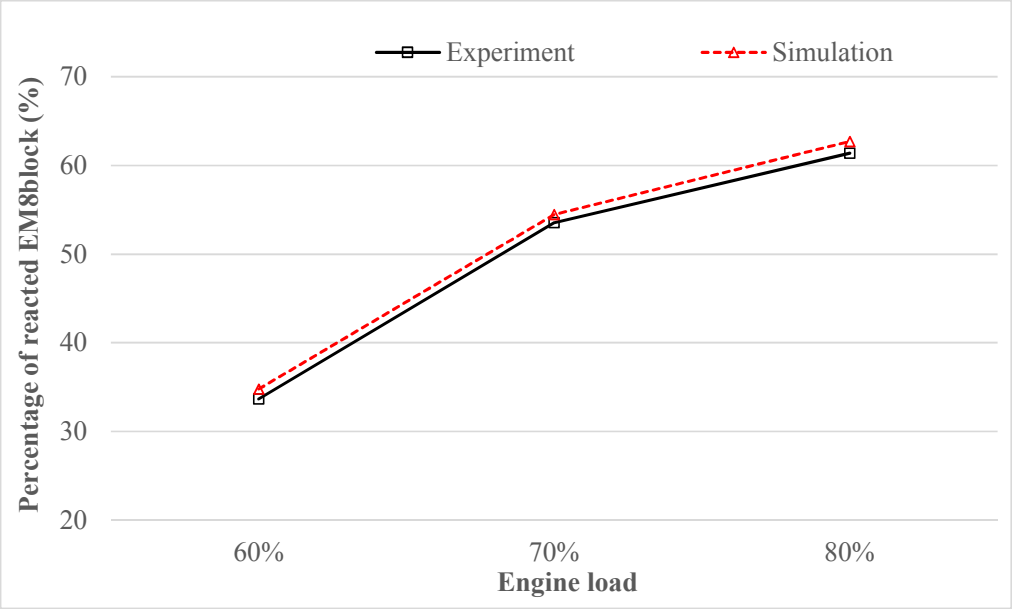

Figure 4.11 *Percentage of reacted EM8block 60 minutes after engine starts at 60%, 70% and 80% engine loads*

4.2.5.2 The heat output process

After the heat storage process, the solid product, $EM8block_p$ was retailed inside the reactor and water was stored in the water tank. In the heat storage in the current study, the stored energy was used to heat the engine intake air. The operation condition of the CHS in the simulation was set based on the experiments and controlled by the mass flow rate of the water vapour moving in the reactor. In the heat output process, the amount of water vapour moving in the reactor was controlled by the electrical resistor and it was measured each two minutes. The parameters in the CFD model are the average ones in the time step (two minutes) of the experimental data.

The temperature of the heated air after going through the reactor depended on the temperature of the reactor wall and the ambient temperature. In the experiments, at the ambient temperature of 23^0C, the temperature of the reactor wall was recorded by a thermostat at the middle of the tube of the reactor. In the CFD model, the checkpoint in the heat output process was set at the same position as the thermostat in the experiment, so that the comparison of the temperature values from experiments and simulation can be used to verify the CFD model. Figure 4.12 shows the comparison of the temperature of the checkpoint in the experiment and simulation at the ambient temperature 23^0C in the heat output process.

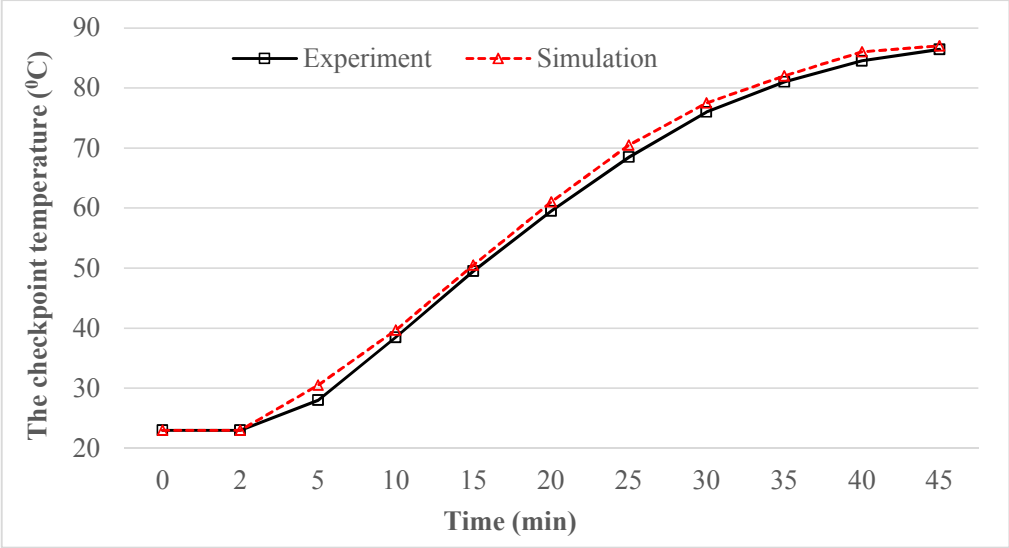

Figure 4.12 *Checkpoint temperature in the experiment and simulation at the ambient temperature of 23^0C*

As shown in Figure 4.12, the difference between the experimental and simulation results is insignificant. The biggest difference between the simulation and experimental results was at 5 minutes (8.9%). The temperature of the checkpoint did not change in the two first minutes because it was the time for evaporating the water liquid inside the reactor

and the heat transfer from the reacted areas inside $EM8block_p$ to the checkpoint. In the heat output process, the hydration reaction took place when the water vapour from the water tank moved into the reactor and reacted with $EM8block_p$ inside the reactor. When the hydration reaction occurred at a node of EM8block, the temperature of the node increased to the reaction temperature of $EM8block_p$, 162^0C. The heat energy after that was transferred to other areas inside $EM8block_p$ and the reactor wall and it made the temperature of the reactor wall increased. Similar to the heat storage process, the difference in the checkpoint temperature between the experimental and simulation results came from the difference between the experimental and simulation conditions, the heat loss from the CHS system to the ambient and the gap contact between $EM8block_p$ and the reactor wall. Moreover, the penetration of water in $EM8block_p$ affected the reaction process inside the reactor in the heat output process.

The temperature of a node inside $EM8block_p$ depends on its positions inside $EM8block_p$. The temperature of the reaction node was higher than other nodes. As shown in Figure 4.13, the temperature at the central and on the top of $EM8block_p$ and opposite with the water vapour port was the highest and decreased towards the lower layer of $EM8block_p$. As discussed above, the hydration reaction occurred when the water vapour reacted with $EM8block_p$ inside the reactor. The water vapour from the water tank moved into the reactor at the vapour port locating on the top of the reactor. Therefore, the hydration reaction of $EM8block_p$ took place firstly in the area located opposite with the vapour port and on the top of $EM8block_p$. After all nodes on the top of $EM8block_p$ reacted, water penetrated and reacted with $EM8block_p$ at the lower areas. The heat energy from the hydration reaction of $EM8block_p$, after that, was transferred to other areas inside $EM8block_p$ and the reactor wall.

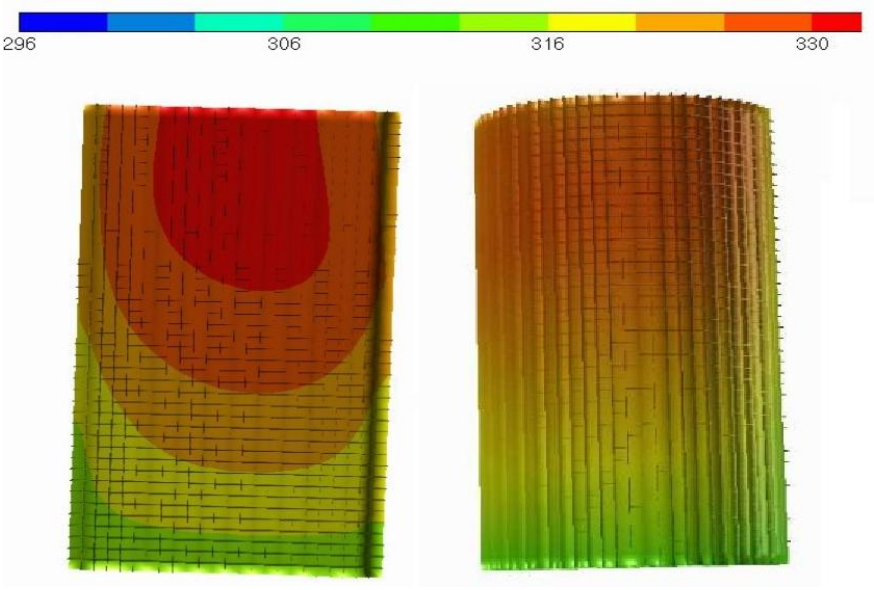

Figure 4.13 *Temperature profile of the surface crossing the centroid and the outside surface of EM8block$_p$ in the heat output process at the ambient temperature of 23^{0}C*

In stage 2 of the heat output process as discussed in 4.1.3, the engine intake air was supported by a fan flowed in the reactor and received heat energy from the reactor wall by convection. The temperature of the intake air increased after going through the reactor. The temperature of the heated air in the experiments and simulation at the ambient temperature of 23^{0}C are shown in Figure 4.14.

Figure 4.14 shows that the difference between the experimental and the simulation result was slightly higher at the higher temperature of the reactor. At the reactor temperature of 41.9^0, the simulation temperature was higher than the experimental one 3.97%. Besides the reasons as mentioned above, at the higher temperature, the heat loss from the reactor to the ambient was higher. It made the difference in the temperature of the heated air in the experiment and simulation was higher.

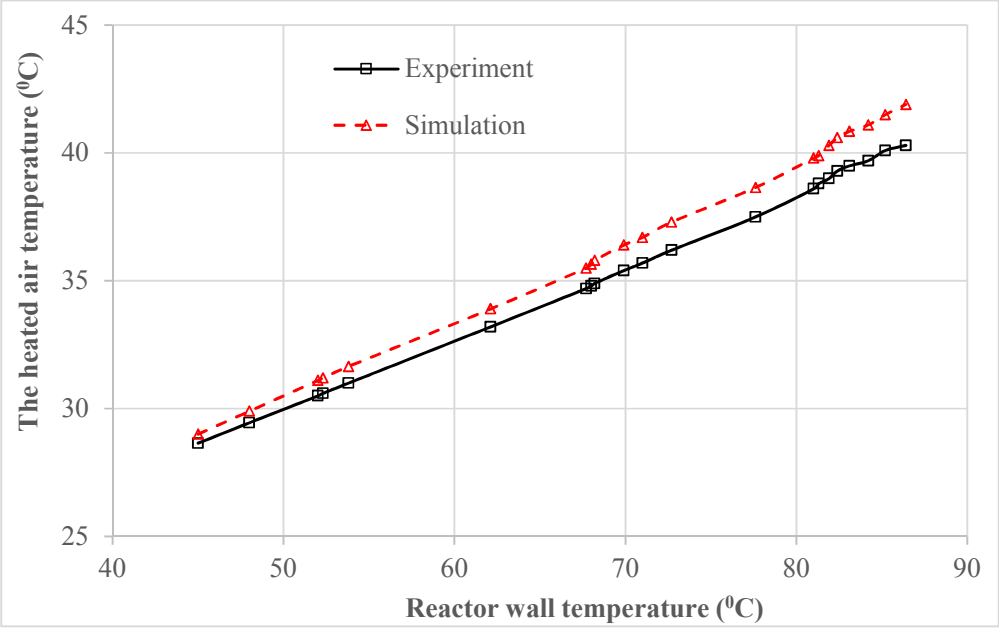

Figure 4.14 *Variation of the heated air temperature with the reactor wall temperature in the experiment and simulation at the ambient temperature of 23^0C*

It can be seen from Figures 4.12 and 4.14, the differences between the experimental and the simulation results are insignificant, so the accuracy of the simulation is considered in heat output process.

4.3 Summary

This chapter presented the experimental and numerical methods. It includes the experiment set up and procedure in the heat storage and heat output processes, and the CFD model code ANSYS FLUENT using to simulate the operation of the CHS system in other operation conditions of the engine and further improved from the one used in the experiments. The major results of this chapter can be concluded as follows:

- The heat storage process occurred in four stages. Stages 1,2,3 were for heating the

reactor, EM8block, and evaporating the moisture inside EM8block (stage 2). The energy of the exhaust gas was stored in stage 4 of the heat storage process.

- The heat output process occurred in two stages. Stage 1 for heating$EM8block_p$ and the reactor. Stage 2 was for heating the engine intake air.
- In the CFD model, half of the reactor was simulated to minimize the simulation time and cost. The simulation model in the heat storage and heat output processes were developed and verified by comparing the simulation results with the experimental results.

Chapter Five

5 CHS in Heat Storage Processes

Experimental and numerical results will be presented and analysed to investigate the performance of the CHS system. The criteria for evaluating the CHS performance will be defined in subsection 5.1, one based on fixed time of 60 minutes and the other on full charge. In 5.2, experimental results will be presented and analysed against the criterion time based to evaluate the performance of the CHS in the heat storage process. CFD simulation results will be reported in 5.3 to further investigate the performance of the CHS system at more engine operation conditions than that in experiments.

5.1 Criteria for evaluating the performance of CHS

In the heat storage process, at an engine load, the performance of the CHS system was evaluated by the percentage of the reacted EM8block, the percentage of the exhaust gas energy stored in the CHS system and the time taken by the heat storage process.

5.1.1 Percentage of reacted EM8block

In the experiment, based on the weight of the condensed water vapour in the water tank, the hydration reaction of $Mg(OH)_2$ and the mass mixing ratio of EM8block, the amount of the reacted EM8block in the heat storage process is calculated as follows:

$$m_{EM8block} = \frac{1}{r_{mix}} M_{Mg(OH)_2} \frac{m_{H_2O}}{M_{H_2O}} \text{(g)} \quad (5.1)$$

Where m_{H_2O} is the weight of the condensed water in the water tank in stage 4 (g), M_{H_2O} is the mole mass of the water (g/mol). From the weight of the reacted EM8block and the total weight of EM8block before the heat storage process, the percentage of the reacted EM8block could be found from Eq. (5.2).

$$r_{EM8block} = 100\frac{m_{EM8block}}{m_{total}} \quad (\%) \tag{5.2}$$

Where m_{total} is the total weight of EM8block (g).

5.1.2 Percentage of stored exhaust gas energy.

In the heat storage process, 81 kJ heat energy will be stored when one mole of $Mg(OH)_2$ inside EM8block reacted, and consequently one mole of water vapour is generated, flows in and condenses in the water tank. In the experiment, the recorded water weight in the water tank will be used to find the stored energy, Q_{stored}(kJ), with Eq. (5.3).

$$Q_{stored} = 81\frac{m_{H_2O}}{M_{H_2O}} \tag{5.3}$$

Where 81 kJ/mol is the reaction enthalpy of $Mg(OH)_2$.

As discussed in 3.3, when the heat loss in the connecting piper between the reactor and the engine was ignored, the parameters of the exhaust gas at the reactor inlet are these at the engine manifold. In the experiments, data were recorded every two minutes (a time step). The parameters of the exhaust gas were assumed as constant in the time step. The total energy of the exhaust gas at the reactor inlet, $Q_{\mathrm{ex,in}}$ (kJ) can be determined as follows:

$$Q_{ex,in} = \sum_0^t E_{ex,in}\, t \tag{5.4}$$

Where t is time taken by the heat storage process (s) and $E_{ex,in}$ (kW) is the exhaust gas energy calculating from Equation 3.6. The percentage of the exhaust gas energy stored in the reactor is calculated from the stored energy and the total exhaust gas energy at the reactor inlet with Eq. (5.5).

$$r_{stored} = 100\frac{Q_{stored}}{Q_{ex,in}}\ (\%) \quad (5.5)$$

5.1.3 Time taken for heat storage process

In the heat storage process, the percentage of the reacted EM8block and stored exhaust gas energy depended on the time taken. The performance of the CHS system in the current study was investigated in two time modes including 60 minutes mode and the full charge mode.

In 60 minutes mode, the engine run in 60 minutes and the criteria for evaluating the performance of CHS includes.

- The percentage of the stored exhaust gas energy.
- The percentage of the reacted EM8block.

In the full charge mode, the engine run until all EM8block inside the reactor reacted. In this mode the performance of CHS is presented by criteria as follows:

- The percentage of the stored exhaust gas energy.
- The full charge time.

5.2 Experimental results

In the experiment, because of the safety requirements, the diesel engine could not run at

the 90% and full engine load in the 60 minutes mode. The experiments of the heat storage process were conducted at 60%, 67% and 80% engine loads in 60 minutes mode. The data was recorded every 2 minutes. From the experimental data, the energy of the exhaust gas at the inlet and outlet were determined based on exhaust gas components, temperature, and Equation 3.6. The captured energy of the reactor ($E_{captured}, kW$) was the energy difference of the exhaust gas between the inlet ($E_{ex,in}$, kW) and outlet ($E_{ex,out}$, kW) of the reactor as shown in Eq. (5.6).

$$E_{captured} = E_{ex,in} - E_{ex,out} \quad (5.6)$$

The percentage of the captured energy, $r_{captured}$, is calculated from the captured energy, $E_{captured}$, and the energy of the exhaust gas at the reactor inlet, $E_{ex,in}$ using Eq. (5.7).

$$r_{captured} = \frac{E_{captured}}{E_{ex,in}} (\%) \quad (5.7)$$

The results were calculated every two minutes (a time step) using the average value of the exhaust gas temperature and components. The exhaust gas energy at the reactor inlet and the percentage of the captured energy at 60%, 70% and 80% engine loads are shown in Figure 5.1.

As shown in Figure 5.1, the exhaust gas energy at the reactor inlet increased with the increase of the engine load. At an engine load, the percentage of the captured energy was the highest after engine start-up and reduce over time. The reason is that at the beginning, the temperature difference between the exhaust gas and the reactor was higher, so the heat transfer process occurred stronger.

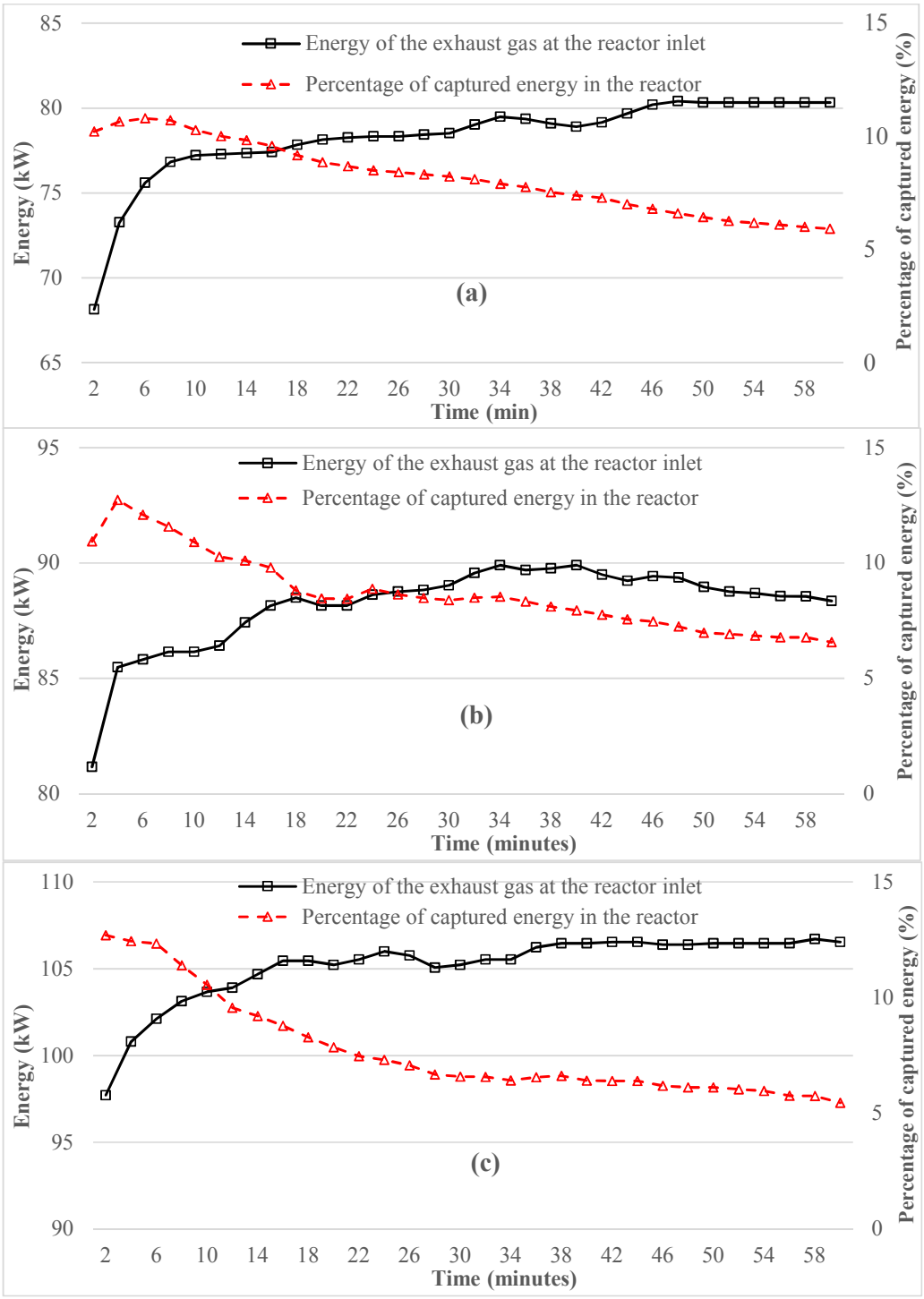

Figure 5.1 *Exhaust gas energy at the reactor inlet and the percentage of captured energy at 60% (a), 70% (b) and 80% (c) engine loads*

In the heat storage process, the captured energy of the reactor could be used for

- heating the reactor to increase the temperature of the reactor (E_{r}).
- heating EM8block inside the reactor to increase EM8block temperature (E_{EM8block}).
- evaporating the moisture inside EM8block (stage 2), energy storage in EM8block (stage 4), other heat losses (connecting pipers, reactor to the environment, etc.) (E_{other}).

Assume that the temperatures of EM8block and the reactor are constant in a time step and they are the average values of the experimental data. Based on the reactor and EM8block temperatures, the heat energy for heating them can be calculated using the Equations 5.8 and 5.9.

$$E_r = \frac{m_r.C_r(T_{r,n+1}-T_{r,n})}{120} \quad (5.8)$$

Where m_{r} is the mass of the reactor (kg), C_{r} is the specific heat of the reactor (kJ/kg.K) and $T_{\mathrm{r,n}}$, $T_{\mathrm{r,n+1}}$ are the average temperatures of the reactor at the time step n and n+1 (K).

$$E_{EM8block} = \frac{m_{total}.C_{EM8block}(T_{EM8block,n+1}-T_{EM8block,n})}{120} \quad (5.9)$$

WhereC_{EM8block} is the specific heat of EM8block (kJ/kg.K),$T_{\mathrm{EM8block,n}}$,$T_{\mathrm{EM8block,n+1}}$ arethe average temperatures of EM8block at the time step n and n+1 (K).

E_{other} (kW), as discussed above, including the energy for evaporating the moisture in stage 2, storing in EM8block in stage 4 and other energy losses could be presented by Eq. (5.10).

$$E_{other} = E_{captured} - E_r - E_{Em8block} \quad (5.10)$$

The distribution of the captured energy at 60%, 70% and 80% engine loads are shown in Figure 5.2.

As shown in Figure 5.2, at 80% engine load, from the engine started to 28th minute is the time for stages 1, 2 and 3 of the heat storage process as discussed in Chapter 4. In this time, the "other energy losses and storage" section, E_{other}, is small compared with the energies for heating the reactor, E_{r}, and EM8block, E_{EM8lock}. After that, the "other heat loss and storage" section increases sharply in stage 4. In this stage, the exhaust gas energy started being stored in the dehydration reaction of EM8block inside the reactor. The energies for heating the reactor and EM8block were smaller in stage 4 because the temperature difference between the exhaust gas and the reactor, EM8block were smaller. The similar processes at 70% and 60% engine loads are shown in Figure 5.2 with the time for stages 1, 2, and 3 is around 34 and 45 minutes, respectively. At the lower engine loads, the time for the heating stages (stages 1, 2, and 3) was longer, so the time left for heat storage stage (stage 4) was shorter in the total time of 60 minutes.

Figure 5.2 *Distribution of the captured energy in the reactor at 60% (a), 70% (b) and 80% (c) engine loads*

Furthermore, as discussed in section 4.1, in stages 2 and 4, water vapour from the evaporating process of the moisture inside EM8block (stage 2) and dehydration reaction of EM8block (stage 4) flowed to the water tank. The water vapour after that condensed inside the water tank, and it made the weight of the water tank increased. Figure 5.3 [98] shows the temporal variation of EM8block temperature (T_3) and the weight of water in the water tank with time in the heat storage process at 60%, 70% and 80 % engine loads.

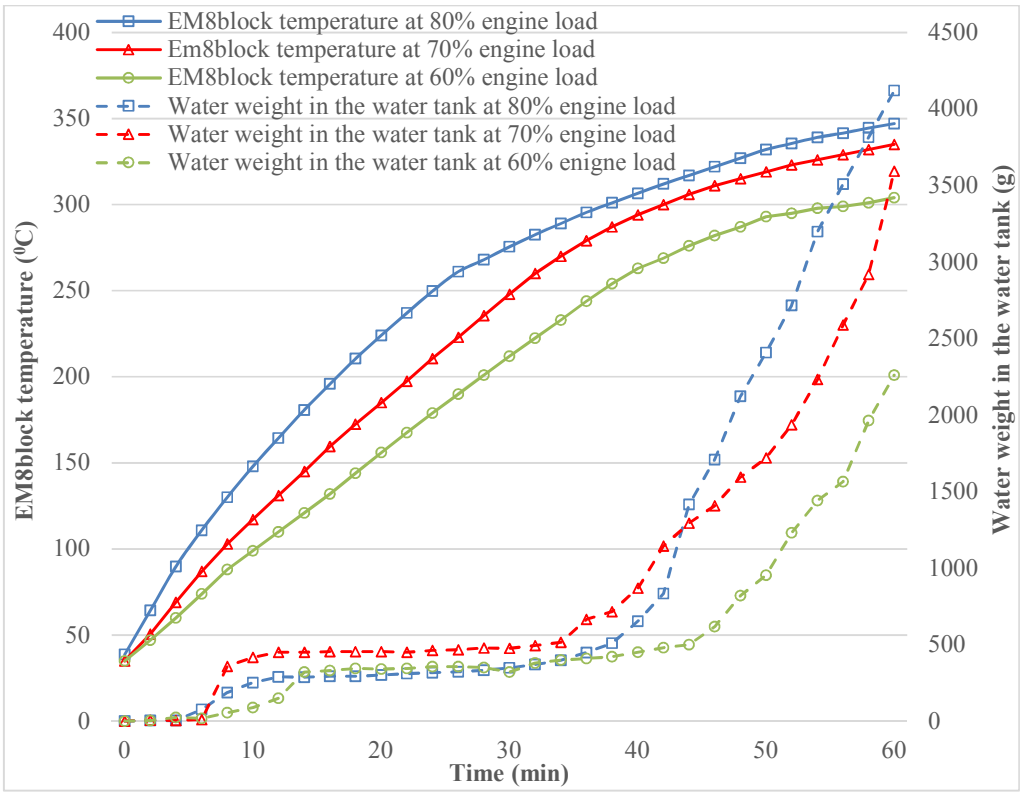

Figure 5.3 *EM8block temperature and the water weight in the water tank in the heat storage process at 60%, 70% and 80% engine loads*

The solid lines in Figure 5.3 show the temporal variation of EM8block temperature (T_3) and dotted lines show the weight of the condensed water accumulated in the water tank. As shown in Figure 5.3, the time for stage 1 as defined in section 4 is 0-4 minutes for

80% engine load, 0-5 minutes for 70% engine load and 0-6 minutes for 60% engine load. In stage 1, the water weight did not change, and the time taken depended on the engine start-up condition.

Stage 2 started when the temperature of EM8block (T_3) reached around 80^0C-90^0C. At this temperature, in the hottest area inside EM8block, the temperature reached to the saturation temperature of the water (100^0C) and the moisture inside EM8block evaporated. As shown in Figure 5.3, it took about 6, 7, and 9 minutes for 80%, 70% and 60% engine loads, respectively. The time for stage 2 depended on the amount of moisture inside EM8block formed in the chemical material built process and the environment. It also depended on the exhaust gas temperature and energy. It increased with the decrease of engine load because the temperature and energy of the exhaust gas reduced with the decrease of the engine load. This stage finished when T_3 reached around 110-120^0C. At this temperature, all moisture inside EM8block evaporated and condensed in the water tank.

In stage 3, EM8block was heated by the exhaust gas continuously from 110 - 120^0C to the reaction temperature of $Mg(OH)_2$, T_3 in a range of 250^0C to 280^0C. As shown in Figure 5.3, the time taken was approximately 18 minutes (from the 10^{th} minute to the 28^{th} minute) at 80% engine load, 22 minutes (from 12^{th} minute to 34^{th} minute) at 70% engine load and 30 minutes (from 15^{th} minute to 45^{th} minute) at 60% engine load. In this stage, when no water vapour was generated, the weight of the water tank was constant.

Stage 4 started when the temperature of EM8block (T_3) reached around 250^0C – 280^0C. At this temperature, the dehydration occurred when the temperature of the hottest area inside EM8block reached the reaction temperature of $Mg(OH)_2$ of 280^0C. In stage 4, the

weight of water in the water tank increased quickly when the water vapour generating from the dehydration reaction of EM8block in the reactor, flowed in and condensed in the water tank.

5.2.1 Percentage of reacted EM8block

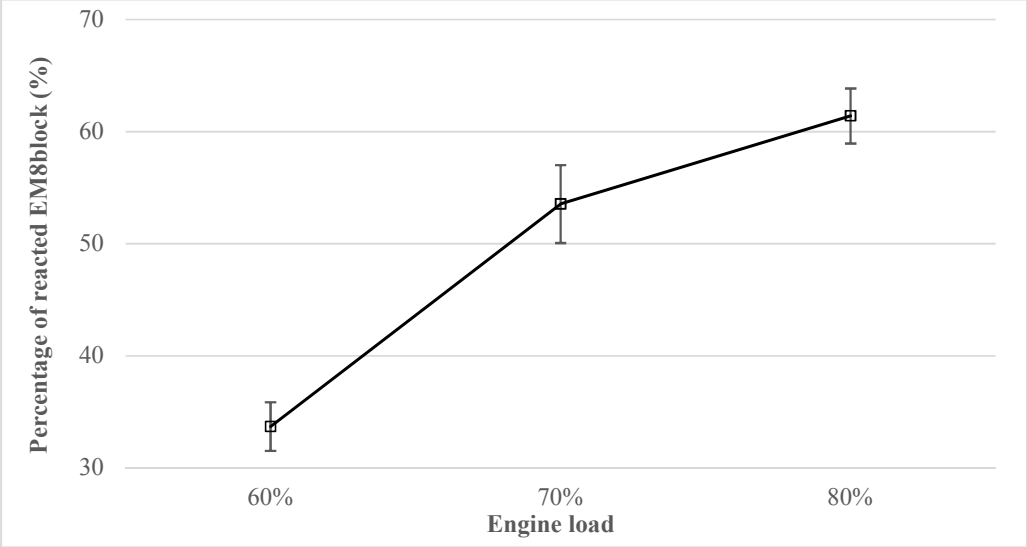

Figure 5.4 *Variation of the percentage of the reacted EM8block and the engine load*

Based on the weight of water in the water tank in stage 4, the percentage of the reacted EM8block were determined based on Equations 5.1 and 5.2. At each engine load, five samples of date were taken to get the average values and the standard deviation such as the ones of the percentage of reacted EM8block shown in Figure 5.4 and that of the percentage of stored exhaust gas energy in Figure 5.5. The main results of the percentage of the reacted EM8block in 60 minutes mode at 60%, 70%, and 80% engine loads are shown in Table 5.1.

Table 5.1 *Percentage of the reacted EM8block*

Parameters	**Unit**	**Engine load**		
		60%	**70%**	**80%**
Weight of water inside the water tank	Kg	2.26	3.59	4.12
Weight of reacted $Mg(OH)_2$	Kg	7.32	11.64	13.35
Weight of reacted EM8block	Kg	8.24	13.12	15.02
Percentage of reacted EM8block	%	33.68	53.54	61.41

As shown in Figure 5.4, at 80% engine load, 60 minutes after engine started, 61.4± 2.5% of EM8block reacted. By taking the same time of 60 minutes, 53.54± 3.4% of EM8block reacted at 70% engine load, and 33.68± 2.2% of EM8block reacted at 60% engine load. In 60 minutes mode, when the engine load increased, the percentage of the reacted EM8block increased. The reason is that at the higher engine load, the exhaust gas temperature was higher so the time taken for the heating stages (stages 1, 2, and 3) were shorter and the time left for the storage stage (stage 4) was longer. The longer time for stage 4 and the higher exhaust gas temperature led to the higher percentage of the reacted EM8block at the high load of the engine.

5.2.2 Percentage of stored exhaust gas energy

Based on the weight of water in the water tank in stage 4, the percentage of the exhaust gas energy stored in the CHS system were determined based on Equations 5.3-5.5 and the results are shown in Figure 5.5.

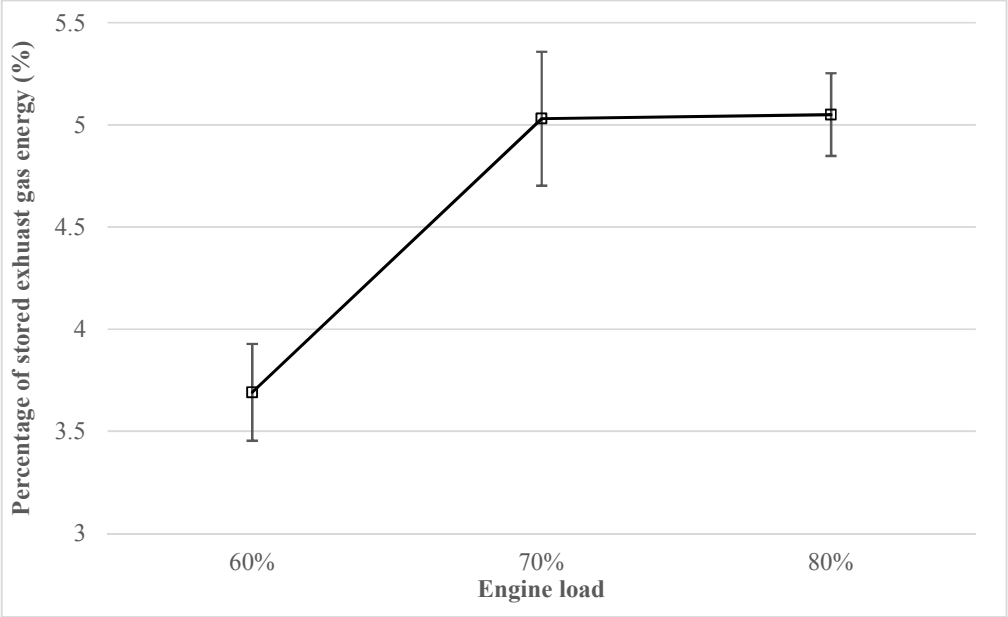

Figure 5.5 *Variation of the percentage of the stored exhaust gas energy with the engine load*

As shown in Figure 5.5, the percentage of the stored exhaust gas energy increased with the increase of the engine load in the 60 minutes mode. At 60% engine load, 3.69± 0.24% of the exhaust gas energy was stored inside the CHS system after 60 minutes. By taking the same time of 60 minutes, 5.03± 0.33% of the exhaust gas energy was stored at 70% engine load, and 5.05± 0.20% at 80% engine load. It can be seen that the difference in the percentage of the exhaust gas energy stored in the CHS system between 70% and 80% engine loads was insignificant. The reason is that although the stored energy increased when the engine load increased from 70% to 80% engine load, the exhaust gas energy also increased accordingly. It led to the percentage of the stored exhaust gas energy changed insignificantly. Compared with 70% and 80% engine loads, at the lower load of the engine (60% engine load), the percentage of the stored energy decreased because the reduction of the stored energy was faster than it of the exhaust gas energy.

5.3 Simulation results

As discussed in 5.2, in the heat storage process, the experiments were conducted at 60 minutes mode at 60%, 70% and 80% engine loads. The verified CFD model was used to investigate the performance of the CHS system at conditions different from that in the experiments in the 60 minutes and full charge modes.

5.3.1 60 minutes mode

5.3.1.1 Percentage of reacted EM8block

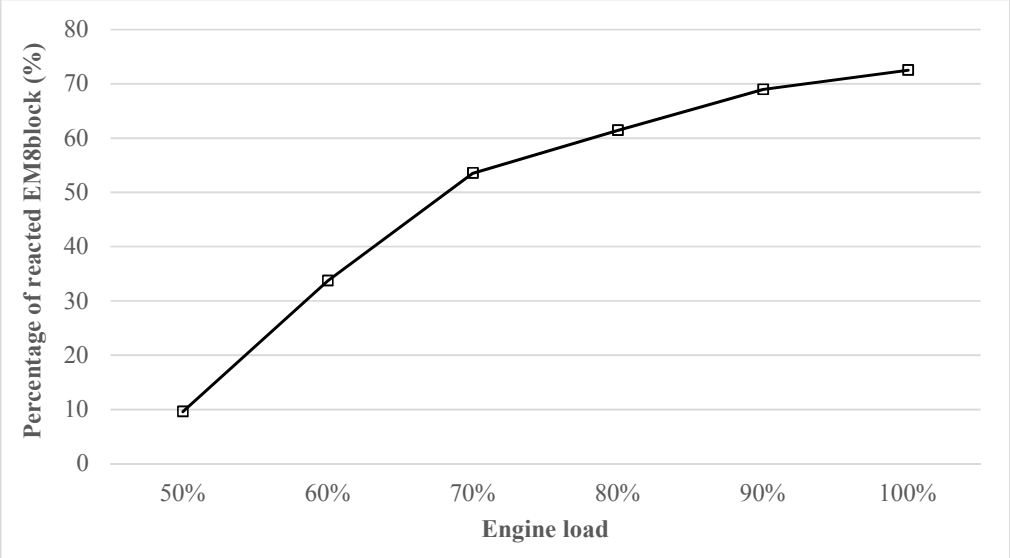

Figure 5.6 *Variation of the percentage of the reacted EM8block in 60 minutes mode with the engine load*

In the simulation, the percentage of reacted EM8block could be found from the temperature history of EM8block in the 60 minutes mode as shown in 4.2.5. The percentage of reacted EM8block as shown in Figure 5.6 was determined by the percentage of EM8block having the temperature higher than the reaction temperature of EM8block in the heat storage process.

It can be seen that the percentage of reacted EM8block in 60 minutes mode highly depends on the engine load. At 50% engine load, 60 minutes after the engine started, only 9.6% EM8block reacted inside the reactor. By take the same time of 60 minutes, the percentage of the reacted EM8block increased 7.55 times to 72.54% at the full engine load. With the CHS system using EM8block as the storage material, heat energy of the exhaust gas was stored in EM8block when the dehydration reaction occurred at the reaction temperature of 280^0C. In the diesel engine in the current study, the temperature of the exhaust gas at the low engine load (50% engine load) was not high enough, so the time for heating stages (stages 1, 2 and 3) were longer. Therefore, the time left for stage 4 decreased in the total time of 60 minutes corresponding to the small percentage of the reacted EM8block. Moreover, at the engine load lower than 50%, the low exhaust gas temperature led to the low performance of the CHS system and applying the CHS system in this case is ineffective.

5.3.1.2 Percentage of stored exhaust gas energy

Another criterion to evaluate the performance of the CHS system in the heat storage process in 60 minutes mode is the percentage of the stored exhaust gas energy. In the simulation, the amount of the reacted EM8block, $m_{EM8block}$ (kg), was calculated from the initial mass of EM8block, m_{total} (kg), and the percentage of reacted EM8block, $r_{EM8block}$ as shown in Eq. (5.11).

$$m_{EM8block} = r_{Em8block}.m_{total} \quad (5.11)$$

Based on the amount of the reacted EM8block, the amount of the stored energy, Q_{stored} (kJ), was determined using Eq. (5.12).

$$Q_{stored} = 81.\frac{r_{mix}.m_{EM8block}}{M_{Mg(OH)_2}} \quad (5.12)$$

The percentage of the stored exhaust gas energy determining from Equation 5.3 depended on the stored energy and the total energy of the exhaust gas in the time of 60 minutes. The total energy of the exhaust gas depended on the engine load and it increased with the increase of the engine load. The amount of the stored energy and the percentage of the stored exhaust gas energy at 60 minutes mode are shown in Figure 5.7.

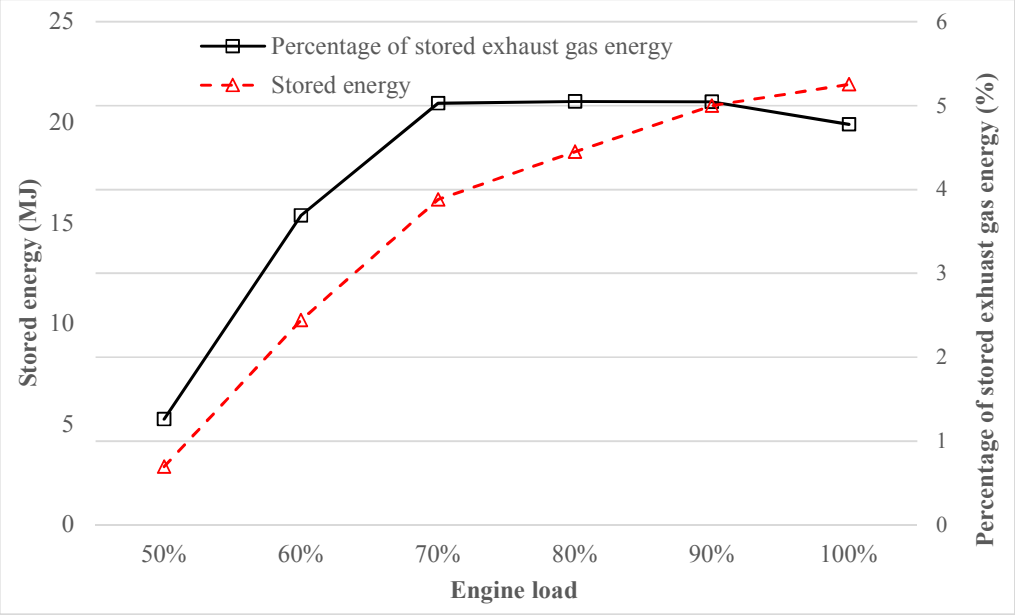

Figure 5.7 *Variation of stored energy and percentage of stored exhaust gas energy in 60 minutes mode with the engine load*

Similar to the percentage of the reacted EM8block, the stored energy, as shown in Figure 5.7, increased with the increase of the engine load from 2.9 MJ at 50 % engine load to 21.9 MJ at the full engine load. However, the variation of the percentage of the stored exhaust gas energy with the engine load as shown in Figure 5.7 is different from the stored energy. The percentage of the exhaust gas energy stored in the CHS system was highest

at 70%, 80%, 90% engine loads with around 5.05% of the energy of the exhaust gas was stored in the 60 minutes mode. This percentage decreased sharply when the engine load was smaller than 70%. In the 60 minutes mode, the percentage of the stored exhaust gas energy decreased to 3.69% at 60% engine load and 1.26% at 50% engine load. The reason was the low temperature of the exhaust gas at the low loads of the engine. The low temperatures at the low loads of the engine led to the longer heating time (stages 1, 2 and 3 of the heat storage process), so the storing time (stage 4) was shorter and the stored energy was smaller. Moreover, compared with 70%, 80% and 90% engine loads, at the full engine load, the percentage of the stored exhaust gas energy was slightly decreased at 4.78%. The reason was that when the engine load increased, the total energy of the exhaust gas increased. However, the increase rate of the exhaust gas energy was higher than the stored energy, so the percentage of the stored exhaust gas energy at the full engine load was smaller than that at 70%, 80% and 90% engine loads.

5.3.2 Full charge mode

After 60 minutes, when the engine kept running, the dehydration reaction of EM8block continuously occurs inside the reactor until all EM8block reacted. In the full charge mode, the verified CFD model was used to investigate the performance of the CHS system. In this mode, as shown in 5.1, the full charge time and the percentage of the stored exhaust gas energy are criteria to evaluate the operation the CHS system.

5.3.2.1 Full charge time

As shown in Figure 5.8, the longest full charge time was at 50% engine load at 110.3 minutes. This time decreased to 95.1 minutes at 60% engine load, 79.05 minutes at 70% engine load, 72.9 minutes at 80% engine load, 70.04 minutes at 90 % engine load and

67.1 minutes at the full engine load. It can be seen that the full charge time highly depended on the engine load. At the higher engine load, the temperature of the exhaust gas was higher and the heating effect of the exhaust gas was stronger. It contributed to the shorter charge time of the CHS system.

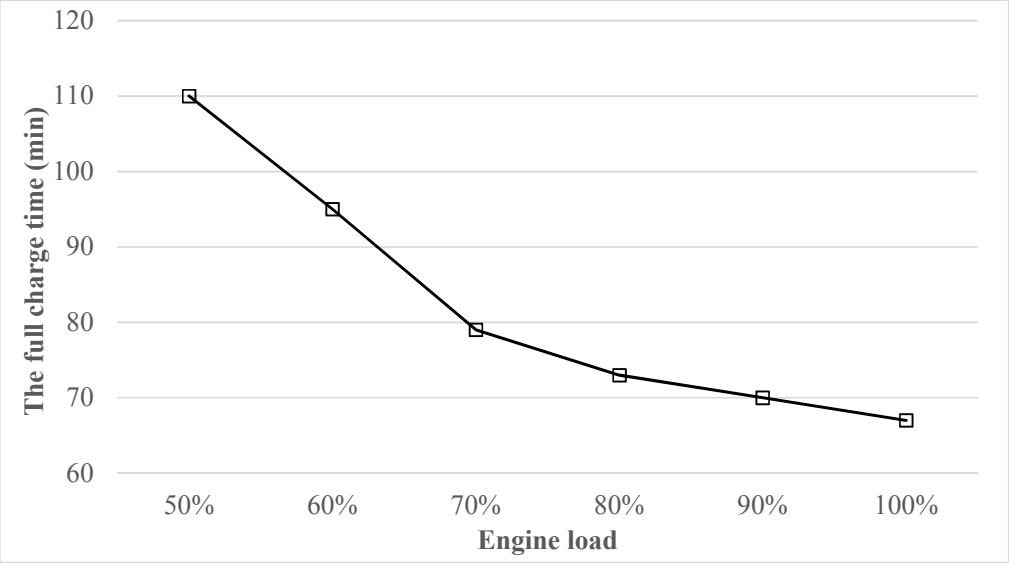

Figure 5.8 *Variation of the full charge time with the engine load*

Compared with the requirement of the CHS system when designing it for D1146TI diesel engine as shown in section 3.2, the full charge time of the CHS at the full engine load in the simulation was higher (67.1 minutes compared with 60 minutes in the design). The reason of the higher full charge time came from the difference in the operation condition of the engine between design and simulation. In the reactor design, the parameter of the exhaust gas was assumed as steady. In the experiment and simulation, the energy and temperature of the exhaust gas was unstable and they were lower in the engine start-up. It led to the longer full charge time in the simulation. However, the difference in the full charge time between design and simulation was insignificant and it can be accepted.

5.3.2.2 Percentage of stored exhaust gas energy

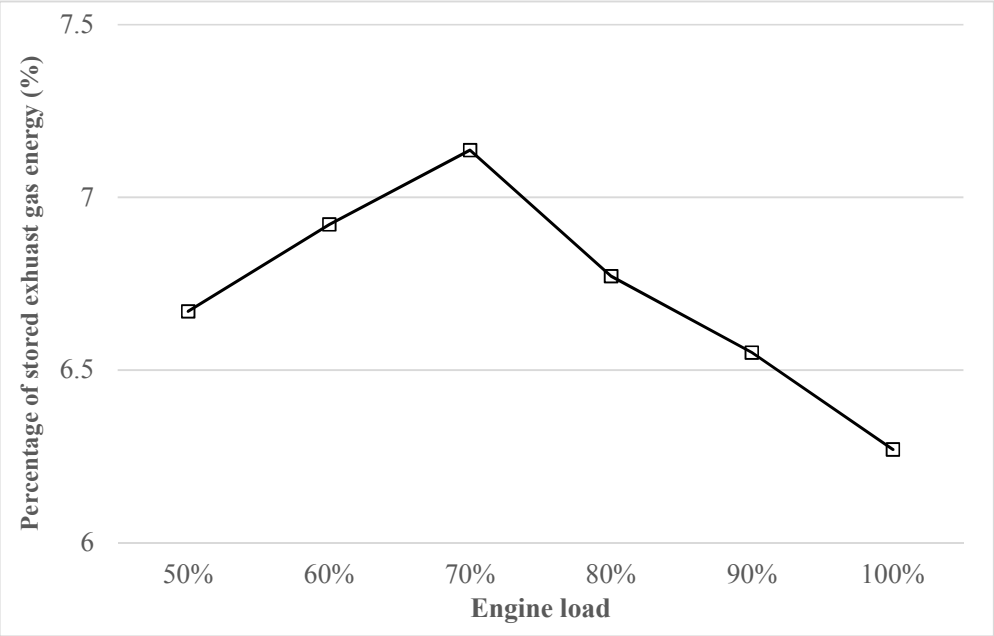

Figure 5.9 *Variation of the percentage of the stored exhaust gas energy in the full charge mode with the engine load*

The percentage of the stored exhaust gas energy could be found from the stored energy and the total energy of the exhaust gas as shown in Equation 5.5. As shown in Figure 5.9, the percentage of the stored exhaust gas energy changed slightly when the engine load changed from 50% to full engine load. At the full charge mode, the stored energy presenting by the amount of reacted EM8block inside the reactor was the same at all engine loads. The difference in the percentage of the stored exhaust gas energy between engine load conditions came from the total energy of the exhaust gas. The highest percentage of the stored exhaust gas energy was 7.14% at 70% of engine load, and it reduced when the engine load increased or decreased. At the higher engine loads, the full charge time decreased; however, the energy of the exhaust gas energy per unit time increased. It led to the total energy of the exhaust gas increase and the percentage of the

exhaust gas energy stored in the CHS system decreased in the full charge mode. On the contrary, at the lower engine loads, the energy of the exhaust gas per unit time decreased, but the full charge time was longer. It led to the total energy of the exhaust gas increased and the percentage of the stored exhaust gas energy in the whole charge time decreased compared with that at 70% engine load.

5.4 Summary

This chapter presented and discussed the experimental and simulation results of the heat storage process. The results were presented in two modes: 60 minutes and full charge modes. The major results of this chapter can be concluded as follows:

- For the diesel engine in the current study, D1146TI diesel engine, the CHS system using EM8block as the storage material was feasible when the engine load was higher than 50%.
- The weight of the water in the water tank was used to recognise stages of the heat storage process of the CHS system.
- At 60 minutes mode, at the higher engine loads, the time for heating stages (stages 1, 2 and 3) were shorter. Therefore, the time left for the heat storage stage (stage 4) was longer and the amount of reacted EM8block, the percentage of reacted EM8block and stored energy were higher. However, the percentage of the stored exhaust gas energy was stable at 70%, 80%, 90% engine loads, slightly decreased at the full engine load and sharply decreased at 60%, 50% engine loads.
- At the full charge mode, the shortest full charge time was 67.1 minutes at the full engine load. This time increased to 110.3 minutes at 50% engine load. The percentage of the exhaust gas energy stored in the CHS system changed

insignificantly with the change of the engine load. This percentage was highest at 70% engine load and decreased when the engine load changed.

Chapter Six

6 CHS in Heat Output Processes

This chapter presents and analyses the experimental and numerical results to investigate the performance of the CHS in the heat output process. The experimental results are presented in subsection 6.1. Subsection 6.2 presents the simulation results. The comparison between the CHS in the current study and other TES systems to evaluate the performance of the CHS is shown in subsection 6.3.

6.1 Experimental results

After the heat storage process, the solid product of the dehydration reaction, $EM8block_p$, was stored inside the reactor and water vapour flowed into and condensed in the water tank. In the storing time, $EM8block_p$ and water liquid were stored separately in the reactor and the water tank at the ambient condition. Therefore, the stored energy of the CHS system could be stored for a long time with small energy loss. The energy loss of the CHS system in the storing time could be come from the penetration of the water vapour in the ambient to the reactor. The water vapour from the ambient will react with $EM8block_p$ inside the reactor to release the energy loss. The energy loss of the CHS system can be avoided if the system is sealed to the environment.

After storing time, the stored energy of the CHS system is used to heat the engine intake air in the heat output process. The heated air then is used for heating purposes of the

vehicle. Therefore, the temperature of the intake air after going through the CHS system is a criterion to evaluate the performance of the CHS system.

In the heat output process, water liquid inside the water tank was heated by an electrical resistor. It evaporated, moved into and reacted with $EM8block_p$ in the reactor. After the hydration reaction between $EM8block_p$ and water vapour in the reactor, the stored energy was released and transferred to the reactor wall. The engine intake air was driven by a fan to flow into the reactor and received heat energy from the reactor by heat convection.

In the experiment, because the laboratory was not air conditioned, the experiments were only conducted at the ambient temperature of 23^0C. The operation of the CHS in the engine intake air heating process at other ambient temperatures were investigated using the verified CFD model. The difference between the temperature of the intake air at the outlet (T_5) and inlet (T_4) of the reactor was used to evaluate the performance of the CHS system in the heat output process.

As discussed in Chapter 2, the temperature of $EM8block_p$ after the hydration reaction depends on the water vapour pressure. For heating purposes of the IC engine, the required temperature of the engine intake air is not too high. Therefore, in the current study, the air heating process was conducted at the ambient pressure. At this pressure, the requirement of pressure vessels to store the water vapour were unnecessary, so it could reduce the initial cost of the CHS system. At the ambient pressure, as shown in Table 2.7, the temperature of $EM8block_p$ after the hydration reaction was $150 – 175^0$C (the reaction temperature). After the hydration reaction, the temperature inside the reaction regions increased quickly. The heat energy was then transferred from the high-temperature regions (reaction regions) to the low-temperature regions (unreacted regions) in

EM8block$_p$ and the reactor wall by heat conduction before transferring to the engine intake air by heat convection.

In the experiment, besides the temperature of the engine intake air at the reactor inlet and outlet (T_4 and T_5), a thermostat was located at the middle of the reactor wall to record the temperature of the reactor wall at this area (T_6). The experimental results showed that when the temperature of the reactor wall was lower than 45^0C, the heating effect of the reactor was insignificant as shown by the small difference between T_4 and T_5 (less than 5^{o}C). Therefore, in the experiment, the engine intake air was not flowing in the reactor until the wall temperature, T_6, reached 45^0C. It took 11 minutes for the reactor wall temperature increased from the ambient temperature of 23^0C to 45^0C.

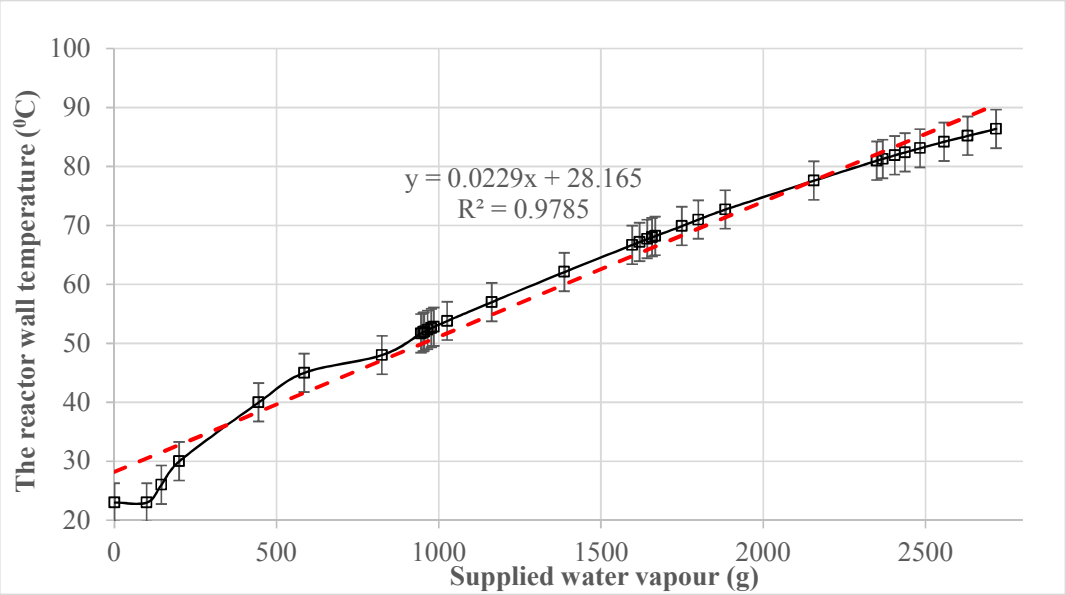

Figure 6.1 *Variation of temperature of the reactor wall with the weight of the supplied water vapour*

The temperature of the reactor wall (T_6) depended on the reaction inside EM8block$_p$, and the reaction carried on with the supplied water vapour moving from the water tank into

the reactor. As shown in Figure 6.1, the temperature of the reactor wall increases linearly with the increase of the weight of evaporated water in the water tank. The solid line shows the experimental data. The dotted line is the linear regression fitting. In the linear regression equation shown in Figure 6.1, the independent variable x is the weight of the evaporated water in the water tank, and the dependent variable y is the temperature of the reactor wall (T_6). The correlation coefficient, R, of 0.9785, shows a good agreement between the experimental data and the data calculated with the linear equation in Figure 6.1, except in the condition when the reactor wall temperature is lower than 48^{o}C. This linear function between the weight of the water and the temperature of the reactor wall can be useful for predicting and controlling the reactor wall temperature and consequently, the heated air temperature.

Figure 6.2 shows the variation of the intake air temperature with the temperature of the reactor wall at the ambient temperature of 23^{0}C. In the linear regression equation, x is the reactor wall temperature, T_6, and y is the temperature of the heated air after going through the reactor, T_5. The correlation coefficient, R, is 0.9966. This linear function can be useful for predicting the heated air temperature based on the reactor wall temperature.

Given the temperature of the heated air, the required temperature of the reactor wall (T_6) can be calculated with the linear regression equation in Figure 6.2. To get T_6 as required, the required weight of water required for the reaction can then be determined based on the linear regression equation shown in Figure 6.1. At the ambient temperature 23^{0}C, the heated air temperature after going through the reactor increased by 5.7 to 17.3^{0}C depended on the temperature of the reactor wall as shown in Figure 6.2.

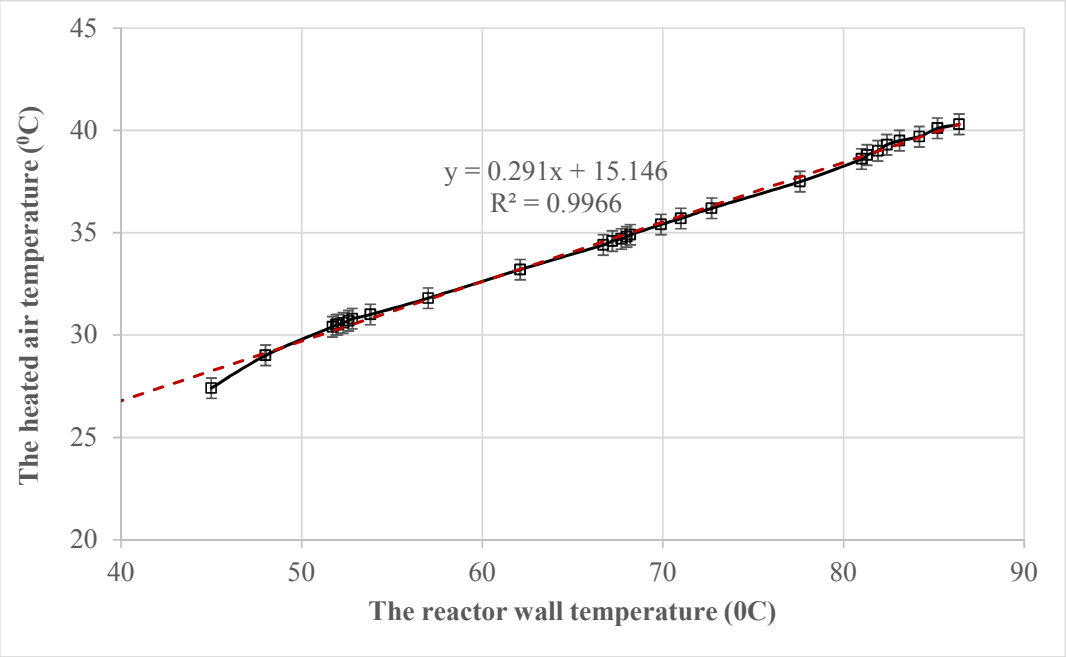

Figure 6.2 *Variation of the heated air temperature with the temperature of the reactor wall at the ambient temperature of 23^{0}C*

6.2 Simulation results

The operation of the CHS system at other ambient temperature was investigated using the verified CFD model. Based on the experimental results, the heat transfer coefficient of the system as shown in Equation 4.7 was determined and used in the CFD model to simulate the operation of the CHS system in the heat output process and at other ambient temperature. The temperature of the heated air, T_5, depended on the temperature of the environment (T_4), and the reactor wall (T_6) as shown in Figure 6.3.

It can be seen in Figure 6.3, even when the ambient temperature is -10^{0}C, after going through the CHS system, the temperature of the heated air increases to higher than the freezing point 0^{0}C, from 2.98 to 12.15^{0}C depending on the reactor wall temperature. At the same reactor wall temperature, the performance of the CHS system presented by the

temperature difference of the intake air between the outlet and inlet of the reactor was smaller at the higher ambient temperature. The reason is that at the lower ambient temperature, the temperature difference between the reactor wall and the engine intake air was higher, so the heating effect of the reactor was stronger leading to the higher temperature difference between the heated air and the ambient. At the reactor temperature 85^0C, the temperature increase of the engine intake air after going through the reactor at the ambient temperature 23^0C was 17.3^0C. However, it increased to around 22.15^0C when the ambient temperature reduced to -10^0C.

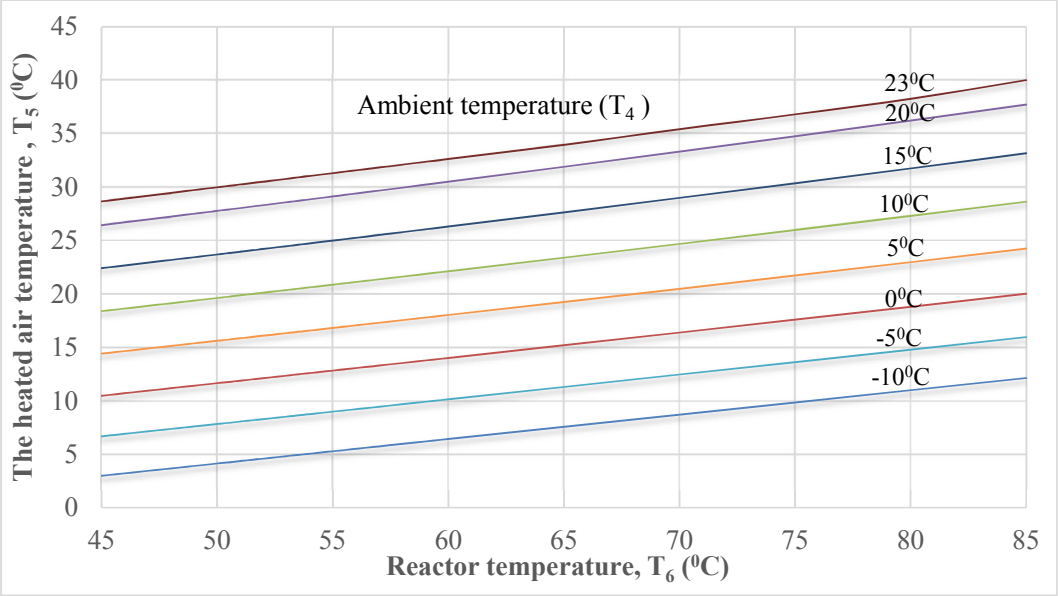

Figure 6.3 *Variation of the heated air temperature with the temperature of the ambient and the reactor*

For the heating purposes, the heated air, after that, could be used for heating the engine or extent to other heating required in IC engine and hybrid vehicles. Based on the required temperature of the heated air in the vehicle and the ambient temperature, the temperature

of the reactor wall can be determined based on Figure 6.3 and the required weight of the water for the reaction could be found from Figure 6.1.

6.3 Comparison between the CHS and other TES systems

TES systems with its advantages as storing and using the heat energy whenever, are being researched and applied to recover the exhaust gas energy of IC engines as shown in Chapter 2. In this section, the advantages and disadvantages of the CHS system in the current study will be compared with other TES systems in recovering the exhaust gas energy of IC engines. The main properties of the CHS system in the current study and other TES systems are shown in Table 6.1.

Table 6.1 *Main properties of CHS system in the current study and other TES systems to recover exhaust gas energy of IC engines*

Parameter	**PandiyarajanTES system [23]**	**Pertti TES system [70]**	**M.Gumus TES system [71]**	**Tessa TES system [72]**	**CHS system in the current study**
Applications	Heating the engine oil	Heating the engine	Heating the engine	Heating the engine, the cabin	Heating the intake air
Size	*A heat exchanger:* 450 mm ID x 720 mm H *A TES tank:* 323 mm ID x 500 mm H	*A accumulator:* 195 mm OD x 300 mm H *Two plate heat exchangers:* 190 mm x 170 mm	*A stored tank:* 220 mm OD x 400 mm L	*A stored tank:*610 W x 710 D x 230 H mm	*A reactor:* 360 mm OD x 500 mm H *A water tank:* 20 mm OD x 30 mm H
Heat storage process					
Stored energy	19.500 kJ	2500 kJ	2277 kJ		**30.197 kJ**

Percentage of stored exhaust gas energy	11% at 50% engine load 14% at 75% engine load 15% at full engine load				6.5% at 50% engine load 7.14% at 70% engine load 6.1% at full engine load
Full charge time	180 min at 50% engine load 150 min at 75% engine load 85 min at full engine load				110 min at 50% engine load 79 min at 70% engine load 67 minutes at full engine load
Storing process					
Storing time	90 hours		12 hours	12 hours	**More than 90 hours with small heat loss**
Heat output process					
The working temperature	120^0C	70-82^0 C	32.4^0 C	230^0 C	90^0 C
Start-up time	Short	Short	Short		**Long**

ID: inside diameter, OD: outside diameter, H: height, W: Width, D: depth, L: length

As discussed in Chapter 2, a combination of a sensible and latent heat storage system was developed to recover the waste heat of the exhaust gas of a Diesel engine in [23] to warming-up the lube oil. Compared with this system, the CHS in the current research has some advantages as follows:

- Size: the size of the CHS in the present study is smaller than that of TES system

in [23]. TES system in [23],as shown in Figure 2.7, included two main devices, a cylindrical vessel of inner diameter 450 mm x height 720 mm for the heat exchanger and a TES tank, 323 mm x 500 mm. In the current study, the reactor is a cylindrical vessel of 360 mm x 500 mm, and the water tank is another cylindrical vessel of 20 mm x 30 mm. It can be seen that the total size of the CHS in the current study is much smaller, so it will be easier to locate in the vehicle than the TES system in [23].

- Stored energy: The stored energy of the CHS system in the current study is higher than the TES system in [23]. The TES system in [23] stored energy based on the sensible and latent heats of paraffin with the total stored energy of the system of 19,500 kJ. The CHS in the current study stored energy based on the reversible reaction of $Mg(OH)_2$.With 24.46 kg of EM8block in the reactor, the stored energy of the CHS system was 30,197 kJ, 1.5 times higher than the TES system in [23].
- Storing time: The CHS system in the current study stored energy in the longer time than the TES system in [23]. In the TES system in [23], the stored energy was stored at the high temperature so it was lost to the environment overtime. The heat loss process of the stored energy of the TES system in [23] occurred in two periods. In the initial period when the temperature of TES was from 120^0C to 65^0C, the temperature of TES system dropped very quickly, and the sensible heat was lost to ambient. When the temperature was 65^0C, the latent heat of paraffin was lost but with the slower speed. As reported in [23], almost the stored energy of the TES system was gone after 5500 minutes. With the CHS in the current study, two products of the dehydration reaction of EM8block was stored separately at the ambient temperature so the heat loss to the ambient was very small. It can came from the penetration of the water vapour in the ambient to the

reactor as discussed in 6.1 and it can be avoided if the system is sealed to the environment.

Besides advantages, compared with the TES system in [23], the CHS in the current study have some drawbacks as follows:

- The start-up time of the heat output process: The CHS system in the current study need a longer start-up time compared with the TES system in [23]. With the TES system in [23], in the heat output process, the liquid paraffin was pump to the heat exchanger to heat the oil so the start – up time was very quick. In the current study, as discussed above, it need time to heat the reactor to the required temperature (stage 1 of the heat output process). This time depended on the required temperature of the reactor wall, T_6, and it was usually higher than 10 minutes.
- The applied temperature in the heat output process: The applied temperature in the heat output process of the CHS system in the current study is lower than the TES system in [23]. The applied temperature in the heat output process of TES in [23] depend on the temperature of paraffin inside the system and the maximum temperature could be 120^0C. In the CHS in the current study, the temperature of the hydration reaction in the heat output process was 150 – 175^0C. However, by the heat transfer to the other part of EM8block$_p$ and the reactor wall, the maximum temperature of the reactor wall, T_6, was only around 90^0C, smaller than the TES system in [23].

Another TES system applying to recover the exhaust gas energy of a Diesel engine as mentioned in Chapter 2 is the combination of the latent TES system and the exhaust gas heat recovery system in [70]. The stored energy was used to pre-heating the engine in the

cool weather. This TES system using Stabilised trisodium phosphate dodecahydrate as the PCM consists of two main devices: a latent heat accumulator and exhaust gas heat recovery system. The accumulator was a cylindrical vessel of outer diameter 195 mm and height 300 mm. The exhaust gas heat recovery system was made by two plate heat exchangers with the parameter 190 mm x 170 mm. It can be seen that the total size and the working temperature in the heat output process of the TES system in [70] and the CHS system in the current study are almost the same. However, the stored energy of the combination system in [70] was only 2500 kJ smaller than in the CHS system in the current study.

With the same purpose for pre-heating the engine, another latent heat storage system using $Na_2SO_4.10H_2O$ was suggested by M.Gumus as presented in [71]. The maximum stored energy of the TES system in [71] with the parameters of outer diameter 220 mm and length 400 mm was 2277 kJ. It can be seen that compare with the TES systems in [71], the total volume of the CHS system in the current study is 3.3 times higher than that of the TES system in [71], however, the stored energy of the CHS is 13 times higher. Moreover, the storing time of the CHS system is longer when the stored energy of the TES system in [71] was only available in 12 hours.

Tessa thermal storage system in [72] was another TES system applying to recover exhaust gas energy of IC engines. The TES system in [72] was tested in a Land Rover Freelander 2 with a 2.2 litre diesel engine. In this system, the exhaust gas energy was stored in the high temperature PCM, which melts at 164^0C. The stored temperature could be up to 230^0C. It can be seen that, the Tessa thermal storage system in [72] can store energy at the higher temperature than other TES systems applying to recover the exhaust gas energy of IC engines including the CHS system in the current study. Therefore, Tessa TES

system can be applied for high temperature applications of the vehicles. The stored energy of Tessa system is the same as the CHS in the current study. However, the total size of Tessa system, 610 x 710 x 230 mm, is two times bigger than that of the CHS in the current study. Moreover, similar to the TES system in [71], the stored energy of Tessa thermal storage system was only available for 12 hours after being fully charged.

In summary, compare with other TES systems applying to recover exhaust gas energy of IC engine vehicles, the CHS in the current study has a higher stored energy and the longer storing time. However, the disadvantage of the CHS system is that it needs a start-up time in the heat output process. This time depends on the requirement of the heated air temperature as discussed in section 6.1.

6.4 Summary

This chapter presented and discussed the experimental and numerical results of the heat output process. This chapter also presented the comparison of the CHS system in the current study with other TES systems applying to recover the exhaust gas energy of IC engines. The main results of this chapter can be concluded as follows:

- The temperature of the heated air depended on the ambient temperature and the temperature of the reactor wall. The temperature of the reactor wall depended on the reaction inside EM8block$_p$ carried on with the supplied water vapour moving into the reactor. Depending on the required temperature of the heated air, and the ambient temperature, the amount of water vapour moving in the reactor can be determined.
- Compared with other TES system applying to recover exhaust gas energy of IC

engine, the CHS in the current study has the higher stored energy and the longer storing time. However, it needs start-up time before the stored energy can be used.

Chapter Seven

7 Numerical Investigation to Improve CHS System

Based on the above experimental and simulation results, the original CHS system was modified with two wings added to enhance the heat transfer process between the exhaust gas and EM8block. Subsection 7.1describesthe modification of the CHS system. The performance of the modified CHS system in the heat storage will be presented and compared with that of the original one in subsections 7.2 and the heat output process in 7.3.

7.1 Modification of the CHS system

As discussed in Chapter 5, the stored energy depends on the amount of the reacted EM8block. The dehydration reaction occurs in EM8block when the temperature of the EM8block is higher than the reaction temperature of 523-553K. Therefore, in the simulation, the stored energy in the CHS system depends on the number of node that have the temperature higher than the reaction temperature of $Mg(OH)_2$. If the number of EM8block nodes with the temperature higher than reaction temperature increases, the amount of the reacted EM8block and the stored energy will increase. Furthermore, the temperature of a node inside EM8block depends on the temperature of the exhaust gas, the heat transfer process inside the reactor and its location in EM8block as shown in Figure 7.1.

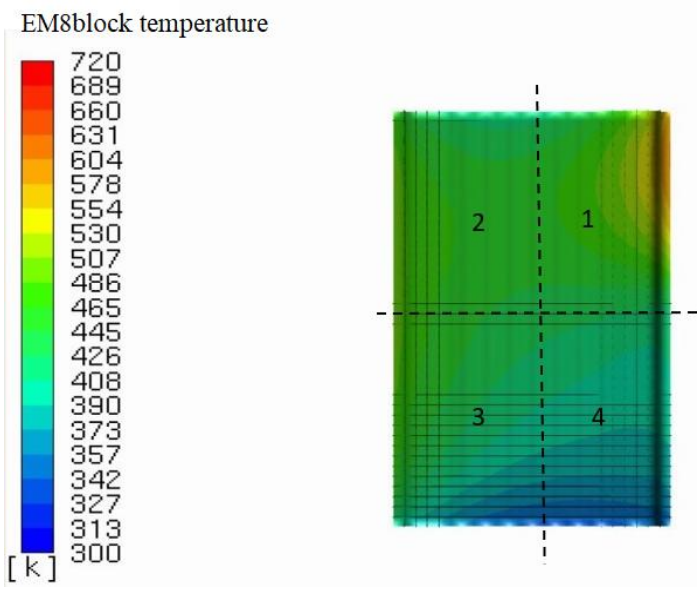

Figure 7.1 *Temperature profile at the cross surface passing through the central of EM8block*

As shown in Figure 7.1, the temperature profile inside EM8block is not uniform. The highest temperature profile is at the first quarter, next to the reactor inlet of EM8block (area 1). The temperature prolife is lower in the areas 2 and 3 (opposite the inlet of the reactor). The lowest temperature profile is at the last quarter of EM8block, area 4, below the reactor inlet and opposite the reactor outlet. The reason is that in the original CHS system, the exhaust gas flowed directly from the inlet to the outlet and the area 4 received the least heat energy from the exhaust gas. It can be seen that, the nodes at the lower temperature areas (areas 2, 3, and 4) are harder than area 1 to reach to the reaction temperature of $Mg(OH)_2$, therefore, increasing the temperature of the low temperature areas could be a solution to improve the efficiency of the CHS system. Furthermore, the temperature of EM8block also depends on the temperature of the exhaust gas and the heat transfer process inside the reactor. The parameters of the exhaust gas are unchanged at an engine load, and they depend on the operation condition of the IC engine. Therefore, to

improve the performance of the CHS system, enhancing the heat transfer process inside the reactor could be a proposed solution.

To enhance the heat transfer process between the exhaust gas and the EM8block, an improvement has been made by adding two wings to the exterior wall of the tube and between the shell and the tube of the reactor as shown in Figure 7.2.

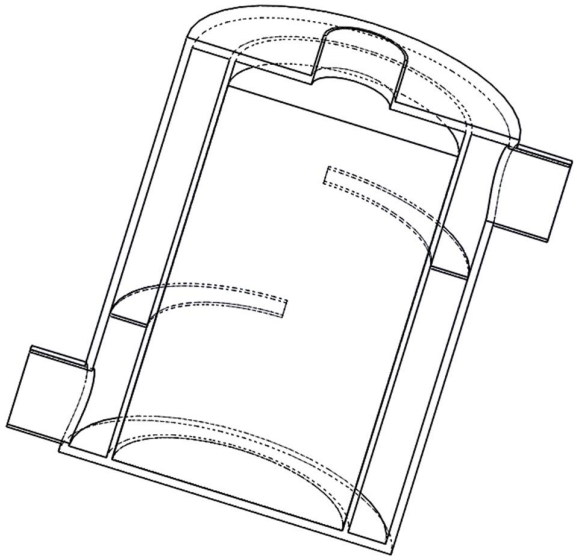

Figure 7.2 *Reactor of the modified CHS system*

The wings were made by the same material with the reactor, steel grade 153MA™, and the thicknesses are 3.05 mm. The wings were located in the exterior wall of the tube, and they divide the volume between the shell and the tube inside the reactor to three equal parts. The modified CHS system, after that, was tested using the verified CFD model.

Figure 7.3 shows the comparison of the temporal variation of the temperature at the checkpoints in the modified and the original CHS systems.

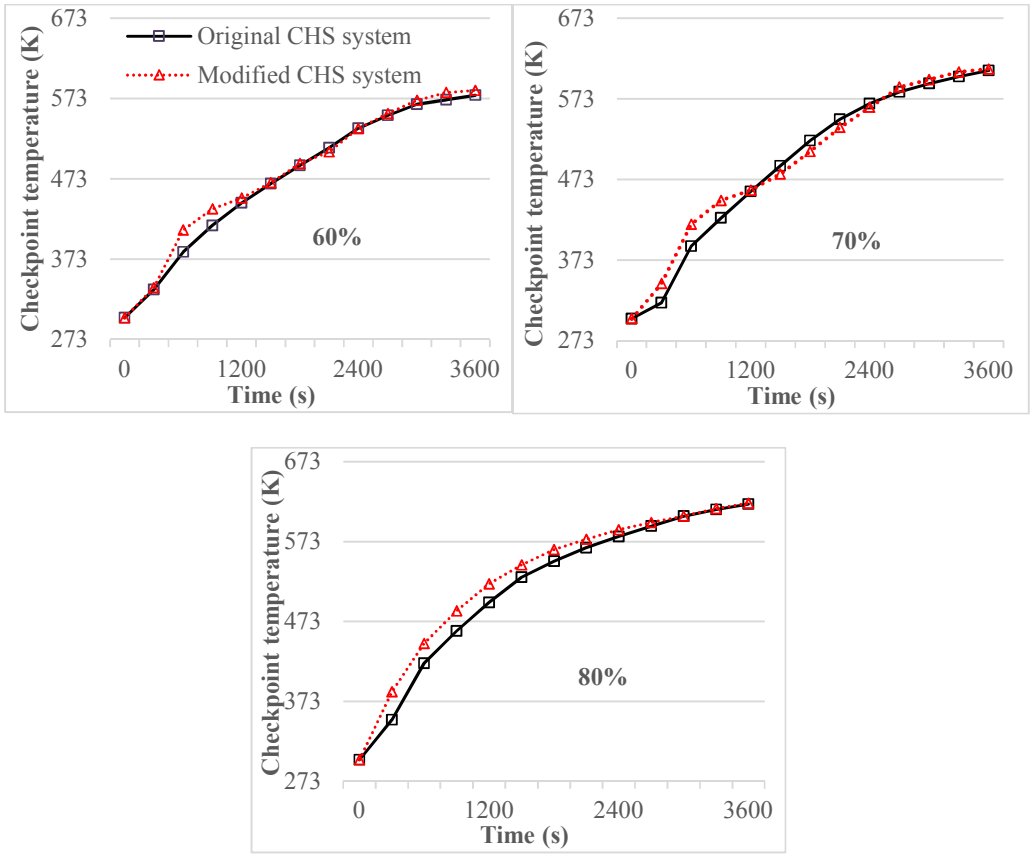

Figure 7.3 *Temporal variation of the temperature at the checkpoint at 60%, 70%, 80% engine loads in the original and modified CHS systems*

As shown in Figure 7.3, the temperature at the checkpoint changed insignificantly in the modified CHS system, compared with the original one (the biggest average difference was 2.06% at 80% engine load). The reason is that the checkpoint was located in the area 1 in both original and modified CHS systems. The exhaust gas flowed directly in area 1 so the difference in the checkpoint temperature between two systems is insignificant.

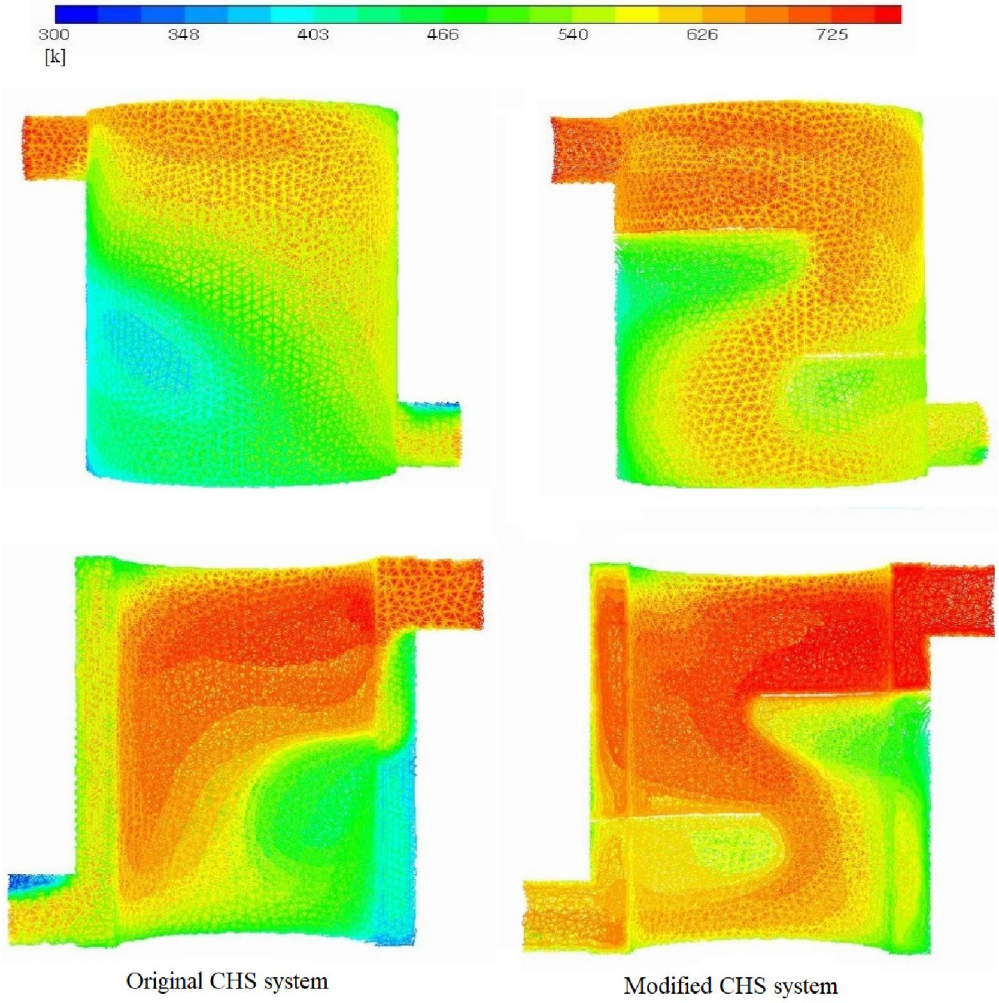

Figure 7.4 *Exhaust gas flow in the original and modified CHS systems at 80% engine load*

Figure 7.4 shows the exhaust gas flow in the original and modified CHS system at 80% engine load. As shown in Figure 7.4, in the original CHS system, the exhaust gas moved directly from the exhaust gas inlet to outlet and rarely to the area 4. It made the temperature profile of this area was lower than other areas inside the reactor. The temperature profile of this area was improved in the modified CHS system. In the modified CHS system, the exhaust gas flowed through most of the areas inside the reactor, and it made more uniform temperature distribution inside the reactor. Furthermore, the

longer movement distance and the smaller velocity of the exhaust gas in the modified CHS system led to the increase of the moving time of the exhaust gas inside the reactor. Therefore, the heat transfer between the exhaust gas and the reactor was enhanced and the amount of EM8block nodes with the temperature higher than the reaction temperature of $Mg(OH)_2$ increased.

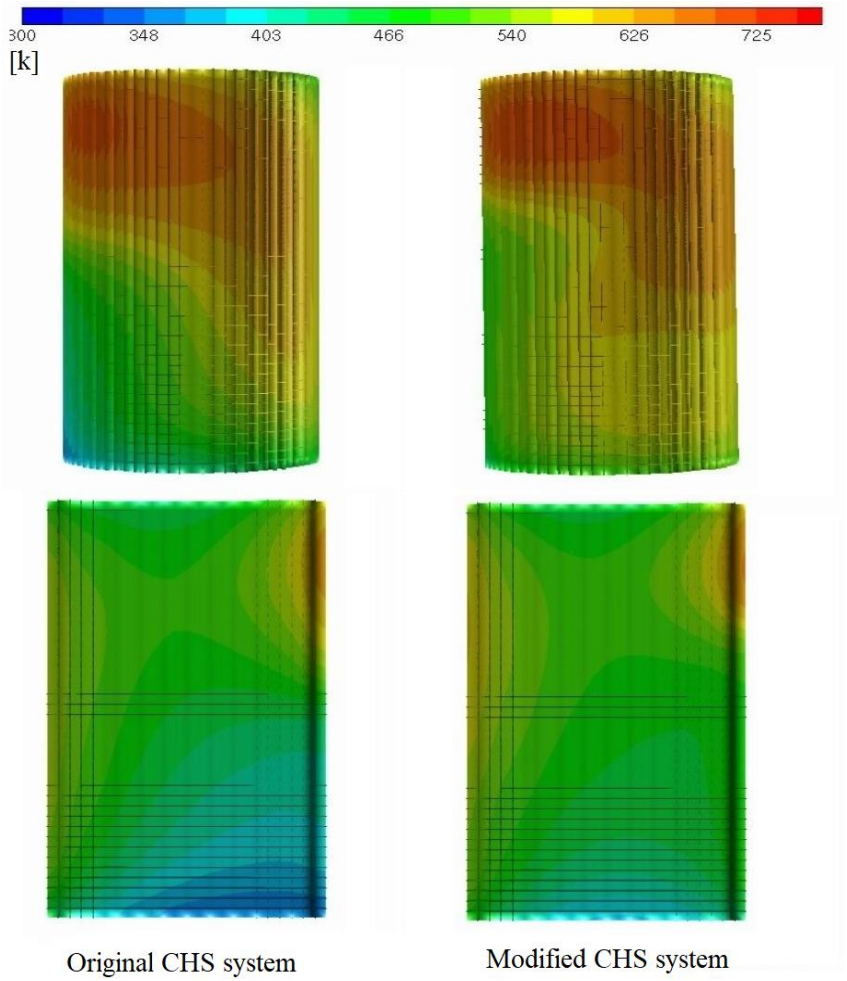

Figure 7.5 *Temperature profile of the outside surface and the cross surface passing through the central of EM8block in the original and modified CHS systems at 80% engine load*

Figure 7.5 shows the temperature profile of EM8block in the original and modified CHS

systems at 80% engine load. As shown in Figure 7.5, the temperature of EM8block in area 4 defined in Figure 7.1 was lower than that in other areas (areas 1, 2, and 3) in the original CHS system because of the movement of the exhaust gas inside the reactor. In the modified CHS system, the temperature profile of EM8block was enhanced, especially in the area 4. The lowest temperature area in the modified CHS system was at the bottom of EM8block. Moreover, as shown in Figure 7.5, the temperature difference between the smallest temperature area and other areas in the modified CHS system was smaller than in the original one. The improvement in the temperature profile of EM8block led to the improvement of the performance of the CHS system in the heat storage process.

The performance of the modified CHS system in the heat storage and heat output processes was investigated using the verified CFD model. The performance of the modified CHS system in the heat storage process is presented in section 7.2 and the heat output process in section 7.3.

7.2 Performance of the modified CHS system in the heat storage process

7.2.1 60 minutes mode

7.2.1.1 Percentage of reacted EM8block

In the modified CHS system, as discussed above, the temperature distribution inside EM8block became more uniform with two wings added. As a consequence, Figure 7.6 compares the volume percentage of the reacted EM8block with the temperature higher than the reaction temperature of $Mg(OH)_2$.

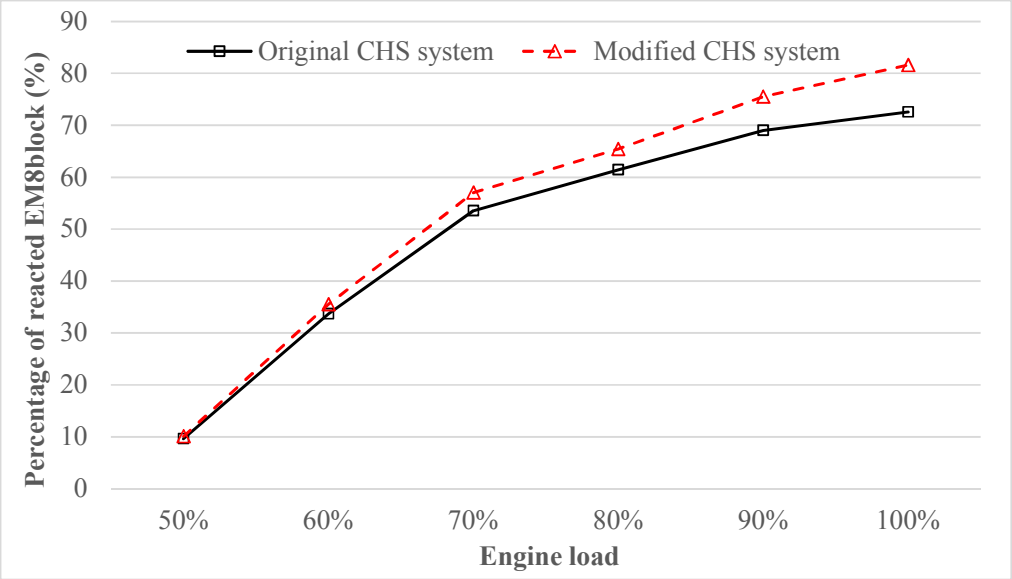

Figure 7.6 *Variation of the percentage of the reacted EM8block in the heat storage process in the original and modified CHS systems with the engine load in the 60 minutes mode*

As shown in Figure 7.6, the percentage of the reacted EM8block in the modified CHS system is higher than the original one in the 60 minutes mode. At the low load of the engine, the heating effect of the exhaust gas is weaker so the difference in the percentage of the reacted EM8block between two CHS systems is smaller. At 50% engine load, the percentage of the reacted EM8block in the modified CHS system was 10.1%. It was 0.49% higher than the original CHS system. The difference in the percentage of reacted EM8block in two CHS system increases to 1.81% at 60% engine load, 3.44% at 70% engine load, 4.04% at 80% engine load, 6.5% at 90% engine load, and 9.06% at the full engine load as shown in Table 7.1.

Table 7.1 *Comparison of percentage of reacted EM8blockin the original and modified CHS system in 60 minutes mode*

	Unit	**Engine load**					
		50%	**60%**	**70%**	**80%**	**90%**	**100%**
Original CHS system	%	9.61	33.69	53.56	61.41	69	72.54
Modified CHS system	%	10.1	35.5	57	65.45	75.5	81.6
Improvement	%	0.49	1.81	3.44	4.04	6.5	9.06

Table 7.1 also shows that in the 60 minutes mode, the maximum percentage of the reacted EM8block increase from 72.54% in the original CHS system to 81.6% in the modified one (12.49% higher) in the full engine load.

7.2.1.2 Percentage of stored exhaust gas energy

Based on the percentage of the reacted EM8block, the stored energy could be found based on Equations 5.11 and 5.12. Figure 7.7 shows the stored energy in the original and modified CHS system in the 60 minutes mode. As shown in Figure 7.7, the effect of the modified CHS on the stored energy is stronger at the high engine load. At 50% engine load, 60 minutes after the engine starts, compared with the original CHS system, using the modified one, the stored energy increased 0.15 MJ from 2.9 MJ to 3.05 MJ. By the taking the same time of 60 minutes, the effect of the modified model increased to 0.55 MJ at 60% engine load, 1.04 MJ at 70% engine load, 1.22 MJ at 80% engine load, 1.96 MJ at 90% engine load and 2.74 MJ at the full engine load as shown in Table 7.2.

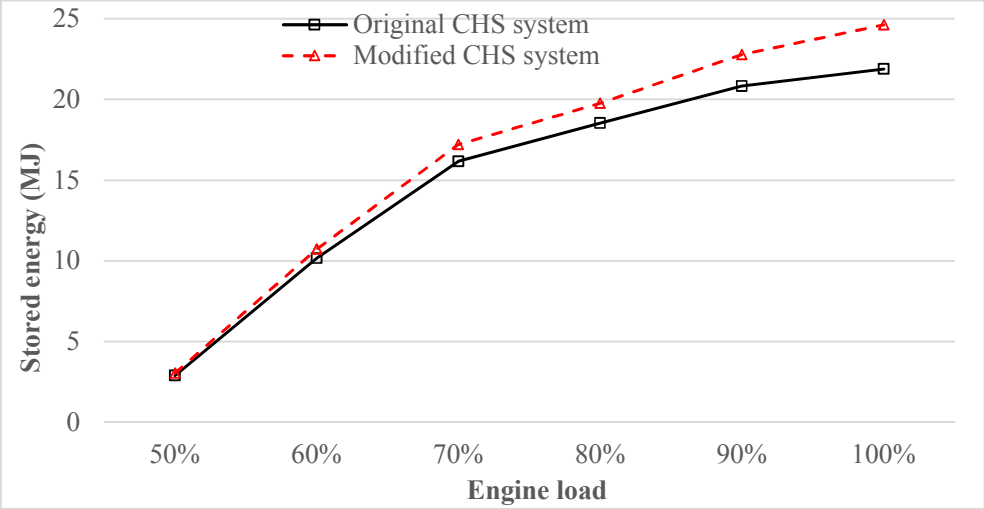

Figure 7.7 *Variation of the stored energy in the 60 minutes mode of the original and modified CHS systems with the engine load*

Table 7.2 *Comparison of stored energy in the original and modified CHS systems in 60 minutes mode*

	Unit	**Engine load**					
		50%	**60%**	**70%**	**80%**	**90%**	**100%**
Original CHS system	MJ	2.9	10.17	16.17	18.54	20.83	21.9
Modified CHS system	MJ	3.05	10.72	17.21	19.76	22.79	24.64
Improvement	MJ	0.15	0.55	1.04	1.22	1.96	2.74

Another criterion for evaluating the performance of the CHS system in the 60 minutes mode as discussed in section 5.1 is the percentage of the stored exhaust gas energy. Based on the stored energy and the total energy of the exhaust gas, the percentage of the exhaust gas energy stored in the CHS system could be determined by Equation 5.3 and shown in Figure 7.8.

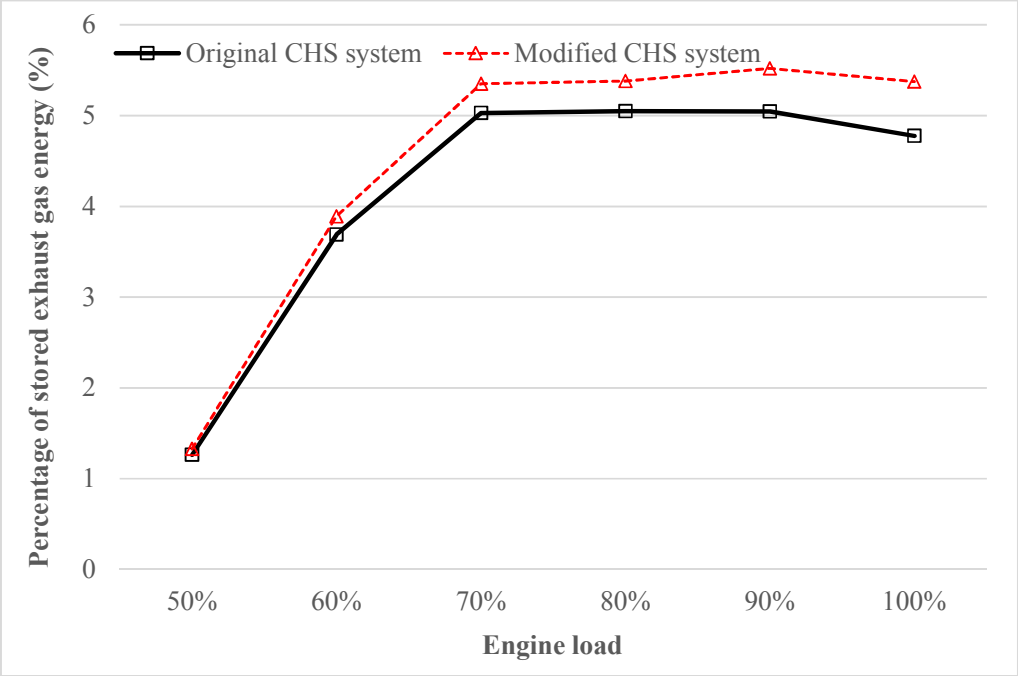

Figure 7.8 *Variation of the percentage of the stored exhaust gas energy of the original and modified CHS systems with the engine load in the 60 minutes mode*

It can be seen that compared with the original CHS system, the percentage of the stored exhaust gas energy in the modified CHS system is improved, especially at the high loads of the engine. In the original CHS system, as discussed in Chapter 5, the maximum percentage of the stored exhaust gas energy is at 70%, 80%, 90% engine loads and it decreased slightly at the full engine load. Difference with the original CHS system, the maximum percentage of the exhaust gas energy stored in the CHS system in the modified one is 5.52% at 90% engine load as shown in Table 7.3. At the full engine load, the percentage of the stored exhaust gas energy of the modified CHS system is 12.49% higher than that of original one (5.37% of the exhaust gas energy stored in the modified CHS system compared with 4.78% in the original one). The difference in the percentage of the stored exhaust gas energy between two CHS system reduced with the decrease of the

engine load. At 50% engine load, this percentage in the modified CHS system is 5.15% higher than that in the original one (from 1.26% exhaust gas energy stored in the original CHS system to 1.33% in the modified one).

Table 7.3 *Comparison of percentage of stored exhaust gas energy in the original and modified CHS systems in 60 minutes mode*

	Unit	**Engine load**					
		50%	**60%**	**70%**	**80%**	**90%**	**100%**
Original CHS system	%	1.26	3.69	5.03	5.05	5.05	4.78
Modified CHS system	%	1.33	3.89	5.35	5.38	5.52	5.37
Improvement	%	0.07	0.2	0.32	0.33	0.47	0.59

It can be seen that both the percentage of the stored exhaust gas energy and the percentage of the reacted EM8block were increased in the modified CHS system, in 60 minutes mode, compared with the original one. The effect of the modified CHS system was stronger at the higher engine loads.

7.2.2 Full charge mode

At the full charge mode of the modified CHS system, as discussed in section 5.1, the criteria for evaluating the performance are the full charge time and the percentage of the stored exhaust gas energy. The difference of the full charge time and the percentage of the stored exhaust gas energy between two CHS systems are shown subsections 7.2.2.1 and 7.2.2.2.

7.2.2.1 Full charge time

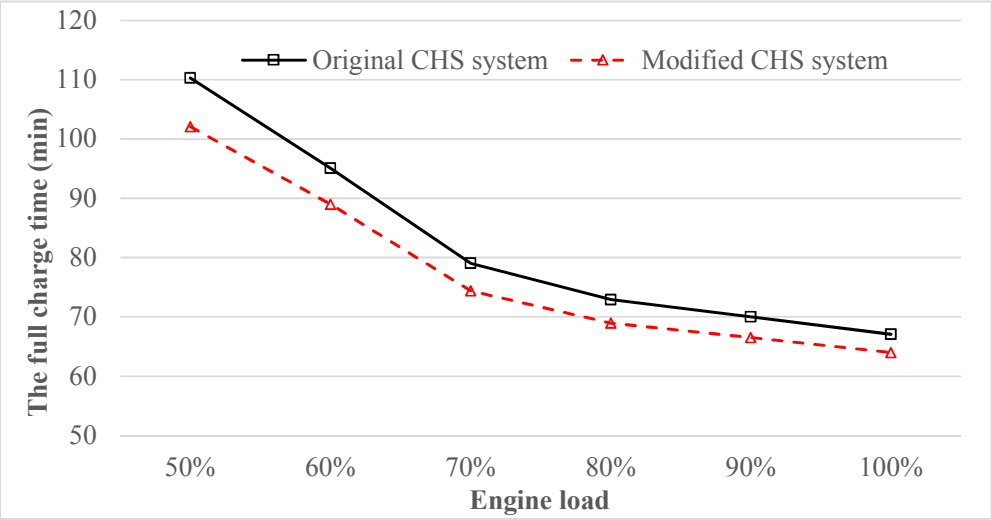

Figure 7.9 *Variation of the full charge time of the original and modified CHS systems with the engine load*

As shown in Figure 7.9, because the heat transfer process inside the reactor was enhanced with two wings added, the full charge time of the reactor was decreased. The full charge time of the modified CHS system was 8.2 minutes shorter than the original one at 50% engine load, 6.1 minutes at 60% engine load, 4.65 minutes at 70% engine load, 3.95 minutes at 80% engine load, 3.54 minutes at 90% engine load, and 3.1 minutes at the full engine load as shown in Table 7.4. The shorter full charge time in the modified CHS system came from the better heat transfer process between the exhaust gas and the reactant when two wings added in the reactor. The effect of the modified CHS system in the full charge time was stronger at the low load of the engine. At 50% of engine load, using the modified CHS system, the full charge time improved 7.43% compared with the original one. It decreased to 4.62% at the full engine load.

Table 7.4 *Comparison of full charge time in the original and modified CHS systems in the full charge mode.*

	Unit	**Engine load**					
		50%	**60%**	**70%**	**80%**	**90%**	**100%**
Original CHS system	Minute	110.3	95.1	79.05	72.9	70.04	67.1
Modified CHS system	Minute	102.1	89	74.4	68.95	66.5	64
Improvement	Minute	8.2	6.1	4.65	3.95	3.54	3.1

7.2.2.2 Percentage of stored exhaust gas energy

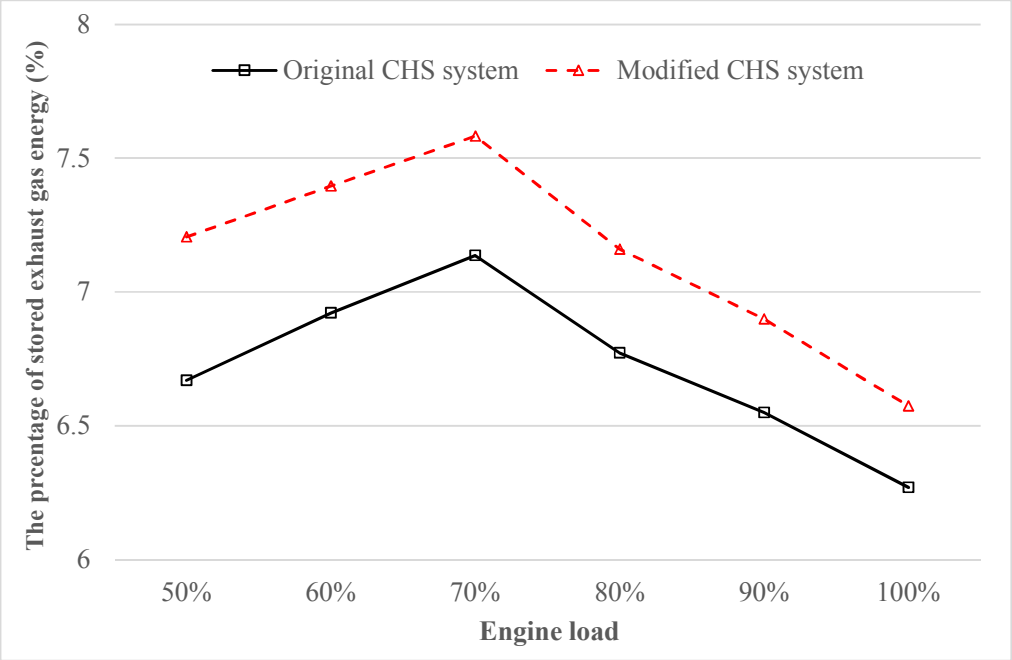

Figure 7.10 *Variation of the percentage of the stored exhaust gas energy of the original and modified CHS systems with the engine load*

The decrease of the full charge time led to the higher percentage of the stored exhaust gas energy in the full charge mode of the modified CHS system. As shown in Figure 7.10 and

Table 7.5, the difference in the percentage of stored exhaust gas energy between two CHS systems was larger at the low load of the engine. At 50% engine load, using the modified CHS system, the percentage of the exhaust gas energy stored in the CHS system could be improved 8.03% (from 6.67% the exhaust gas energy stored in the original CHS system to 7.21% in the modified one). The improvement in the percentage of the stored exhaust gas energy in the modified CHS system decreased to 6.85% at 60% engine load (from 6.92% to 7.4%), 6.25% at 70% engine load (from 7.14% to 7.58%), 5.73% at 80% engine load (from 6.77% to 7.16%), 5.32% at 90% engine load (from 6.55% to 6.9%) and 4.84% at the full engine load (from 6.27% to 6.57%). Similar to the original one, the maximum percentage of exhaust gas energy stored inside the reactor in the modified CHS system was 7.58 % at 70% engine load.

Table 7.5 *Comparison of stored exhaust gas energy in the original and modified CHS systems in the full charge mode*

	Unit	**Engine load**					
		50%	**60%**	**70%**	**80%**	**90%**	**100%**
Original CHS system	%	6.67	6.92	7.14	6.77	6.55	6.27
Modified CHS system	%	7.21	7.4	7.58	7.16	6.9	6.57
Improvement	%	0.54	0.47	0.45	0.39	0.35	0.3

In summary, in the heat storage process, the performance of the CHS system was improved in both the 60 minutes and full charge modes with two wings added. In the 60 minutes mode, both the percentages of stored exhaust gas energy and reacted EM8block were higher, especially at the high loads of the engine. At the full charge mode, the higher

performance of the modified CHS system was presented by the shorter full charge time and the higher percentage of the stored exhaust gas energy. The improvement of the modified CHS system can be up to 7.43% in the full charge time and 8.03% in the percentage of the exhaust gas energy stored in the CHS system at 50% engine load.

7.3 Performance of the modified CHS system in the heat output process

In the heat output process, the stored energy of the CHS system was used to heating the engine intake air. When two wings added in the reactor, similar to the heat storage process, the heat transfer coefficient and the moving time of the intake air inside the reactor increased leading to the increase in the absorbed energy of the intake air. The higher absorbed energy of the intake air was presented by the higher temperature of the heated air after going through the CHS system. The difference between the temperature of the heated air in two CHS systems are shown in Figure 7.11.

The solid lines in Figure 7.11 show the variation of the heated air temperature with the reactor and ambient temperatures in the original CHS system, and the dotted lines show the variation in the modified one. As shown in Figure 7.11, at a fixed ambient temperature, the heated air temperature in the modified CHS system is higher than that in the original one. The difference between two systems is higher at the lower ambient temperature and higher temperature of the reactor wall. The reason is that at the higher temperature of the reactor wall and lower temperature of the ambient temperature, the difference between two temperatures is higher. It leads to the stronger heat transfer process inside the reactor. At the ambient temperature -10^0C, the temperature of the heated air in the modified CHS system increases from 0.7 to 1.2^0C compared with the

original CHS system when the reactor wall increases from 45^0C to 85^0C.

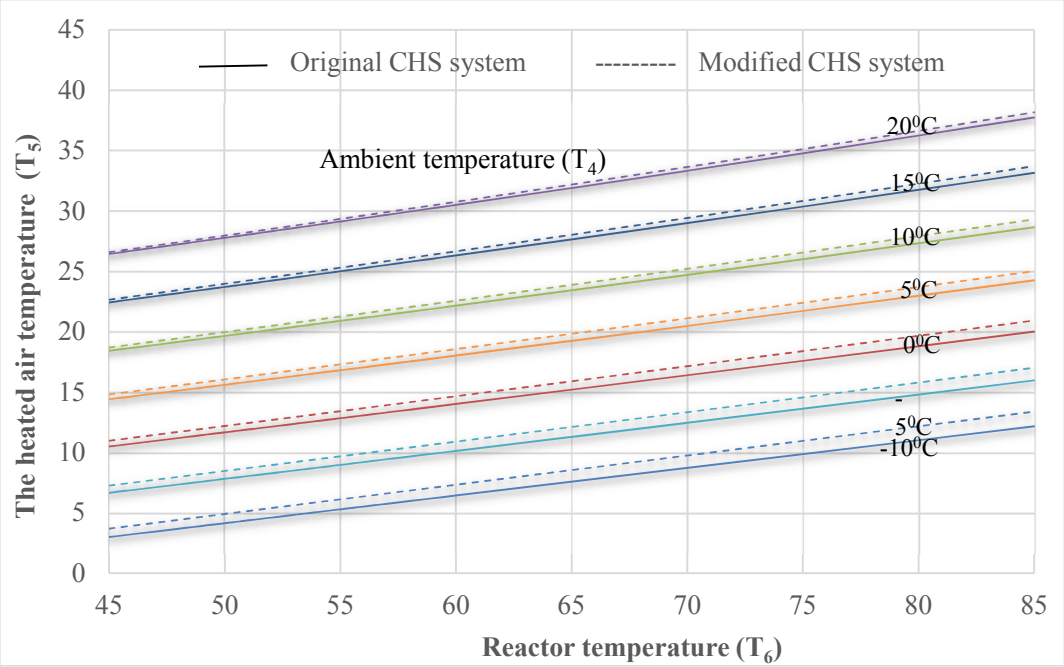

Figure 7.11 *Variation of the heated air temperature with the temperature of the ambient and reactor wall in the original and modified CHS systems*

In the modified CHS system, based on the required temperature of the heated air and the ambient temperature, the temperature of the reactor wall could be founded from Figure 7.11. Similar to the original CHS system, based on the reactor wall, the amount of water vapour required for the reaction inside the reactor could be determined from Figure 6.1.

7.4 Summary

This chapter presented the modified CHS system when two wings added in the exterior wall of the tube of the reactor. The chapter also presented and discussed the simulation results of the heat storage process in both the 60 minutes and full charge modes and the heat output process of the modified CHS system. The results of the modified CHS system

after that were compared with the original one. The main results of this chapter can be concluded as follows:

- To improve the heat transfer process inside the reactor, two wings added in the exterior wall of the tube of the reactor (the modified CHS system). Using the modified CHS system, the low temperature issue of EM8block in the area 4 was solved. The temperature profile of EM8block in the modified CHS system was higher and more uniform than the original one.
- In the heat storage process, both the percentages of the stored exhaust gas energy and the percentage of the reacted EM8block were improved in the 60 minutes mode. The maximum improvement of the modified CHS system was at the full engine load with 2.74 MJ stored energy and 12.49% of the percentage of the reacted EM8block higher than the original CHS system at the same engine load. In the full charge mode, using the modified CHS system, the full charge time was reduced 3.1 minutes at the full engine load and 8.2 minutes at 50% engine load. Furthermore, the maximum percentage of the exhaust gas energy stored in the modified CHS system increased to 7.58% compared with 7.14% in the original one at 70% engine load.
- In the heat output process, at a fixed ambient temperature, the heated air temperature after going through the modified CHS system was slightly higher than that in the original one. The obvious difference in the heated air temperature between two CHS systems was at the high temperature of the reactor wall and the low temperature of the ambient.

Chapter Eight

8 Conclusions and Future Work

8.1 Conclusions

To investigate the performance of the CHS using $Mg(OH)_2$, experiments were conducted in both heat storage and heat output processes. In the heat storage process, the experiments were conducted at 60%, 70% and 80% engine loads in 60 minutes. In the heat output process, the stored energy was used to heat the engine intake air at the ambient temperature of 23^0C.

Numerical simulations were performed using the commercial CFD code ANSYS FLUENT as the platform and verified by comparing the simulation and experimental results. The verified model was used to investigate the performance of the CHS system at condition different from that in experiments.

To improve the performance of the CHS system, an improvement was made in the reactor design with two wings added to the exterior wall of the tube of the reactor. The performance of the modified reactor was simulated using the verified CFD model.

8.1.1 CHS for heat storage

In the heat storage process, the experiments were conducted at 60%, 70%, 80% engine loads of the 60 minutes mode. At the other engine loads of the 60 minutes mode and the full charge mode, the performance of the CHS system was estimated based on the verified CFD model. The majors results in the heat storage process of the original CHS system

can be concluded as follows:

- For D1146TI diesel engine, using the original CHS system to recover the wasted heat of the exhaust gas was feasible at the engine loads higher than 50%. At the lower engine load, the temperature of the exhaust gas was not high enough, so the time for heating stages (stages 1, 2 and 3) were higher and using the CHS system at these engine loads was ineffective.
- In 60 minutes mode of the heat storage process, the maximum percentage of the reacted EM8block was 72.5% at the full engine load. This number decreased to 9.6% at 50% engine load. The highest percentage of the stored exhaust gas energy was 5.05% at 80% engine load and it dropped to 1.26% at 50% engine load.
- In the full charge mode, the full charge time of the CHS system depended on the engine load, and the shortest time was 67.1 minutes at the full engine load. This time increased with the decrease of the engine load and it took 110.3 minutes at 50% of engine load. The variation of the percentage of stored exhaust gas energy with the engine load was insignificant. The highest percentage was 7.14% at 70% engine load, and it decreased slightly when the engine load changed. The smallest percentage of the stored exhaust gas energy was 6.27% at the full engine load.

8.1.2 CHS for heat output

In the heat output process, the CHS system was used to pre-heating the engine intake air. The experiments were conducted at the ambient temperature of 23^0C. At other ambient temperature, the verified CFD model was used to investigate the performance of the CHS system in the heat output process. The major results of the heat output process of the CHS system can be concluded as follows:

- The temperature of the heated air after going through the reactor depended on the temperature of the reactor wall and the ambient temperature. The temperature of the reactor wall depended on the amount of the water vapour supporting from the water tank in the heat output process. Based on the required temperature of the heated air and the ambient temperature, the amount of water required for the reaction could be found based on Figures 6.1 and 6.3.
- The temperature of the heated air could be kept at 12.15^0C when the ambient temperature was 10^0C below freezing point, increased to 20.1^0C when the ambient temperature was at the freezing point 0^0C and was 40.02^0C when the ambient temperature was 23^0C.

8.1.3 Modification of the CHS system

In the modified CHS system, when two wings added on the exterior wall of the tube of the reactor, the heat transfer process inside the reactor was enhanced, resulting in increased average temperature of EM8block and more uniform temperature distribution in the reactor. The simulation results showed that the performance of the CHS system in both heat storage and heat output process were improved. The major results of the modified CHS system can be concluded as follows:

- In 60 minutes mode of the heat storage process, the improvement in the performance of the CHS system was evaluated in both the percentages of the stored exhaust gas energy and the reacted EM8block. The effect of the modified CHS system was stronger at the high load of the engine and it decreased with the decrease of the engine load. The percentage increase in the percentage of the reacted EM8block and the percentage of the exhaust gas energy stored in the

modified CHS system increased from 5.15% to 12.49% when the engine load increased from 50% to full engine load.

- In the full charge mode of the heat storage process, the maximum percentage of the exhaust gas energy stored by the CHS system raised to 7.58% at 70% engine load and it decreased when the engine load changed. Moreover, using the modified CHS system, the shortest full charge time was 64 minutes at the full engine load, 4.48% shorter than in the original one. In the full charge mode, the effect of the modified CHS system was stronger at the low load of the engine that was presented by the higher percentage increase in the full charge time and the percentage of the exhaust gas energy.
- In the heat output process, at a fixed ambient temperature, the heated air temperature in the modified CHS system was slightly higher than that in the original one. At the lowest ambient temperature of -10^0C in the simulation, the heated air temperature increased by 0.7 to 1.2 ^{0}C when the reactor wall temperature was changed from 45^0C to 85^0C compared with the original CHS system.

8.2 Suggestion for future work

8.2.1 Suggestion for applications of the heated air in the vehicle

As shown in Figure 6.3 for the original CHS system and Figure 7.10 for the modified one, even when the ambient temperature is below 0^0C, the temperature of the heated air after going through the reactor can increase to 10^0C or more depending on the ambient and reactor temperatures. Furthermore, the stored energy of the CHS system in the current study was absorbed by the air that is easy to transport to other parts of the vehicle.

Therefore, the high temperature of the heated air after going through the CHS system can be used not only for a fixed system but also simultaneously for many different applications of the vehicle such as: heating the engine, the lube oil of the IC engine vehicles or the batteries, cabin of the hybrid vehicles or defogging system of the vehicles in the ice regions.

Heating the engine is a possible application of the CHS system. As discussed in Chapter 2, heating the engine resulted in lower fuel consumption in the cold-start process. Compared with other TES systems applying to heat the engine in the engine start-up as discussed in section 6.2, the CHS system using EM8block with the higher stored energy and storing time could become a candidate for this heating purpose.

Heating the lube oil in the cold weather is another possible application of the CHS system. As discussed in Chapter 2, heating the lube oil can decrease the friction losses and increase the efficiency of the IC engine. From the results of the air heating process of the original CHS system in 6.2 and the modified one in 7.3, it can be seen that using the heated air from the CHS systems to increase the lube oil temperature to the effective operation range is possible or this application is very feasible.

In the hybrid vehicles, the operation of a battery in a hybrid vehicle highly depends on the surrounding temperature. The battery is designed to get the highest efficiency at a fixed range of temperature, from 25^0C to 45^0C [99]. If the temperature of the battery is lower than that required, the change of the viscosity inside the battery may lead to sluggish ion transport. The mobility of the ions decreases causing a rise in internal resistance [100]. The increase in the inside resistance of the battery leads to lower battery performance and it impacts the power capacity of motor and vehicle acceleration. The

capacity of a battery collapses rapidly at the low temperature, especially at the temperature lower than 0^0C [101]. In the version 3.2.3 of the Tesla app publishing on 22nd December 2017, Tesla gave a recommendation for the batteries of their electric vehicles in the cold weather "When temperatures are near freezing, preconditioning will also heat your battery for better driving and charging performance. We recommend you plug in to reduce range loss, and start pre-conditioning about an hour before you plan to leave since it can take some time to warm up the battery in colder weather". This recommendation can also apply for the battery of the electric motor in the hybrid vehicles. Therefore, for the battery of the hybrid vehicle, pre-heating it in the cool weather is a requirement to increase the capacity and maintain the lifespan of the battery. In this case, the high temperature of the heated air after going through the CHS systems can be used to heat the battery without engine start-up.

Moreover, the high temperature of the heated air after going through the reactor could be used as a heating assistance system to heat the cabin of the hybrid vehicle when the electric motor is in being used. Electric motors are different from IC engines. When the IC engine is in being used, the waste heat from IC engine could be provided for thermal requirement of the passenger, so the energy cost for heating the cabin could be reduced. However, with electric motors, they do not make much heat energy in operation as IC engines. Therefore, using the electric motors, the vehicles need more energy from the battery for heating purpose in the cool weather, and it affects the operation and the efficiency of the vehicles. As reported in [102], the average heating requirement of an electric vehicle in Edinburgh was 18% of the energy consumption. Matthew in [103] reported that a electric vehicle cabin heating at 20^0F ambient can reduce electric vehicle range by 20% - 59% compared with no heating. It can be seen that heating the cabin in

the cold weather adversely affect to the operation of the electric vehicles. Similar to that is the hybrid vehicles when the electric motors are in being used. Some solutions for this problem are using a bigger battery, electrical heaters [104], or heat pumps [105]in the winter. However, they will add more to the cost of the vehicles, and they still use a lot of energy from the batteries for their operation. Using the CHS system in the current study, as shown in Figures 6.3 and 7.10, the heated air temperature after going through the reactor can reach to around 20^0C even when the ambient temperature is 0^0C. This temperature is very suitable for heating the cabin of the hybrid vehicle in the cold weather.

In ice regions, warming up the vehicles a few minutes before driving is necessary, especially when frosted windshields appears. Heating the vehicle in the ice weather helps protect the engine and extend the life of the vehicle. To defrost the car's windshield, the hot air is provided to the inside of the windshields. It makes the temperature of the windshields increases and the ice melts. However, the hot air creating from HVAC system also increases the fuel consumption and polluting emissions of the vehicle, especially in the cold start of IC engine. As shown in Figures 6.3 and 7.10, even when the ambient temperature is smaller than -10^0C, the heated air temperature after going through the reactor should increase to higher than 10^0C. The high temperature of the heated air from the CHS system can be used in the defrosting assistance system to reduce the fuel consumption and emission of the vehicle.

In summary, besides heating the engine intake air, the CHS in the current study can be applied for many different applications of the vehicle such as heating the lubricant, engine in IC engine vehicles or the batteries, cabin in hybrid vehicles or the defrosting system in both IC engine and hybrid vehicles.

8.2.2 Suggestion for future work

Based on the current results of the research, some suggestion for future work may be adopted as follows:

1. Firstly, in the current research, as presented above, the laboratory was not air conditioned, the experiments on the intake air heating process were only conducted at the ambient temperature 23^0C. The intake air heating process at other ambient temperatures was investigated using the verified CFD simulation. However, experiments are still needed to verify the current simulation results.
2. Secondly, based on the heated air temperature, some possible application were suggested in 8.2. However, the applications suggested above still need a more detailed study.
3. Thirdly, in the current study, the reactor was designed based on the shell-tube heat exchanger. To improve the performance of the CHS system, in the modified CHS system, two wings added in the improvement model. However, a different design with higher efficiency could be developed in future work.
4. Finally, the gasoline engine with the higher exhaust gas temperature is the potential object of the CHS system in the current study. The higher temperature of the exhaust gas of the gasoline engine makes the heating time of the CHS system (stages 1, 2 and 3) is shorter, so the full charge time, accordingly, will be shorter. A CFD model was developed based on a tested gasoline engine, Camry Aurion, at the engine laboratory at University of Technology Sydney[94, 106]. However, it still needs a more detailed research.

References

1. *Energy effciency opportunities: Energy-mass balance: Transport Version 1.0*, Department of Resources Australian Goverment, Energy and Tourism, Editor. 2010.
2. Guruprasad Alva, Yaxue Lin, Guiyin Fang, *An overview of thermal energy storage systems.* Energy, 2017. **144**: p. 341-378.
3. Hasnain, S. M., *Review of sustainable thermal energy storage technologies, part 1: heat storage material and techniques* Energy Conversion and Management, 1998. **39**: p. 1127-1138.
4. Ming Liu, N.H.Steven Tay, Stuart Bell, Martin Belusko, Rhys Jacob, Geoffrey Will, Wasim Saman, Frank Bruno, *Review on concentrating solar power plants and new developments in high temperature thermal energy storage technologies.* Renewable and Sustainable Energy Reviews, 2016. **53**: p. 1411 - 1432.
5. Behnaz Rezaie , Bale V. Reddy , Marc A. Rosen *Assessment of the thermal energy storage in friedrichshafen district energy systems.* Energy Procedia, 2017. **116**: p. 91-105.
6. (IRENA), The International Renewable Energy Agency, *Renewable energy in district heating and cooling: Case Studies*, A renewable Energy Roadmap, Editor. 2017: www.irena.org/publications.
7. Dirk Mangold, Manfred Reuß, *Solar district heating in Germany - Finding and Prospects* in *ISES Solar World Congress 2011*. 2011: Kassel, Germany.
8. Duncan Gibb, Antje Seitz, Maike Johnson, Joaquim Romaní, Jaume Gasia, Luisa F. Cabeza, Richard Gurtner, *Applications of thermal energy storage in the energy transition: Benchmarks and Developments* in *Public Report of IEA ECES Annex 30*. 2018: IEA Technology Collaboration Programme on Energy Conservation through Energy Storage.
9. Eric Serge Kenda, Kokouvi Edem N'Tsoukpoe, IgorW.K. Ouédraogo, Yézouma Coulibaly, Xavier Py, Fabrice Marie Armel W. Ouédraogo, *Jatropha curcas crude oil as heat transfer fluid or thermal energy storage material for concentrating solar power plants.* Energy for Sustainable Development, 2017. **40**: p. 59-67.

10. Rhys Jacob, Martin Belusko, A. Inés Fernández, Luisa F. Cabeza, Wasim Saman, Frank Bruno, *Embodied energy and cost of high temperature thermal energy storage systems for use with concentrated solar power plants.* Applied Energy, 2016. **180**: p. 586 - 597.
11. Zhen Yang, Suresh V. Garimella, *Molten-salt thermal energy storage in thermoclines under different environmental boundary conditions.* Applied Energy, 2010. **87**: p. 3322–3329.
12. J.Pacioa, A. Fritsch; C. Singer, R. Uhlig, *Liquid metals as efficient coolants for high-intensity point-focus receivers: implications to the design and performance of next-generation CSP systems.* Energy Procedia, 2014. **49**: p. 647 - 655.
13. Robert Lugolole, Ashmore Mawire, Denis Okello, Katlego A. Lentswe, Karidewa Nyeinga, Adedamola B. Shobo, *Experimental analyses of sensible heat thermal energy storage systems during discharging.* Sustainable Energy Technologies and Assessments, 2019. **35**: p. 117 - 130.
14. Li, Gang, *Sensible heat thermal storage energy and exergy performance evaluations.* Renewable and Sustainable Energy Reviews, 2016. **53**: p. 897–923.
15. Valentina A. Salomoni, Carmelo E. Majorana, Giuseppe M. Giannuzzi, Adio Miliozzi, Rosa Di Maggio, Fabrizio Girardi, Domenico Mele, Marco Lucentini, *Thermal storage of sensible heat using concrete modules in solar power plants.* Solar Energy, 2014. **103**: p. 303–315.
16. P. Ohanessian, W. W. S. Charteres, *Thermal simulation of a passive solar house using a Trombe-Michel wall structure.* Solar Energy, 1978. **20**: p. 275 - 281.
17. Magdalena Nem´s, Artur Nem´s, Jacek Kasperski, Michał Pomorski, *Thermo-Hydraulic Analysis of Heat Storage Filled with the Ceramic Bricks Dedicated to the Solar Air Heating System.* Materials, 2017. **10**.
18. Atul Sharma, V.V. Tyagi, C.R. Chen, D. Buddhi, *Review on thermal energy storage with phase change materials and applications.* Renewable and Sustainable Energy Reviews, 2009. **13**: p. 318–345.
19. Skogsberg, Kjell, *Seasonal Snow Storage for Space and Process Cooling.* Thesis, 2005: Luleå University of Technology, Sweden.
20. *Cool Energy: Case examples of the ultilization of snow and ice cryogenic energy*. Hokkaido Bureau of Economy, Trade and Industry Ministry of Economy, Trade and Industry

21. Tan, Pepe, *On the Design Considerations for Thermal Energy Storage with Phase Change Materials: Material characterization and Modelling.* Thesis, 2018: Chalmers university of technology, Sweden.
22. Bo He, Fredrik Setterwall, *Technical grade paraffin waxes as phase change materials for cool thermal storage and cool storage systems capital cost estimation.* Energy Conversion and Management, 2002. **43**: p. 1709–1723.
23. Pandiyarajan, V., M. Chinna Pandian, E. Malan, R. Velraj, and R. V. Seeniraj, *Experimental investigation on heat recovery from diesel engine exhaust using finned shell and tube heat exchanger and thermal storage system.* Applied Energy, 2011. **88**: p. 77-87.
24. Yanping Yuan , Nan Zhang, Wenquan Tao, Xiaoling Cao, Yaling He, *Fatty acids as phase change materials: A review.* Renewable and Sustainable Energy Reviews, 2014. **29**: p. 482–498.
25. Aran Solé, Hannah Neumann, Sophia Niedermaier, Ingrid Martorell, Peter Schossig, Luisa F.Cabeza, *Stability of sugar alcohols as PCM for thermal energy storage.* Solar Energy Materials & Solar Cells, 2014. **126**: p. 125–134.
26. Henri Schmita, Werner Pfeffera, Christoph Rathgeber, Stefan Hiebler, *Experimental investigation of the concentration dependent maximum storage capacity of two inorganic phase change materials.* Energy Procedia, 2015. **73**: p. 231 – 238
27. Luisa F. Cabeza , GustavSvensson, Stefan Hiebler, Harald Mehling, *Thermal performance of sodium acetate trihydrate thickened with different materials as phase change energy storage material.* Applied Thermal Engineering, 2003. **23**: p. 1697–1704.
28. A. Inés Fernándeza, Camila Barreneche, Martin Belusko, Mercè Segarra, Frank Bruno, Luisa F. Cabeza, *Considerations for the use of metal alloys as phase change materials for hightemperature applications.* Solar Energy Materials and Solar Cells, 2017. **171**: p. 275 - 281.
29. E. Risueña, A.Faika, J. Rodríguez-Aseguinolaza, P. Blanco-Rodríguez, A.Gil, M. Tello, B. D'Aguanno, *Mg-Zn-Al eutectic alloys as phase change material for latent heat thermal energy storage.* Energy Procedia, 2015. **69**: p. 1006 – 1013.
30. P. Blanco-Rodríguez, J. Rodríguez-Aseguinolaza, E. Risueno, M. Tello, *Thermophysical characterization of Mge51%Zn eutectic metal alloy: A phase*

change material for thermal energy storage in direct steam generation applications. Energy, 2014. **72**: p. 414 - 420.

31. Vineet Veer Tyagi, D. Buddhi, *PCM thermal storage in buildings: A state of art.* Renewable and Sustainable Energy Reviews, 2007. **11**: p. 1146 - 1166.
32. Vincent Basecq , Ghislain Michaux , Christian Inard, Patrice Blondeau, *Short-term storage systems of thermal energy for buildings: a review.* Advances in Building Energy Research, 2013. **7**: p. 66– 119.
33. Ioan Sarbu, Calin Sebarchievici, *A Comprehensive Review of Thermal Energy Storage.* Sustainability, 2018. **10**.
34. Valeria Palomba, Vincenza Brancato, Andrea Frazzica, *Experimental investigation of a latent heat storage for solar cooling applications.* Applied Energy, 2017. **199**: p. 347 - 358.
35. M. Johnsona, J. Vogel, M. Hempel, A. Dengel, M. Seitz, B. Hachmann, *High temperature latent heat thermal energy storage integration in a co-gen plant.* Energy Procedia, 2015. **73**: p. 281 – 288.
36. Zamengo, M, *A Study on Heat Transfer-Enhanced Composites for a Magnesium Oxide/Water Chemical Heat Pump.* Thesis, 2014: Tokyo Institute of Technology.
37. Pardo, Pedro, Deydier, Alexandre, Anxionnaz-Minvielle, Zoe, Rouge, Sylvie, Cabassud, Michel, Cognet, Patrick, *A review on high temperature thermochemical heat energy storage.* Renewable and Sustainable Energy Reviews, 2014. **32**: p. 591-600.
38. Devrim Aydin, Sean P.Casey, Saffa Riffat, *The latest advancements on thermochemical heat storage systems.* Renewable and Sustainable Energy Reviews, 2015. **41**: p. 356–367.
39. Azpiazu, M. N., J. M. Morquillas, and A. Vazquez, *Heat recovery from a thermal energy storage based on the Ca(OH)2/CaO cycle.* Applied Thermal Engineering, 2003. **23**: p. 733-741.
40. A.Amhalhel, Gamal and Piotr Furmanski, *Theoritical and technical aspects of thermochemical conversion of concentrated solar energy.* 2004.
41. Lovegrove, K., A. Luzzi, I. Soldiani, and H. Kreetz, *Developing ammonia based thermochemical energy storage for dish power plants.* Solar Energy, 2004. **76**: p. 331-337.

42. Dunn, Rebecca, Keith Lovegrove, and Greg Burgess, *A Review of Ammonia-Based Thermochemical Energy Storage for Concentrating Solar Power.* IEEE, 2011.
43. Qiusheng Liu, Akira Yabe, Shiro Kajiyama, Katsuya Fukuda, *A Review of Study on Thermal Energy Transport System by Synthesis and Decomposition Reactions of Methanol.* JSME International Journal Series B Fluids and Thermal Engineering, 2002. **45**: p. 473-480.
44. Nobuyuki Gokona, Yusuke Osawa, Daisuke Nakazawa, Tatsuya Kodama, *Kinetics of CO_2 reforming of methane by catalytically activated metallic foam absorber for solar receiver-reactors.* International Journal of Hydrogen Energy, 2009. **34**: p. 1787 - 1800.
45. Xin, Fang, Min Xu, Xiulan Huai, and Xunfeng Li, *Study on isopropanol–acetone–hydrogen chemical heat pump: Liquid phase dehydrogenation of isopropanol using a reactive distillation column.* Applied Thermal Engineering, 2013. **58**: p. 369-373.
46. KlinSoda, Itikorn and Pornpote Piumsomboon, *Isopropanol–acetone–hydrogen chemical heat pump: A demonstration unit.* Energy Conversion and Management, 2007. **48**: p. 1200-1207.
47. Wentworth, W.E., *Thermochemical cycles for Energy storage: Thermal decomposition of $ZnSO_4$ systems* 1992: National Renewable Energy Laboratory, the U.S. Department of Energy.
48. Yan, T., R. Z. Wang, T. X. Li, L. W. Wang, and Ishugah T. Fred, *A review of promising candidate reactions for chemical heat storage.* Renewable and Sustainable Energy Reviews, 2015. **43**: p. 13-31.
49. M.A.Fahim and J.D.Ford, *Energy Storage Using the BaO_2-BaO Reaction Cycle.* 1982.
50. Agrafiotis, Christos, Martin Roeb, and Christian Sattler, *Exploitation of thermochemical cycles based on solid oxide redox systems for thermochemical storage of solar heat. Part 4: Screening of oxides for use in cascaded thermochemical storage concepts.* Solar Energy, 2016. **139**: p. 695-710.
51. Block, Tina and Martin Schmücker, *Metal oxides for thermochemical energy storage: A comparison of several metal oxide systems.* Solar Energy, 2016. **126**: p. 195-207.

52. Yukitaka Kato, Tadashi O-shima and Yoshio Yoshizawa, *Energy Analysis of a High-Temperature Chemical Heat Pump.* SAE technical paper series, 1999.

53. Kyaw Kyaw, Hitoki Matsuda, Masanoubu Hasatani, *Applicability of Carbonation/Decarbonation Reactions to High-Temperature Thermal Energy Storage and Temperature Upgrading.* Journal of chemical engineering of Japan, 1996. **29**: p. 119-125.

54. S. Fujimoto, E. Bilgen, H. Ogura, *$CaO/Ca(OH)_2$ chemical heat pump system.* Energy Conversion andManagement, 2002. **43**: p. 947–960.

55. F. Schaube, L. Koch, A. Wörner, H. Müller-Steinhagen, *A thermodynamic and kinetic study of the de- and rehydration of $Ca(OH)_2$ at high H_2O partial pressures for thermo-chemical heat storage.* 2012. **523**: p. 9 -20.

56. W.Wongsuan, S.Kumar, P.Neveu, F.Meunier, *A review of chemical heat pump technology and application.* Applied Thermal Engineering, 2001. **21**: p. 1489-1519.

57. Jane H. Davidson, Josh Quinnell, Jay Burch, H.A. Zondag, Robert de Boer, Christian Finck, Ruud Cuypers, Luisa F. Cabeza, Andreas Heinz, Dagmar Jahnig, Simon Furbo, Florian Bertsch, *Development of Space Heating and Domestic Hot Water Systems with Compact Thermal Energy Storage*, in *A report of the IEA Solar Heating and Cooling / Energy Conservation through Energy Storage programme – Task 42/Annex 24:*. 2013: International Energy Agency (IEA).

58. Valeria Palomba, Salvatore Vasta, Angelo Freni, *Experimental testing of AQSOA FAM Z02/water adsorption system for heat and cold storage.* Applied Thermal Engineering, 2017. **124**: p. 967–974

59. P. Pardo, Z. Anxionnaz-Minvielle, S. Rouge´, P. Cognet, M. Cabassud, *$Ca(OH)_2$/ CaO reversible reaction in a fluidized bed reactor for thermochemical heat storage.* Solar Energy 2014. **107**: p. 605–616.

60. Sylvie Rougé, Yolanda A. Criado, Olivier Soriano, J. Carlos Abanades, *Continuous $CaO/Ca(OH)_2$ fluidized bed reactor for energy storage: first experimental results and reactor model validation.* Industrial & Engineering Chemistry Research, 2017. **56 (4)**: p. 844-852.

61. Jorge Vázquez, Miguel A. Sanz-Bobi, Rafael Palacios, *Antonio Arenas *State of the Art of Thermoelectric Generators Based on Heat Recovered from the Exhaust Gases of Automobiles*, in *7th European Workshop on Thermoelectrics.* 2002.

62. Yuchao Wang, Chuanshan Dai, Shixue Wang, *Theoretical analysis of a thermoelectric generator using exhaust gas of vehicles as heat source.* Applied Energy, 2013. **112**: p. 1171–1180.

63. Vaka Devi, Karteek Naidu Mariserla *Waste Heat Recovery in Automobile Engines Potential Solutions and Benefits.* International Journal of Mechanical Engineering and Computer Applications, 2015. **3**: p. 99-104.

64. Orr, Bradley Glenn, *Power production from a car exhaust heat recovery system utilising thermoelectric generators and heat pipes.* 2016.

65. R. Saidur , M.Rezaei , W.K.Muzammil , M.H.Hassan , S.Pariaa, M.Hasanuzzaman *Technologies to recover exhaust heat from internal combustion engines.* Renewable and Sustainable Energy Reviews, 2012. **16**: p. 5649-5659.

66. Energy, US Department of, *Thermoelectric Conversion of Waste Heat to Electricity in an IC Engine Powered Vehicle*, Final report, Editor. 2011: United State Govenrment.

67. Pulkrabek, Willard W., *Engineering Fundementals of the Internal Combustion Engine*. 1997.

68. Gordon E. Andrews, Ali. M. Ounzain, Hu Li, Margaret Bell, James Tate and Karl Ropkins, *The Use of a WaterLube Oil Heat Exchanger and Enhanced Cooling Water Heating to Increase Water and Lube Oil Heating Rates in Passenger Cars for Reduced Fuel Consumption and CO2 Emissions During Cold Start.* SAE 2007-01-2067.

69. Will, Frank and Alberto Boretti, *A New Method to Warm Up Lubricating Oil to Improve the Fuel Efficiency During Cold Start.* SAE International Journal of Engines, 2011. **4**: p. 175-187.

70. Kauranen, Pertti, Tuomo Elonen, Lisa Wikström, Jorma Heikkinen, and Juhani Laurikko, *Temperature optimisation of a diesel engine using exhaust gas heat recovery and thermal energy storage (diesel engine with thermal energy storage).* Applied Thermal Engineering, 2010. **30**: p. 631-638.

71. Gumus, M., *Reducing cold-start emission from internal combustion engines by means of thermal energy storage system.* Applied Thermal Engineering, 2009. **29**: p. 652-660.

72. TESSA *Thermal Energy Saving and Storage on Automobiles* 2018.

73. Innovations, UK-based Atmos. *TESSA — the Thermal Energy Storage and Saving in Automobile* 2017.
74. Satoshi Hariu, Takafumi Yamasaki, *Chemical heat storage device*. 2016, Kabushiki Kaisha Toyota Jidoshokki: United States.
75. Satoshi Hariu, Takafumi Yamasaki, Yukihiro Noguchi, Hiroyasu Kawauchi, Hideaki Suzuki, *Chemical heat storage decide*. 2016, Kabushiki Kaisha Toyota Jidoshokki: United States.
76. Kenji Mori, Satoshi Hariu, Takajumi Yamasaki, *Chemical heat storage device*. 2016, Kabushiki Kaisha Toyota Jidoshokki: United States.
77. Satoshi Hariu, Takafumi Yamasaki, *Chemical heat storage devide*. 2017, Kabuchiki Kaisha Toyota Jidoshokki: United States.
78. Zamengo, Massimiliano, *A Study on Heat Transfer-Enhanced Composites for a Magnesium Oxide/Water Chemical Heat Pump.* Thesis, 2014: Tokyo Institute of Technology.
79. Massimiliano Zamengo, Yukitaka Kato, *A study on heat tranfer-enhanced composites for a Magnesium Oxide/Water Chemical Heat Pump.* 2014.
80. Zamengo, Massimiliano, Junichi Ryu, and Yukitaka Kato, *Composite block of magnesium hydroxide – Expanded graphite for chemical heat storage and heat pump.* Applied Thermal Engineering, 2014. **69**: p. 29-38.
81. Zamengo, Massimiliano, Junichi Ryu, and Yukitaka Kato, *Thermochemical performance of magnesium hydroxide–expanded graphite pellets for chemical heat pump.* Applied Thermal Engineering, 2014. **64**: p. 339-347.
82. Thomas B. Gatski, Jean-Paul Bonnet, *Compressibility, Turbulence and High Speed Flow*. 2013: Elsevier.
83. Spalart, P.R., *Strategies for turbulence modelling and simulations.* International Journal of Heat and Fluid Flow, 2000. **21**: p. 252 - 263.
84. T. van Hooff, B. Blocken, Y. Tominaga, *On the accuracy of CFD simulations of cross-ventilation flows for a generic isolated building: Comparison of RANS, LES and experiments.* Building and Environment, 2017. **114**: p. 148 - 165.
85. Pope, Stephen B, *Ten questions concerning the large-eddy simulation of turbulent flows.* New Journal of Physics, 2004. **4**.
86. *ANSYS Fluent Tutorial Guide*. Vol. ANSYS 18. 2017: ANSYS, Inc.

87. Guangliang Chen, Zhijian Zhang, Zhaofei Tian, Lei Li, Xiaomeng Dong, Haoran Ju, *Design of a CFD scheme using multiple RANS models for PWR.* Annals of Nuclear Energy, 2017. **102**: p. 349–358.
88. C.-H. Hu, Takashi Kurabuchi, M. Ohba, *Numerical study of cross-ventilation using two-equation RANS turbulence models.* International Journal of Ventilation, 2005. **4**: p. 123-132.
89. Frank P.Incropera, David P.Dewitt, Theodore L.Bergman, Adrienne S.Lavine, *Fundamentals of Heat and Mass Transfer*. 6th ed. 2007: Wiley.
90. J.P.Holman, *Heat transfrer*. 10th ed. 2010: McGraw-Hill
91. Mahan, J. Robert, *Radiation Heat Transfer: A Statistical Approach*. 2002: Wiley.
92. WenqiZhong, AibingYu, GuanwenZhou, JunXie, HaoZhang, *CFD simulation of dense particulate reaction system: Approaches, recent advances and applications.* Chemical EngineeringScience, 2016. **140**: p. 16–43.
93. Ravi Inder Singh, Anders Brink, Mikko Hupa, *CFD modeling to study fluidized bed combustion and gasification.* Applied Thermal Engineering, 2013. **52**: p. 585 - 614.
94. Duc Luong Cao, Guang Hong, Jianguo Wang. *Preliminary investigation to the feasibility of chemical heat storage for saving the exhaust gas energy in a spark ignition engine*. in 20th Australasian Fluid Mechanics Conference. 2016. Perth, Australia.
95. Duc Luong Cao, Guang Hong, Tuan Le Anh. *Preliminary comparison of chemical heat storage systems for saving exhaust gas energy in gasoline and diesel engines*. in 11th Asia-Pacific Conference on Combustion. 2017. Sydney, Australia.
96. Tianyou Wang, Jie Zhang, Yajun Zhang, Zhijun Peng, *Energy Analysis for Recoverable Exhaust Heat in a Gasoline Engine*, in *Sustainable Thermal Energy Management in the Process Industries*. 2011: Newcastle.
97. Outokumpu, *Stainless steels for high service temperatures: Outokumpu Therma range datasheet*, Outokumpu, Editor. 2018: https://www.outokumpu.com/products/ranges/therma.
98. Duc Luong Cao, Guang Hong, Tuan Le Anh. *Investigation of chemical heat storage processes for recovering exhaust gas energy in internal combustion engines*. in 21st Australasian Fluid Mechanics Conference. 2018. Adelaide, Australia.

99. Ahmad A. Pesaran, Andreas Vlahinos, Tom Stuart. *Cooling and Preheating of Batteries in Hybrid Electric Vehicles*. in 6th ASME-JSME Thermal Engineering Joint Conference. 2003. Hawaii, United States.

100. Shuai Ma, Modi Jiang, Peng Tao, Chengyi Song, Jianbo Wu, Jun Wang, Tao Denga, Wen Shang, *Temperature effect and thermal impact in lithium-ion batteries: A review.* Progress in Natural Science: Materials International, 2018. **28**: p. 653-666.

101. Ahmad Pesaran, Shriram Santhanagopalan, Gi-Heon Kim, *Addressing the Impact of Temperature Extremes on Large Format Li-ion Batteries for Vehicle Applications*, in *30th International Battery Seminar* 2013: Ft. Lauderdale, Florida.

102. Muneer, Aisling Doyle and Tariq, *Energy consumption and modelling of the climate control system in the electric vehicle.* Energy Exploration & Exploitation, 2019. **37**: p. 519 - 543.

103. Matthew Jeffers, Lawrence Chaney, and John Rugh, *Climate Control Load Reduction Strategies for Electric Drive Vehicles in Cold Weather*, in *AE 2016 World Congress & Exhibition*. 2016: Detroit, Michigan.

104. A. Hande, T.A.Stuart, *AC Heating for EV/HEV Batteries*, in *7th IEEE Workshop on Power Electronics in Transportation*. 2002: Detroit, MI.

105. *Heat-Pump Cabin Heater*. 2019, Nissan motor corporation: https://www.nissan-global.com/en/technology/overview/heat_pump_cabin_heater.html.

106. Duc Luong Cao, Guang Hong, Jack Wang, *Chemical heat storage for saving the exhaust gas energy in a spark ignition engine.* Journal of Clean Energy Technologies 2018. **6**: p. 41-46.